

**HISTOGRAM OF GRADIENT ORIENTATIONS OF EEG SIGNAL  
PLOTS FOR BRAIN COMPUTER INTERFACES**

por  
Rodrigo Ramele



EN CUMPLIMIENTO PARCIAL DE LOS  
REQUISITOS PARA OPTAR AL GRADO DE  
DOCTOR EN INGENIERÍA INFORMATICA

DEL  
  
INSTITUTO TECNOLÓGICO DE BUENOS AIRES  
BUENOS AIRES, ARGENTINA  
30 DE NOVIEMBRE, 2018

INSTITUTO TECNOLÓGICO DE BUENOS AIRES

DEPARTAMENTO DE DOCTORADO

Los aquí suscriptos certifican que han asistido a la presentación oral de la Tesis  
**“Histogram of Gradient Orientations of EEG Signal Plots for Brain Computer Interfaces”** cuyo autor es **Rodrigo Ramele** completando parcialmente, los requerimientos exigidos para la obtención del Título de **Doctor en Ingeniería Informatica**.

Fecha: 30 de Noviembre, 2018

Directores:

---

Dr. Juan Miguel Santos

---

Dra. Ana Julia Villar

Tribunal de Tesis:

---

Dra. Jurado

---

Dr. Jurado

---

Dr. Jurado

INSTITUTO TECNOLÓGICO DE BUENOS AIRES

Fecha: **30 de Noviembre, 2018**

Autor: **Rodrigo Ramele**

Título: **Histogram of Gradient Orientations of EEG Signal Plots for  
Brain Computer Interfaces**

Departamento: **Doctorado**

Título Académico: **Doctor en Ingeniería Informática** Convocatoria: **Mes Año**

Por la presente se otorga permiso al Instituto Tecnológico de Buenos Aires (ITBA) para: (i) realizar copias de la presente Tesis y para almacenarla y/o conservarla en el formato, soporte o medio que la Universidad considere conveniente a su discreción y con propósitos no-comerciales; y, (ii) a brindar acceso público a la Tesis para fines académicos no lucrativos a los individuos e Instituciones que así lo soliciten (incluyendo, pero no limitado a la reproducción y comunicación al público no comercial de toda o parte de la Tesis, a través de su sitios o páginas Web o medios análogos que en el futuro se desarrollen).

A excepción de lo autorizado expresamente en el párrafo precedente, me reservo los demás derechos de publicación y, en consecuencia, ni la Tesis ni extractos de la misma podrán ser impresos o reproducidos de otro modo sin mi previo consentimiento otorgado por escrito.

Declaro que he obtenido la autorización para el uso de cualquier material protegido por las leyes de propiedad intelectual mencionado o incluido en la tesis (excepto pasajes cortos, transcripciones, citas o extractos que solo requieran ser referenciados o citados por escrito) y que el uso que se ha hecho de estos está expresamente reconocido por las leyes aplicables en la materia.

Finalmente, manifiesto que la presente autorización se firma en pleno conocimiento de la Política de Propiedad Intelectual del ITBA y, en forma específica, del Capítulo 2.3. referido a la titularidad de derechos de propiedad intelectual en el ITBA y/o, según el caso, a la existencia de licencias no exclusivas de uso académico o experimental por parte del ITBA de la Tesis o la obra o de las invenciones allí contenidas o derivadas de ella.

Hago entrega en este acto de un ejemplar de la Tesis en formato impreso y otro en formato electrónico.

---

Firma del Autor



# Contents

<b>Abstract</b>	<b>ix</b>
<b>Resumen</b>	<b>xiii</b>
<b>Lists of Publications</b>	<b>xv</b>
<b>Acknowledgements</b>	<b>xvii</b>
<b>List of Acronyms</b>	<b>xx</b>
<b>List of Tables</b>	<b>xxi</b>
<b>List of Figures</b>	<b>xxv</b>
<b>List of Symbols</b>	<b>xxvii</b>
<b>Introduction</b>	<b>1</b>
0.1 Significance . . . . .	3
0.2 Summary . . . . .	3
<b>Chapter 1     The Brain, The Computer and The Interface</b>	<b>5</b>
1.1 Brain Computer Interface Model and Architecture . . . . .	7
1.2 Signal Processing . . . . .	9
1.3 The Forward and Inverse Model . . . . .	10
1.4 Brain Imaging Technologies . . . . .	12
1.5 Electroencephalography . . . . .	12
1.6 BCI EEG Paradigms . . . . .	16
1.7 State of the Art of BCI Algorithms for EEG processing . . . . .	17
1.8 EEG Waveform Analysis . . . . .	18
1.8.1 EEG Waveform Characterization . . . . .	18
1.8.2 EEG Waveform Analysis Algorithms . . . . .	20

<b>Chapter 2 From signals to images</b>	<b>27</b>
2.1 Electroencephalographic Plotting . . . . .	27
2.2 Signal to Image transformation . . . . .	28
2.3 EEG Signal Plot . . . . .	31
2.3.1 Standardized plotting . . . . .	32
2.3.2 Autoscaled plotting . . . . .	32
2.3.3 Zero-Level . . . . .	33
2.3.4 Image Size . . . . .	34
2.3.5 Interpolation . . . . .	34
2.3.6 Resolution and Precision . . . . .	36
<b>Chapter 3 The Histogram of Gradient Orientations of Signal Plots</b>	<b>39</b>
3.1 Introduction . . . . .	39
3.2 Feature Extraction: Histogram of Gradient Orientations . . . . .	40
3.3 Keypoint Location . . . . .	41
3.4 Patch Geometry . . . . .	43
3.4.1 Oscillatory Processes . . . . .	44
3.4.2 Transient Events . . . . .	45
3.5 Classification . . . . .	45
3.6 BCI Algorithm . . . . .	45
3.7 Implementation . . . . .	47
3.7.1 Matlab, C++ and VLFeat . . . . .	47
3.8 Mapping Cheat-Sheet . . . . .	47
<b>Chapter 4 Alpha Wave: inhibition signal</b>	<b>49</b>
4.1 Introduction . . . . .	49
4.2 Materials and Methods . . . . .	50
4.2.1 Dataset I - Emotiv EPOC alpha waves own dataset . . . . .	50
4.2.2 Dataset II - AlphaNet Dataset . . . . .	52
4.2.3 Parameters . . . . .	52
4.3 Results . . . . .	52
4.4 Conclusion . . . . .	53

<b>Chapter 5</b>	<b>Motor Imagery: the hunt for a greek letter</b>	<b>57</b>
5.1	Introduction . . . . .	57
5.2	Materials and Methods . . . . .	57
5.3	Results . . . . .	58
5.4	Conclusion . . . . .	60
<b>Chapter 6</b>	<b>Event Related Potential: The P300 Wave</b>	<b>61</b>
6.1	Introduction . . . . .	61
6.2	Materias and Methods . . . . .	62
6.2.1	Feature Extraction from Signal Plots . . . . .	62
6.2.2	Experimental Protocol . . . . .	66
6.3	Results . . . . .	72
6.4	Conclusion . . . . .	77
<b>Chapter 7</b>	<b>Conclusions and Future Work</b>	<b>83</b>
<b>Appendix A</b>	<b>BCI en Argentina</b>	<b>85</b>
<b>Bibliography</b>		<b>88</b>



# Abstract

Brain Computer Interface (BCI) or Brain Machine Interfaces (BMI), has proved the feasibility of a distinct non-biological communication channel to transmit information from the Central Nervous System (CNS) to a computer device. Promising success has been achieved with invasive BCI, though biocompatibilities issues and the complexity and risks of surgical procedures are the main drive to enhance current non-invasive technologies.

Electroencephalography (EEG) is the most widespread method to gather information from the CNS in a non-invasive way. Clinical EEG has traditionally focused on temporal waveforms, but signal analysis methods which follow this path has been overshadow in BCI research.

This thesis propose a method and framework to analyze the waveform, the shape of the EEG signal, using the histogram of gradient orientations, a fruitful technique from Computer Vision which is used to characterize image local features. Inspiration comes from what traditionally electroencephalographers have been doing for almost a century: visually inspecting raw EEG signal plots.

This technique can be outlined in five steps, (1) signal preprocessing, (2) signal segmentation, (3) transformation on a channel by channel basis of each signal segment into a binary image of a signal plot, (4) assignment of keypoint location on a position over the newly created image depending on the physiological phenomena under study and finally (5) the calculation of the histogram of gradient orientations using finite differences from the image around this keypoint. This method generates a feature, a normalized 128-dimension descriptor. This feature is used to compare the signal segments that were used to generate them, hence to analyze the underlying cognitive phenomena.

The validity of the method is verified by studying three cognitive patterns. First, Visual Occipital Alpha Waves are analyzed. An experimental protocol is designed and a dataset is produced using a commercial-grade EEG device. Additionally, the ability of the method to capture oscillatory processes is verified by analyzing a public dataset. Moreover, this methodology is extended to study a related oscillatory process: Motor Imagery Rolandic Mu rhythms. The performance of the method to discriminate right vs left motor imagery

against a public dataset of healthy subjects, is verified. Results are informed and reported.

Finally, the method is modified to capture transient events, particularly the P300 Event Related Potential (ERP). A description on how to extract the ERP from the EEG segment is offered, and a detailed depiction of how to implement a P300-Based BCI Speller application is outlined. Its performance is verified by processing a public dataset of Amyotrophic Lateral Sclerosis (ALS) patients and contrasted against an own dataset produced in-house replicating the same experimental conditions. Results are compared against other methods referenced in the bibliography

The benefits of the approach presented here are twofold, (1) it has a universal applicability because the same basic methodology can be applied to detect different patterns in EEG signals with applications to BCI and (2) it has the potential to foster close collaboration with physicians and electroencephalograph technicians because this direction of work follows the established procedure of the clinical EEG community of analyzing waveforms by their shapes.





# Resumen

Las interfaces BCI (Brain Computer Interfaces, interfaces cerebro computadora) o BMI (Brain Machine Interfaces, interfaces cerebro máquina) han surgido como un nuevo canal de comunicación entre el cerebro y las computadoras, máquinas o robots, distinto de los canales biológicos estándar. Se han obtenido resultados prometedores en el empleo de la variante invasiva de BCI pero, además de los problemas de biocompatibilidad, los procedimientos quirúrgicos requeridos son complejos y riesgosos. Estas razones, han impulsado las mejoras de las tecnologías no invasivas.

La electroencefalografía (EEG) es el método más difundido para obtener información del sistema nervioso central de manera no invasiva. La electroencefalografía clínica se ha enfocado tradicionalmente en el estudio de las formas de ondas temporales, pero los métodos de procesamiento de señales que exploren esta metodología han sido ignorados en las investigaciones sobre BCI.

Esta tesis propone un método y un marco para analizar las formas de las señales de EEG utilizando los histogramas de gradientes orientados, una técnica de visión por computadora que es utilizada para identificar y clasificar características locales en regiones de una imagen. Este procedimiento está inspirado en lo que tradicionalmente los técnicos electroencefalógrafos han realizado por casi un siglo: inspeccionar visualmente los registros electroencefalográficos.

El método propuesto puede resumirse en 5 pasos, (1) preprocesamiento de la señal cruda, (2) segmentación de la señal, (3) obtención de una gráfica blanco y negro de la señal canal por canal, (4) asignación de una localización dentro de la imagen para posicionar un parche de un determinado tamaño y escala dependiendo del fenómeno cognitivo en estudio, y (5) cálculo del histograma de los gradientes orientados de la intensidades de los pixeles usando diferencias finitas. Este mecanismo genera un vector de 128 dimensiones, que se utiliza para comparar los segmentos de señales entre sí, y que permite entonces analizar el fenómeno cognitivo subyacente.

La validez del método se verifica estudiando tres patrones cognitivos. Primero se analizan las ondas alfa de la corteza visual occipital sobre dos conjuntos de registros: uno obtenido

a partir de la aplicación de un protocolo experimental y mediante la utilización de un dispositivo electroencefalográfico digital de uso comercial, y otro obtenido de una base de datos pública de registros electroencefalográficos. Segundo, se analiza otro tipo de onda oscilatoria conocida como ritmo mu correspondiente a la corteza motora que puede ser también activada si el sujeto imagina una actividad motora. Se reporta la efectividad del método para discriminar entre la actividad de la corteza motora derecha e izquierda en base al estudio de otro conjunto de registros público de pacientes sanos. Los resultados son reportados y publicados.

Finalmente, el método propuesto se utiliza para estudiar eventos transitorios, particularmente, el potencial evocado P300. La eficiencia del sistema es verificada mediante el procesamiento de un conjunto de registros público de pacientes con esclerosis lateral amiotrófica, y corroborada contra un conjunto de registros de sujetos sanos obtenidos de manera experimental, replicando el mismo protocolo. Para ambos conjuntos de registros, se realiza una descripción detallada de cómo extraer este potencial de la señal de EEG, y se implementa un procesador de texto basado en P300 para comparar el desempeño del método propuesto respecto de otros citados en la bibliografía.

Los beneficios de esta propuesta se resumen en, (1) tiene una aplicación potencialmente universal, debido que el mismo tipo de metodología puede ser aplicada para detectar cualquier tipo de patrón obtenido en la señal de EEG con potenciales aplicaciones a BCI, y (2) ofrece la posibilidad de incentivar la colaboración y utilización de estas técnicas en la clínica médica especializada en electroencefalografía ya que esta perspectiva basada en el estudio de las formas de onda de las señales, es un procedimiento conocido y ya establecido por esa comunidad.

# Lists of Publications

The following publications are the basis of this thesis

- Ramele, R., A.J.Villar, and J.M.Santos."A Brain Computer Interface Classification Method Based on SIFT Descriptors." VI Latin American Congress on Biomedical Engineering CLAIB 2014, Paraná, Argentina 29,30,31 October 2014. Springer International Publishing, 2015.
- Ramele, R., A. J. Villar, and J. M. Santos. "A Brain Computer Interface Classification Method Based on Signal Plots." 4th Winter Conference on Brain Computer Interfaces, Yongpyong, Korea, February 2016. IEEE Signal and Processing, 2016.



# Acknowledgements

Es un falacia creer que existe alguna actividad en nuestra vida que la hacemos solos. Todos nosotros tenemos una interminable lista de personas a quienes le debemos agradecimiento, desde el primer segundo respirado hasta el último, y especialmente por aquellos actos ciclópeos que nos demandan todo lo que tenemos.



# List of Acronyms

The following abbreviations are used in this thesis:

EEG: electroencephalography

BCI: Brain Computer Interfaces

BMI: Brain Machine Interfaces

BNCI: Brain-Neural Computer Interfaces

SNR: Signal to Noise Ratio

CNS: Central Nervous System

DC: Direct Current

ERP: Event-Related Potential

P300: Positive deflection of an Event-Related Potential which occurs 300 ms after onset of stimulus

ITR: Information Transfer Rate

BTR: Bit Transfer Rate

SIFT: Scale Invariant Feature Transform

SHCC: Slope Horizontal Chain Code

PE: Permutation Entropy

MP: Matching Pursuit

ICU: Intensive Care Unit

EKG: Electrocardiogram

PAA: Period Amplitude Analysis

SVM: Support Vector Machine



# List of Tables

2.1	Reference Values for Precision and Resolution . . . . .	37
6.1	Single Channel Character Recognition Rates for ALS patient's Dataset	72
6.2	Single Channel Character Recognition Rates for Healthy Subject's Dataset . . . . .	73
6.3	Character Recognition Rates for ALS patient's dataset . . . . .	75
6.4	Character Recognition Rates for Healthy Subject's Dataset . . . . .	75
6.5	Speller classification performance obtained for all the waveform-based algorithms: MP Matching Pursuit, SIFT Scale Invariant Feature Transform, PE Permutation Entropy and SHCC Slope Horizontal Code Chain. Additionally, the control algorithm SVM Support Vector Machines is included for comparison. All the methods process the signal on a channel-by-channel basis, hence the best performing channel is also shown. In this case with absence of null-signals, it can be interpreted as the channel that adds less noise to the ERP template. All the methods used 10 intensification sequences to coherently average the trials to obtain the averaged signal. . . . .	81
6.6	Speller classification performance obtained for the dataset IIb of the BCI Competition II (2003) for each one of the algorithms using 15 repetitions of intensification sequences. The first 42 trials are used for training to build the template dictionary and the remaining 31 for testing. The channel where the best performance is attained, is also shown. . . . .	82



# List of Figures

1.1	BCI Block Diagram . . . . .	8
1.2	Neuroanatomical structures of the brain . . . . .	10
1.3	EEG Volume Conduction . . . . .	11
1.4	Sample Multichannel EEG signal . . . . .	13
1.5	Electrode Locations . . . . .	14
1.6	Wearable portable Digital Electroencephalograph . . . . .	14
2.1	EEG Signal Mapping to Images . . . . .	29
2.2	Image Coordinate System . . . . .	30
2.3	Signal plot of an impulse response . . . . .	33
2.4	Signal Plotting: Interpolation . . . . .	35
3.1	Histogram of Gradient Orientations for ERP . . . . .	41
3.2	Keypoint Locations . . . . .	42
3.3	Patch Geometry . . . . .	44
3.4	NBNN Classification . . . . .	46
4.1	Alpha Waves Wiggles . . . . .	50
4.2	Spectrum components obtained by the FFT of Alpha Waves . . . . .	51
4.3	EPOC Emotiv Alpha Waves Dataset . . . . .	52
4.4	Power Spectral Density of the Dataset I . . . . .	53
4.5	Dataset I Classification Rate . . . . .	54
4.6	PhysioNet Dataset Classification Rate . . . . .	54
5.1	Motor Imagery Experimental Protocol . . . . .	59
5.2	Motor Imagery Accuracy . . . . .	60
6.1	P300 Speller Matrix . . . . .	62
6.2	P300 Speller Matrix Letter Identification . . . . .	63

6.3	ERP Template obtained from the coherent point-to-point ensemble average from the signals of Subject Number Eight of the BNCI Horizon public dataset 008-2014. The template is 1s long which is 256 sample points, and the eight channels are superimposed with different colors. The P3b component can be seen around the sample index 150 and 200.	69
6.4	g.Tec devices and subjects . . . . .	70
6.5	Eight-channel EEG signal without and with the superimposed ERP Template. The channel L, the mark which identifies where to superimpose the P300 ERP, is shown as well as the channel S which identifies the stimulus that was presented. On (c) and (d) the small variation that was introduced by the superimposition of the ERP can be seen enclosed by the vertical bars, where the slope of the bump on subfigure (d) is slightly bigger . . . . .	71
6.6	Point-to-point averaged signals for the first letter identification trial. The ERP is superimposed on classes 3 and 9. Class 3 is obtained while averaging the segments where the row of the speller matrix is intensified whereas class 9 is calculated from the intensification of the corresponding column. . . . .	71
6.7	P300 Performance Curves . . . . .	73
6.8	P300 Classification Boxplots . . . . .	74
6.9	Sample P300 Patches . . . . .	76
6.10	Speller performance obtained for each method for the Experiment 1. Y-axis shows performance accuracy while X-axis shows the number of intensification sequences used to calculate the point-to-point signal average. . . . .	79
6.11	Speller performance obtained for each method while latencies are artificially added to each single-intensification segment corresponding to the Experiment 2. The achieved performance is significantly reduced for all methods. Y-axis shows letter identification performance while X-axis shows the number of intensification sequences used to calculate the ensemble average. . . . .	80

6.12	Speller performance obtained for the Experiment 3 while the amplitudes of the P3b component of the superimposed ERP is randomly reduced. Y-axis shows performance accuracy while X-axis shows the number of intensification sequences. . . . .	80
6.13	Speller performance obtained for the Dataset IIb of the BCI Competition II (2003) for each one of the algorithms. An offline BCI Simulation is performed using the first 42 trials as training and the remaining 31 as testing. The horizontal axis show the number of intensification sequences, from 0 to 15 for this dataset, while the vertical axis show the performance rate. . . . .	81



# List of Symbols

$N$	Sample points
$F_s$	Sampling Frequency
$w$	Signal Segment Size
$W_x$	Image Width
$H_y$	Image Height
$\gamma_t$	Time Scale Factor
<b>kp</b>	Keypoint
$S_x$	Patch Width
$S_y$	Patch Height
$S_t$	Patch Horizontal Scale
$\lambda$	Signal Span
$\Delta_s$	Pixels in unit scale
$\Delta\mu V$	Peak-to-peak Amplitude
$S_v$	Patch Vertical Scale
$\gamma$	Signal Amplitude Scale Factor
<b>p</b>	Pixel

# Introduction

The brain is a machine with the sole purpose to respond appropriately to external and internal events, and to spread its own presence into the environment where it belongs<sup>1</sup>. Hence, the brain needs to communicate and it posses mainly two natural ways to do it: hormonal or neuromuscular. When those natural channels are interrupted, they are not available or when it needs to increase or enhance the communication alternatives, a new artificial communication channel which is not based on them, is needed. It is based, instead, on a new technology feat that decode the information from the CNS and transmit it directly to a computer or machine.

Brain Computer Interface, BCI, is a system that measures brainwaves and converts them into artificial output that replaces, restores, enhances, supplements or improves natural CNS output and changes the ongoing interactions between the Central Nervous System (CNS) and its external or internal environment [102]. Brain Machine Interface (BMI) generally refers to invasive devices. Brain Neural Computer Interfaces (BNCI) may refer to devices that do not exclusively use information from the CNS, they also may use any kind of biological signal that can be harnessed with the purpose of volitionally transmit information. Above all, every kind of BCI system is after all a communication device.

There are five motives behind BCI: the **first** is the Aging of Societies: estimated for 2025, 800 millions people will be over 65 years old, and 2/3 of them on developing countries [55]. This may lead to an increased tendency to develop diseases that affect motor pathways and require some form of assistance from technology. The **second** reason is the digital world that calls for more methods of interactions. This digital society demands more mechanisms to interpret the surrounding world and to translate human intentions through digital gadgets. Additionally, the advancement of smart wearable devices that can be used over the skin is also pushing the frontiers to go deeper into the body to find there useful information. The **third** motive is the impulse of Neuroscience Research and the advances that this discipline is having worldwide. The **fourth** reason is the potentialities of BCI as a clinical tool which can help to diagnose diseases, as aid in the field of neurorehabilitation, or to

---

<sup>1</sup>The sensorimotor Hypothesis [105, 102] and The Extended Mind Thesis [19]

provide neurofeedback. The **fifth**, final and most important motive, the reason behind Brain Computer Interfaces, is the still unfulfilled societal promise of social inclusion of people with disabilities. It is known that the ability to walk and live independently is a key indicator of psychological and physical health, and we have to do all we can to provide the technological tools to achieve this goal [78, 21, 102, 43].

In line with the aforementioned motives, there are several applications currently under development for BCI. People affected by any kind of neurodegenerative diseases, particularly those affected by advanced stages of amyotrophic lateral sclerosis (ALS) with locked-in syndrome may find in BCIs the only remaining alternative to communicate. Other applications targeted for the general population include alertness monitoring, telepresence, gaming, education, art, human augmentation [106] biometric identification, virtual reality avatar, assistive robotics and education. Novel niches where this new communication channel can be useful are found routinely [65]. In spite of all this hype [2], there is still a long way ahead. This area advanced rapidly but the complexity of brain signals in all their forms is still a big problem to tackle.

Electroencephalography (EEG) is the most widespread device to capture electrical brain information in a non-invasive and portable way, and it is the most used device in BCI research and applications. The clinical and historical tactic to analyze EEG signals were based on detecting visual patterns out of the EEG trace or polygraph[39]: multichannel signals were extracted and continuously plotted over a piece of paper. Electroencephalographers or Electroencephalography technician have decoded and detected patterns along the signals by visually inspecting them [85]. Nowadays clinical EEG still entails a visually interpreted test [39].

In contrast, automatic processing, or quantitative EEG, was based first on analog electronic devices and later on computerized digital processing methods [46]. They implemented mathematically and algorithmically complex procedures to decode the information with good results [106]. The best materialization of the automatic processing of EEG signals rests precisely in the BCI discipline, where around 71.2% is based on noninvasive EEG [35].

Hence, the traditional strategy of analyzing the electroencephalography by signal shapes on plots, was mainly overshadow in BCI research, and the waveform of the EEG was replaced by procedures that were difficult to link to existing clinical EEG knowledge.

On the other hand, the Histogram of Gradient Orientations is a method from Computer Vision useful to image recognition that aims to mimetically reproduce how the Visual Cortex

discriminate shapes.

This thesis tries to unravel the following question: is it possible to analyze and discriminate Electroencephalographic signals by automatic processing the shape of the waveforms using the Histogram of Gradient Orientations ?

To do that, I humbly ask the reader to join me in this brief journey: Chapter 1 gives details of what is Brain Computer Interfaces and the particularities of the first window of the electric mind: the EEG. It also covers the state of the art in the methods that explore the waveform automatically. The Chapter 2 provides an overview on the procedure to construct a plot representing the signal. Chapter 3 is the core of this thesis and describes the Histogram of Gradient Orientations and how it can be used to process one-dimensional signals. Next, results and experimental procedures are described for the experimented EEG signals and BCI paradigms: Alpha Waves are covered in Chapter 4 and Motor Imagery in Chapter 5. The P300 Wave is studied in Chapter 6. Future Work and Conclusions are addressed in 7. Finally, appendixes provide extra additional information regarding the state-of-the-art of this discipline in Argentina, and also outlines particularities of the SIFT method and the theory behind the Histogram of Gradient Orientations of Signal Plots.

## 0.1 Significance

This thesis propose

- A procedure to construct analyzable 2D-images based on one-dimensional signals.
- A mapping procedure to link time-series characteristics based on feature of the 2D-image representation.
- A feature extraction method for EEG signals that can be used objectively to construct a representation of the waveform.
- A classification algorithm that can be used effectively with these features.

## 0.2 Summary

- What is this all about?: a method to analyze EEG signals based on extracting local feature from their 2D image representation.
- What you won't find in this thesis?: yet another description of BCI.

- What you will find in this thesis?: a point of view that emphasizes the importance of providing mechanisms that help to understand signals based on how they look like on plots.
- Does it work?: It works when the waveform contains the discriminative information. If a person is able to discriminate the signals, this method would also do that.
- Can I use it?: Yes you can. The software to use it is open-source and you can use out-of-the-box. It is particular useful when you need to have an explanation of the classification procedure.
- Why I do not use something else?: If you need to emphasize the shape of the waveform, this is what you are looking for.

# Chapter 1

## The Brain, The Computer and The Interface

Deus ex machina!

---

Aeschylus

With Vidal's work in 1970s, Brain-Computer Interfaces started as a technological amusement, and it steadily moved toward a mature and highly researched area of work. Outstanding success has been achieved with invasive BCI, i.e. with surgically implanted electrodes. Success stories have been made public like Braingate's implant on Jan Scheuermann, Cathy Hutchinson and Dennis Degray [71]. Other works include the total reproduction of arm movement [40], the restoration of reaching and grasping movements through a brain-controlled muscle stimulation device on a person with tetraplegia [3] and the remote control of a manipulator by a macaque using brainwave information [101] albeit of persistent biocompatibility issues and the pervasive complexity and risks of surgical procedures. One noteworthy aspect of this novel communication channel is the ability to transmit information from the Central Nervous System (CNS) to a computer device and from there use that information to control a wheelchair [15], as input to a speller application [36], in a Virtual Reality environment [58] or as aiding tool in a rehabilitation procedure [50]. Other novel applications include the real-time control of flight simulators [68] and the implementation of neuroadaptive interfaces where the computer detects the correctness of a given command based on brainwave analysis [108].

Overall, the holly grail of BCI is to implement a new complete and alternative pathway to restore lost locomotion [102].

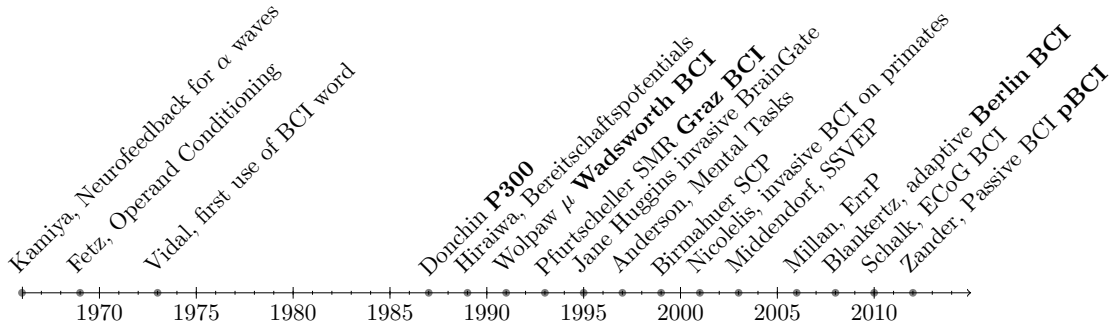


Figure 1 shows a brief chronology of the main events in BCI history, starting from the early works on Neurofeedback in the 70s and walking through the different paradigms. In recent years, this discipline has gained mainstream public awareness with worldwide challenge competitions like Cybathlon [81, 69] and even been broadcasted during the inauguration ceremony of the 2014 Soccer World Cup. New developments are approaching the out-of-the-lab high-bar and they are starting to be used in real world environments [35, 42]. Moreover, BCI research had rampantly been advanced accomplishing a BCI Society, a BCI Journal, BCI Award, annual conference meetings, practical applications, myriads of startups companies and even included in the Gartner list of Hype technologies [2].

From its root as assistive technology it has now expanded to include several application niches like Temporal induced disability, Neuroergonomics, early detection of human error, affective computing, biometric authentication, telepresence (improvement of haptic interface), cyberinfrastructure and assistive robotics. Intensive care units (ICU) and disorders of consciousness (DoC) [6] (detection of remaining brain activity in comatose patients) are recent disciplines where BCI is showing tremendous prospects and possible applications.

Their adoption as a clinical tool is still years ahead. Stroke Rehabilitation is the only area where clinical trials for BCI are being conducted. It is understood that the neurofeedback provided by a BCI interface improves the prognosis of motor rehabilitation [5].

### BCI Definition (circa 2018)

**Definition 1.0.1.** *A system that measures central nervous system activity and converts it into artificial output that replaces, restores, enhances, supplements, or improves natural CNS output and thereby changes the ongoing interactions between the CNS and its external and internal environment [102].*

Despite all this, its primary objective, its core motive of moving into real applications for disabled people has yet to come [13, 49, 1]. They still lack the necessary robustness, and

its performance is well behind any other method of human computer interaction, including any kind of detection of residual muscular movement [20]. Among the many and current challenges of BCI [13] one which is still perennial is precisely their inability to be used and applied outside the BNCI community and specifically in clinical context.

Quoting experts in the field,

*"We yet have an impractical and inaccessible exotica for very specific user groups"*  
(Allison 2010)

*"Effectiveness of non-invasive BCI systems remain limited..." (Wolpaw 2011)*

*"...to ponder if BCIs are really promising and helpful, or if they are simple a passing rod, reinforced by their sci-fi side..." (Lotte 2016)*

The feasibility of the system has been proved but there are several challenges in BCI that need to be tackled. They can be summarizing as increasing the ITR, the pervasive low signal-to-noise ratio of brainwaves, particularly of noninvasive signals [56], the reliability of the system, its portability, and the usability of the system [99], and at the same time decreasing the setup, the training and calibration time and the subject's inter/intra variability. The search for practical, relevant, and invariant *features* that convey good-enough information about the underlying cognitive process is still a goal to be achieved [73]. Ethical aspects of BCI [106] must also be considered and handled: cybersecurity threats and privacy concerns, agency and identity issues that might be occurring by deleterious plasticity with BCI users and the strict peg to the *Primum non vocere*<sup>1</sup> mandate.

## 1.1 Brain Computer Interface Model and Architecture

The draft architecture of a BCI system can be summarized in Fig 1.1. A volitional control, a will to transmit information, is exerted by a user. A brain imaging device captures his/her signals using a measurement modality. A signal acquisition module obtains the brainwaves and the information is digitalized and transmitted to a computer device. Signal preprocessing is applied to eliminate nuisances and artifacts and to enhance the Signal to Noise Ratio (SNR), or to apply spatial or frequency filters. In the next step, a *feature* is carefully constructed in order to differentiate at least between two different mental states. Finally a classification step is applied to derive the actual information bit out of the system.

---

<sup>1</sup>*First, do not harm*, in reference to the Hippocratic Oath

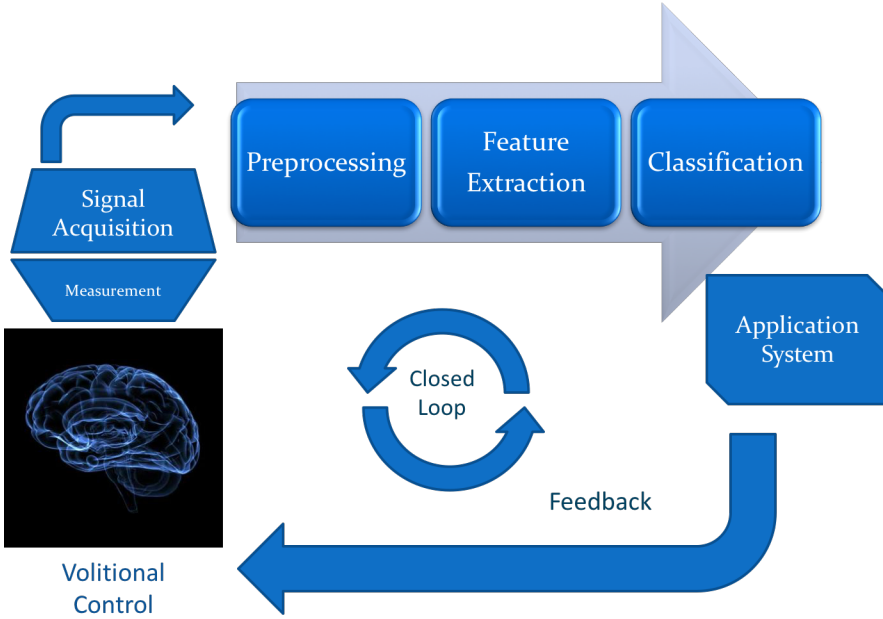


Figure 1.1: General components of a BCI system.

An Application System uses this information to affect some external device. By visual or any other sensory means, the feedback is fed back to the user and a loop is finally closed.

The central point of this system is called the *Brain Machine Dilemma* [102]. The underlying idea is that the BCI system adapts to the user's thinking patterns but at the same time the brain is adapting to what the system is doing, and changing their own signals in the process. This is the reason why it is often called, a *co-adaptive system*, where two different intelligent devices, one biological and the other electronic, try to adapt to each other.

The basic model of any BCI is to take a multichannel digital signal  $\mathbf{x}(n)$ , and transform it to an output control signal  $y(n)$  which can be a scalar or binary function. The BCI system can be modeled as the transformation  $T$ .

$$y(n) = T[\mathbf{x}(n)] \quad (1.1)$$

What a BCI system must do, is to take at least a single bit of information out of  $y(n)$  and use that information to derive some action.

## 1.2 Signal Processing

From this signal processing point of view, BCIs are:

- Causal:  $y(n) = f(\mathbf{v}(m))$ , where  $m \leq n$ . The action of a BCI system depends on the history of the captured brainwaves.
- Dynamic:  $y(n) = f(\mathbf{v}(m), \dot{\mathbf{v}}(m), \ddot{\mathbf{v}}(m), \dots)$ . A BCI system is dynamic, where the output function do not depend only on the current value being observed, it does depend on its dynamic interactions.
- Time invariant:  $y(n) = T[\mathbf{v}(n)] \Rightarrow y(n - k) = T[\mathbf{v}(n - k)]$ . The output of a BCI system does not depend on the particular time frame where it is being used. However, Adaptive BCI, which do adapt to the user behavior are in general time variant.
- Nonlinear: a system is linear when  $T[a_1\mathbf{v}(n) + a_2\mathbf{v}(n)] = a_1T[\mathbf{v}(n)] + a_2T[\mathbf{v}(n)]$ . Due to brainwave complexity, BCI systems are not linear.
- Multirate or broadband [?]: The energy of brainwave spectrum is not confined to a certain band, and almost all frequency channels convey some information.

There are several filters that can be applied to the system to eliminate artifacts, enhance the signal, and to ease the detection of the discriminative information.

**Static Filters** like square or logarithmic were traditionally used in analog signal processing and are currently already embedded in the measuring device. Wiener and Kallman Filters are usually applied to invasive techniques [?]. The filter, particularly when it is linear, can be viewed as the matrix  $M$  in:

$$y(n) = MT[\mathbf{x}(n)] \quad (1.2)$$

**Spatial filters** are carefully adapted to the arrangement of sensors around or within the head and they emphasize the spatial structure of the information that is being captured. Derived from neuroscience research, locations on the head are structured according to neuroanatomical planes or axes and normally the brain, or the head, are divided in different anatomical regions (Figure 1.2).

**Spectral Filters**, on the other hand, do consider brainwaves as another digital signal, and they perform different transformations based on the spectral information contained within the signal  $\mathbf{x}(n)$ . They can be combined and aggregated creating *Filter Banks* to enhance signal quality.

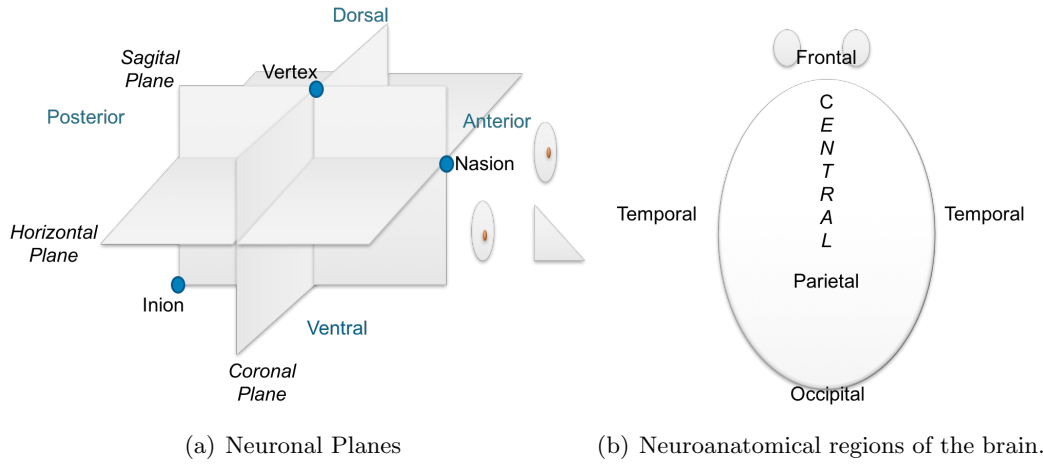


Figure 1.2: Neuronal Planes regularly used in neuroscience research. In BCI they are used to understand electrode location and spatial filters.

### 1.3 The Forward and Inverse Model

Brainwaves are obtained via sensors. Each one of them captures only a part or a version of the information. However, whatever is actually happening inside the brain can be only recovered indirectly from the *Sensor Space*. From there, the information can be traced back to the real landscape where the information source is located, inside the *Source Space*. This is a regular problem found in Engineering and it is not different in BCI. *Calculating* the signal on each a sensor from a projection of a known source of information from within the head is called *The Forward Problem*[72, 102] and doing the opposite, *estimating* the contributions of different sources to whatever activity is found on sensors is called *The Inverse Problem*. The latter is more relevant in BCI because it allows to determine source origins that can be mapped more directly to cognitive activities. However, this kind of problem is highly ill-posed and it is precisely where the majority of the efforts of this discipline are concentrated due to its complexity.

Particularly for noninvasive electrophysiological modalities, an additional problem makes things harder. Due to its electromagnetic properties, the brain acts like conductive gel, and any signal that is generated inside the brain is irradiated to every direction and it can influence every sensor regardless of its position. This is called *Volume conduction* [65, 14] and can be visualized in Figure 1.3.

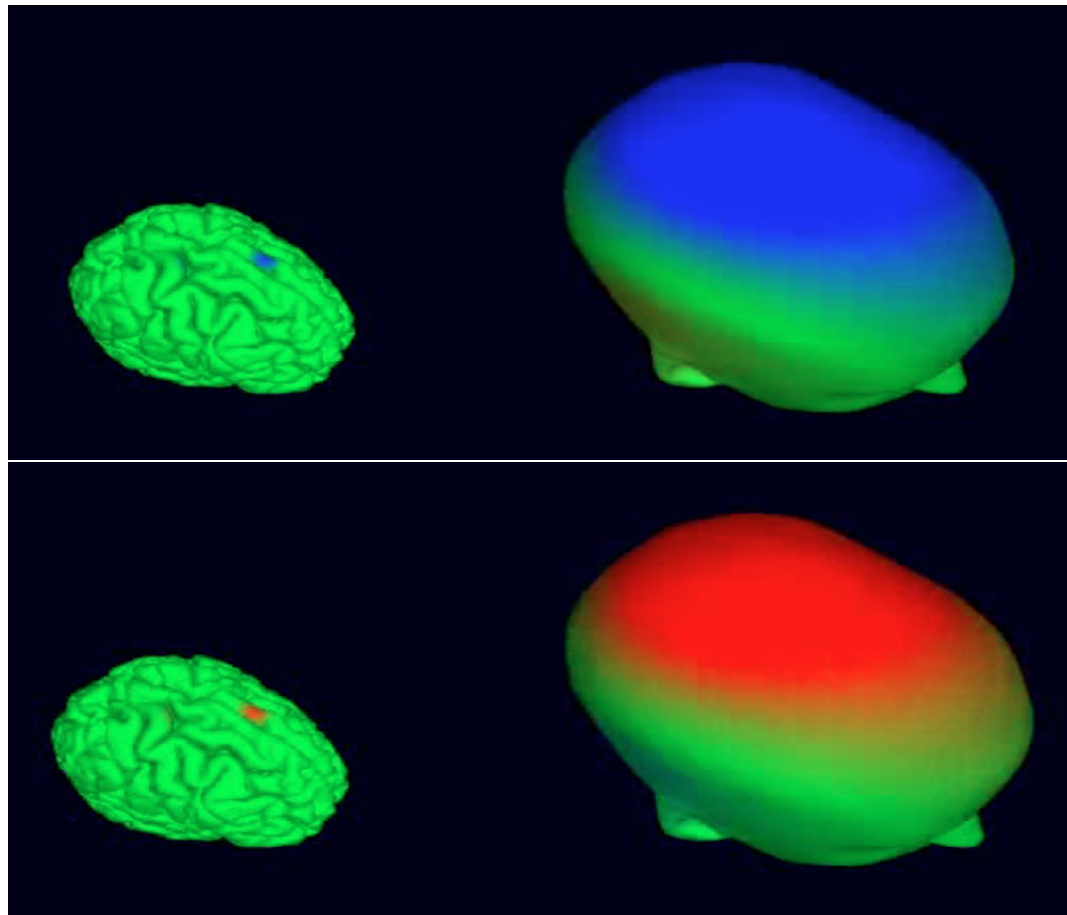


Figure 1.3: A source signal with positive/negative polarity is generated in a very specific region of the brain but due to volume conduction their influence affects a widespread area of the scalp where sensors are located (Image from Swartz Center for Computational Neuroscience)

## 1.4 Brain Imaging Technologies

The measuring technique determines the most important taxonomic differentiation in BCI, according to how they extract the information from the CNS.

1. fNIRS: functional Near Infra Red Spectroscopy.
2. EEG: Electroencephalography
3. MEG: Magnetoencephalography
4. PET: Positron Emission Tomography
5. fMRI: functional Magnetic Resonance Imaging
6. ECoG: Electrocorticography
7. INR: Intracortical Neuron Recordings. Particularly LFP (iEEG, intracranial EEG[14]) and microelectrodes (Utah array).

ECoG and INR are invasive technologies that require some neurosurgery and an implantation of electrodes inside the skull the former, and inside the brain the latter. All the remaining imaging techniques are external or noninvasive. Hybrid BCI, or Brain Neural Computer Interface, are BCI devices that use not only signals from the CNS, they utilize any kind of available biosignal that can be volitionally modulated to transmit information (this is called dependant BCI). On the other hand, when the pace of the BCI is regulated by external stimulus it is called synchronous and when the user choose their own pace to transmit information, it is often called asynchronous or self-paced BCI.

Recent years have seen an incredible advance of Passive BCI, pBCI [107]. The original definition of BCI did not include Passive modalities but per definition 1.0.1 it is now part of this discipline. The important aspect is that passive technologies do not entail necessary the volitional requirement to transmit information. EEG-based passive BCI is a promising and advancing area of research and of commercial applications.

## 1.5 Electroencephalography

Above all, Electroencephalography (EEG), is the most widespread method to gather information from the CNS in a non-invasive way. They are of particular interest in BCI mainly

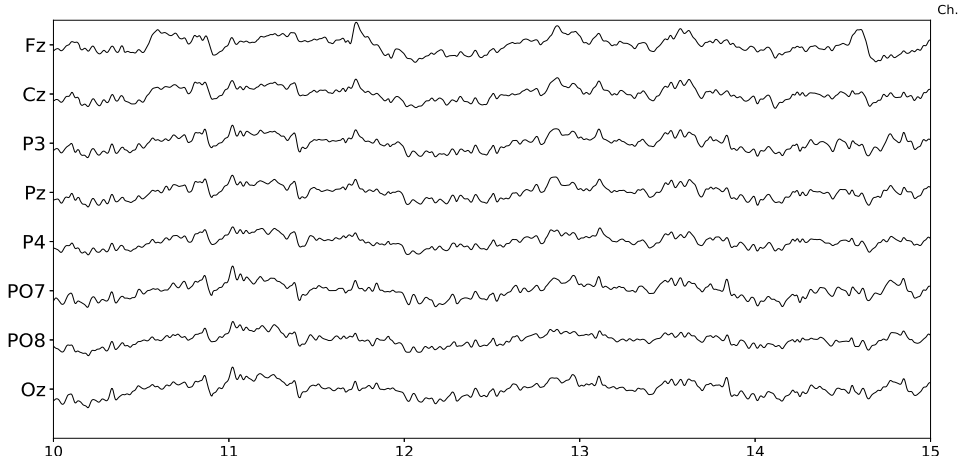


Figure 1.4: Sample EEG signal obtained from (g.Nautilus, g.Tec, Austria). Time axis is in seconds and five seconds are displayed. The eight channels provided by this device are shown.

because of their non-invasiveness, their optimal time resolution and acceptable spatial resolution. Moreover, they are portable, cheap, wearable and can be more easily integrated into fashionable designs aimed for real users, which prefer cap-like devices [43].

The Electroencephalography consists on the measurement of small variations of electrical currents over the scalp. This represents the summed activity of post-synaptic potentials PSPs of pyramidal neurons located perpendicular to the scalp [65]. Only one percent of synchronized activity of pyramidal neurons are stronger than the remaining desynchronized neurons [85] and explain ninety-nine percent of the signals obtained from EEG. This brain imaging technology is one of the most widespread used methods to capture brain signals and was initially developed by Hans Berger in 1924 and has been extensively used for decades to diagnose neural diseases and other medical conditions.

The first characterization that Dr. Berger detected was the Visual Cortical Alpha Wave, the *Berger Rythm* [46]. He understood that the amplitude and shape of this rhythm was coherently associated to a cognitive action (eyes closing). We should ask ourselves if the research advancement that came after that discovery would have happened if it weren't so evident that the shape alteration was due to a very simple and verifiable cognitive process.

The EEG signal is a highly complex multi-channel time-series. It can be modeled as a linear stochastic process with great similarities to noise [90]. It is measured in microvolts, and those slightly variations are contaminated with heavy endogenous artifacts and exogenous spurious signals.

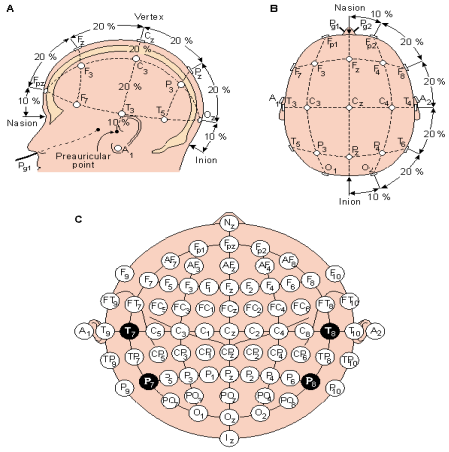


Figure 1.5: International 10-20 system that standardize electrode locations over the scalp.



Figure 1.6: Consumer-grade digital electroencephalograph.

The device that captures these small variations in current potentials over the scalp is called the Electroencephalograph (Figure 1.6). Electrodes are located in predetermined positions over the head, usually embedded in saline solutions to facilitate the electrophysiological interface and are connected to a differential amplifier with a high gain which allowed the measurement of tiny signals. Although initially analog devices were developed and used, nowadays digital versions connected directly to a computer are pervasive. A detailed explanation on the particularities and modeling of EEG can be obtained from [44], and a description of its electrophysiological aspects from [37].

Overall, EEG signals can be described by their phase, amplitude, frequency and *waveform*. The following components regularly characterize EEG signals:

- Artifacts: These are signal sources which are not generated from the CNS, but can be detected from the EEG signal. They are called endogenous or physiological when they are generated from a biological source like muscles, ocular movements, etc., and

exogenous or non-physiological when they have an external electromagnetic source like line induced currents or electromagnetic noise[100]. Ambulatory studies or out-of-the lab studies introduces artifacts that are derived from the person movement from the FES and also from other devices in hybrid BCI, or multi-modal BCIs.

- Non-Stationarity: the statistical parameters that describe the EEG as a random process are not conserved through time, i.e. its mean and variance, and any other higher-order moments are not time-invariant [46].
- DC drift and trending: in EEG jargon, which is derived from concepts of electrical amplifiers theory, Direct Current (DC) refers to very low frequency components of the EEG signal which varies around a common center, usually the zero value. DC drift means that this center value drifts in time. Although sometimes considered as a nuisance that needs to get rid of, it is known that very important cognitive phenomena like Slow Cortical Potentials or Slow Activity Transients in infants do affect the drift and can be used to understand some particular brain functioning [85].
- Basal EEG activity: the EEG is the compound summation of myriads of electrical sources from the CNS. These sources generate a baseline EEG which shows continuous activity with a small or null relation with any concurrent cognitive activity or task.
- Inter-subject and intra-subject variability: EEG can be affected by the person's behavior like sleep hygiene, caffeine intake, smoking habit or alcohol intake previously to the signal measuring procedure [29].

Regarding how the EEG activity can be related to an external stimulus that is affecting the subject, it can be considered as

- Spontaneous: generally treated as noise or basal EEG.
- Evoked: activity that can be detected synchronously after some specific amount of time after the onset of the stimulus. This is usually referred as time-locked. In contrast to the previous one, it is often called Induced activity.

Additionally, according to the existence of a repeated rhythm, the EEG activity can be understood as

- Rhythmic: EEG activity consisting in waves of approximately constant frequency. It is often abbreviated RA (regular rhythmic activity). They are loosely classified by their frequencies, and their naming convention was derived from the original naming used by Hans Berger himself:
  - Alpha Waves (10 Hz)
  - Delta (0-4 Hz)
  - Theta (4-8 Hz)
  - Sigma (12-16 Hz)
  - Beta (12-30 Hz)
  - Gamma (30-100 Hz)
  - Omega (60-120 Hz)
  - Rho (250 Hz) hippocampal
  - Sigma Thalamocortical burst (600 Hz)
- Arrhythmic: EEG activity in which no stable rhythms are present.
- Dysrhythmic: Rhythms and/or patterns of EEG activity that characteristically appear in patient groups and rarely seen in healthy subjects.

The number of electrodes and their positions over the scalp determines a Spatial Structure: signal elements can be generalized, focal or lateralized, depending on in which channel (i.e. electrode) they are found.

## 1.6 BCI EEG Paradigms

*BCI Paradigms* are referred to noninvasive EEG-based BCI configurations that can be used to transmit volitional information. The popularity of EEG (71.2% of the BCI projects submitted to BCI Award 2016 were with EEG) [35] pushed the adoption of paradigms exclusively for noninvasive BCI. Their chronology can be found in Figure 1. They are

1. Steady State Visual Evoked Potentials
2. Bereitschaftspotentials, Readiness Potential or Movement-Related Potentials
3. Motor Imagery

4. ERD/ERS: Event Related
5. Wadsworth BCI
6. Graz BCI
7. Selective Attention
8. P300
9. N400
10. Mental Tasks
11. Operant Conditioning
12. Slow Cortical Potentials
13. Berlin BCI

## 1.7 State of the Art of BCI Algorithms for EEG processing

According to general layout of any BCI, Figure 1.1, specific algorithms or techniques are derived for both the Feature extraction and classification step.

The most relevant features used in BCI are:

- Time points: the sequence of time series, often, concatenated in time or space.
- Band Power: frequency based features.
- Complexity: based on complexity measurements like entropy, fractal.
- Statistical: AR parameters, covariances matrix.

The most successfull used and verified classification methods for BCI [57] can be described as linear versions of popular Machine Learning tools. Particularly, Support Vector Machines SVM, Linear Discriminant Analysis LDA and its variant SWLDA. This one was also relevant for two reasons: the first is that the stepwise identification of features improves the selection criteria and also the spatial filter that this procedure encompass. Additionally, and more from a more pragmatic perspective, this method was included in the popular BCI2000 [84] package and was the default option for anyone doing ERP identification. Spatial Filters have

also being incorporated and have shown substantial improvement in classification accuracies. The now classical Common Spatial Patterns CSP for the identification of Motor Imagery as well as the xDAWN algorithm for P300 identification.

Recent years (circa 2018) have seen the evolution of the methodology but the focus was not centered on any particular classification algorithm. Instead how they are used became much more important [56].

- Ensemble Classifiers: SVM ensembles [75] and variants of Random Forest [88]. Features are segmented and divided and the forest performs a classification step on each part and maximizes classification accuracies.
- Cross-Paradigm BCI: the use of Reinforced Signal RS with ErrP feedback or the use of SSVEP in combination with P300 detection [56].
- Adaptive Classifiers: the parameters of the classifiers are adapted continuously and online adapting to the natural variation of the EEG signals [56].
- Transfer Learning: transfer the calibration information obtained by users to new subjects. This aims to eases the issue of the intra-subject variability in BCI .
- RGC: Riemann Geometry Classifiers
- Tensor-based BCI
- Deep Learning: heavily tried but without significant success.

## 1.8 EEG Waveform Analysis

### 1.8.1 EEG Waveform Characterization

The shape of the signal, the waveform, can be defined as the graphed line that represents the signal's amplitude plotted against time. It can also be called EEG biomarker, EEG pattern, motifs, signal shape, signal form and a morphological signal [46].

The signal context is crucial for waveform characterization, both in a spatial and in a temporal domain [46]. Depending on the context, some specific waveform can be considered as noise while in other cases is precisely the element which has a cognitive functional implication.

A waveform can have a characteristic shape, a rising or falling phase, a pronounced plateau or it may be composed of ripples and wiggles. In order to describe them, they are characterized by its amplitude, the arch, whether they have (non)sinusoidal shape, by the presence of an oscillation or imitating a sawtooth (e.g. Motor Cortical Beta Oscillations). The characterization by their sharpness is also common, particularly in Epilepsy, and they can also be identified by their resemblance to spikes (e.g. Spike-wave discharge).

Other depictions may include, subjective definitions of sharper, arch comb or wicket shape, rectangular, containing a decay phase or voltage rise, peaks and troughs, short term voltage change around each extrema in the raw trace. Derived ratios and indexes can be used as well like peak and trough sharpness ratio, symmetry between rise and decay phase and slope ratio (steepness of the rise period to that of the adjacent decay period). For instance, wording like "Central trough is sharper and more negative than the adjacent troughs" are common in the literature.

Other regular characterizations which are based on shape features may include:

- Attenuation: Also called suppression or depression. Reduction of amplitude of EEG activity resulting from decreased voltage. When activity is attenuated by stimulation, it is said to have been "blocked" or to show "blocking".
- Hypersynchrony: Seen as an increase in voltage and regularity of rhythmic activity, or within the alpha, beta, or theta range. The term suggest an increase in the number of neural elements contributing to the rhythm and a synchronization of neurons with similar firing patterns [14].
- Paroxysmal: Activity that emerges from background with a rapid onset, reaching (usually) quite high voltage and ending with an abrupt return to lower voltage activity.
- Monomorphic: Distinct EEG activity appearing to be composed of one dominant activity
- Polymorphic: distinct EEG activity composed of multiple frequencies that combine to form a complex waveform.
- Transient. An isolated wave or pattern that is distinctly different from background activity.

The traditional clinical approach consists in analyzing the paper strip that is generated by the plot of the signal obtained from the device. Expert technician and physicians

analyze visually the plots looking for specific patterns that may give a hint of the underlying cognitive process or pathology. Atlases and guidelines were created in order to help in the recognition of these complex patterns. Even Video-electroencephalography scalp recordings are routinely used as a diagnostic tools [32]. The clinical EEG research has also focused on temporal waveforms, and a whole branch of electrophenomenology has arisen around EEG *graphoelements* [85].

Sleep Research has been studied in this way by performing Polysomnographic recordings (PSG) [82], where the different sleep stages are evaluated by visually marking waveforms or graphoelements in long-running electroencephalographic recordings, looking for patterns based on standardized guidelines. Visual characterization includes the identification or classification of certain waveform components, or transient events, based on a subjective characterization (e.g. positive or negative peak polarity) or the location within the strip. It is regular to establish an amplitude difference between different waveforms from which a relation between them is established and a structured index are created (e.g. sleep K-Complex is well characterized based on rates between positive vs negative amplitude) [93]. Other relevant EEG patterns for sleep stage scoring are alpha, theta, and delta waves, sleep spindles, polysplindles, vertex sharp waves (VSW), and sawtooth waves (REM Sleep).

Moreover, EEG data acquisition is a key procedure during the assessment of patients with focal Epilepsy for potential seizure surgery, where the source of the seizure activity must be reliably identified. The onset of the Epileptic Seizure is defined as the first electrical change seen in the EEG rhythm which can be visually identified from the context and it is verified against any clinical sign indicating seizure onset. The interictal epileptiform discharges (IEDs) are visually identified from the paper strip, and they are also named according to their shape: spike, spike and wave or sharp-wave discharges[12].

### 1.8.2 EEG Waveform Analysis Algorithms

Shape or waveform analysis methods are considered as nonparametric (in opposition to statistical or dynamical models). They explore signal's time-domain metrics or even derive more complex indexes from it [91].

One of the earliest approach to automatically process EEG data is the Peak Picking method. Although of limited usability, peak picking has been used to determine latency of transient events in EEG [47, 109]. Straightforward in its implementation, it consists in selecting a component, a simple component based on the expected location of its more

prominent deflection [70]. Evoked Potentials (EPs) and Event Related Potentials (ERPs) are transient component that may arise as a brain response to an external visual, tactile or auditory stimulus. Particularly, EPs are regularly used to assess auditory response in infants. ERPs are precisely characterized in this manner, where the name of many of the EEG features evoke directly a peak within the component, e.g. P300 or P3a, P3b or N100. This leads to a natural procedure to classify them visually by selecting appropriate peaks and matching their positions and amplitudes in an orderly manner. The letter provides the polarity (Positive or Negative) and the numbering shows the time referencing the stimulus onset, or the ordinal position of each peak (first, second, etc).

A related method is used in [4] where the area under the curve of the EEG is summarized to derive a feature. This was even used in the seminal work of Farwell and Donchin on P300 [28, 102]. Additionally, a logarithmic graph of the peak-to-peak amplitude which is called amplitude integrated EEG (aEEG) [87] is used nowadays in Neonatal Intensive Care Units.

Other works on EEG explored the idea to extend human capacities analyzing EEG waveforms [30] where a feature from the amplitude and frequency of its signal and its derivative in time-domain is used. Moreover, other works explored the use of Mathematical Morphology [104], where the time-domain structure of contractions and dilations were studied. Finally the proposals of Burch, Fujimori, Uchida and the Period Amplitude Analysis (PAA) [94] algorithm are few of the earliest proposals where the idea of capturing the shape of the signal were established.

*Pursuit* algorithms refer, in their many variants, as blind source separation [98] techniques that assume the EEG signal as a linear combination of different sparse sources extracted from a template's dictionaries. Matching Pursuit *MP* [62], the most representative of this algorithms, is a greedy variant that decomposes a signal into a linear combination of waveforms, called atoms, that are well localized in time and frequency [17]. This method has been used to identify epileptogenetic patterns from EEG traces [95].

Another method that explores the waveform is Bond and Pompe Permutation Entropy [8]. This has been extensively used in EEG processing, with applications on Anesthesia, Sleep Stage evaluation and increasingly for Epilepsy pre-ictal detection . This method generates a code based on the orderly arrangement of sequential samples, and then derives a metric which is based on the number of times each sequence is found on the signal. This numeric value can be calculated as information entropy [66].

A related method is Slope Horizontal Chain Code and Slope Chain Code (SCC) [4]. This algorithm proceeds by generating a coding scheme from a sequence of sample points. This encoding is based on the angle between the horizontal line on a 2D-plane and any segment produced by two consecutive sample points, regarding them as coordinates on that plane. Similar works were provided in Local Binary Patterns (1-D LNBP, 1D-LBP and LBP)[45] algorithms. Finally, the MIDS Merging of Increasing and Decreasing Sequences [110] do not generate a feature but it provides a filter or downsampling scheme which is based on the waveform structure.

Similar to this proposal, all these methods provide a feature that can be used as a template, whereas all of them are based on metrics that can be extracted from the shape of the signal. These features can be used to create dictionaries or template databases. These templates provide the basis for the pattern matching algorithm and offline classification.

Details for these methods are provided in the following sections

### Matching Pursuit - MP 1 and MP 2

*Pursuit* algorithms refer, in their many variants, as blind source separation [98] techniques that assume the EEG signal as a linear combination of different sparse sources extracted from a template's dictionaries. Matching Pursuit *MP* [62], the most representative of these algorithms, is a greedy variant that decomposes a signal into a linear combination of waveforms, called atoms, that are well localized in time and frequency [17]. Given a signal, this optimization technique, tries to find the indexes of  $m$  atoms and their weights (contributions) that minimize,

$$\varepsilon = \left\| x(n) - \sum_{i=1}^m w_i g_i(n) \right\| \quad (1.3)$$

which is the error between the signal and its approximation constructed by the weighted  $w_i$  atoms  $g_i$ , and calculating the euclidean norm  $\|\cdot\|_2$ . The algorithm goes by first setting the approximating signal  $\tilde{x}_0$  as the original signal itself,

$$\tilde{x}_0(n) = x(n) \quad (1.4)$$

and setting the iterative counter  $k$  as 1. Hence, it searches recurrently the best template

out of the dictionary that matches current approximation.

$$g_k = \arg \max_{g_i} \left| \sum_{n=1}^N \tilde{x}_{k-1}(n) g_i(n) \right| \quad (1.5)$$

where  $g_i$  are all the available scaled, translated and modulated atoms from the dictionary. The operation  $|\cdot|$  corresponds to the absolute value of the inner product. This step determines the atom selection process, and their contribution is calculated based on

$$w_k = \frac{\sum_{n=1}^N \tilde{x}_{k-1}(n) g_k(n)}{\|g_k\|^2} \quad (1.6)$$

with  $k$  representing the index of the selected atom  $g_k$  and  $\|\cdot\|$  its euclidean norm. Finally the contribution of each atom is subtracted from the next approximation [22, ?, 62]

$$\tilde{x}_k(n) = \tilde{x}_{k-1}(n) - w_k g_k(n) \quad (1.7)$$

The stopping criteria can be established based on a limiting threshold on Equation 1.3 or based on a predetermined number of steps and selected atoms. Two variants of this algorithm are evaluated. In *MP 1* the dictionary is constructed with the normalized templates directly extracted from the real signal segments which is a straightforward implementation of the pattern matching technique. In *MP 2* the coefficients of Daubechies least-asymmetric wavelet with 2 vanishing moments atoms are used to construct the dictionary [95]. For the first version, the matching against the template is evaluated according to Equation 1.3 directly, whereas for the latter each feature is crafted by decomposing the signal in its coefficients and building, an eventually sparse, vector with them:

$$f = \left\{ w_i \right\}_1^D \quad (1.8)$$

where  $D$  is the size of the dictionary.

### Permutation Entropy - PE

Bond and Pompe Permutation Entropy has been extensively used in EEG processing, with applications on Anesthesia, Sleep Stage evaluation and increasingly for Epilepsy pre-ictal detection [8]. This method generates a code based on the orderly arrangement of sequential samples, and then derives a metric which is based on the number of times each sequence is

found along the signal. This numeric value can be calculated as information entropy [66]. Let's consider a signal on a window of length  $W$  represented by the sample points

$$(x_1, x_2, \dots, x_W) \quad (1.9)$$

and resampled by  $\tau$  intervals, starting from the sampling point  $n$ , doing

$$(x_n, x_{n+\tau}, x_{n+2\tau}, \dots, x_{n+(m-1)\tau}). \quad (1.10)$$

This sequence is of order  $m$ , which is the number of sample points used to derive the ordinal element called  $\pi$ . There are  $m!$  ways in which this sequence can be orderly arranged, according to the position that each sample point holds within the sequence in a strict order relationship. For example if  $m = 3$ , and the first sample point is the bigger, the second is the smaller and the third one is in the middle, the ordinal element  $\pi$  corresponds to  $(3, 1, 2)$ . Thus, along the signal window there can be at most  $k$  different ordinal (and overlapping) elements  $\pi_s$

$$(\pi_1, \pi_2, \dots, \pi_k) \quad (1.11)$$

with  $k = W - (m - 1)\tau$ . The probability density function  $pdf$  for all the available permutations of order  $m$  should be  $\mathbf{p} = (p_1, p_2, \dots, p_m)$  with  $\sum_{i=1}^{m!} p_i = 1$ .

Hence, the time series window is mapped to a new set of  $k$  ordinal elements, and the  $pdf$  can be calculated by the empirical permutation entropy,

$$p_i = \frac{1}{k} \sum_{s=1}^k [\pi_s = \pi_i] \quad (1.12)$$

with  $1 \leq i \leq m!$ . The Iverson Bracket  $[\cdot]$  resolves to 1 when their logical proposition argument is true, 0 otherwise. Therefore, for each  $i$  only those ordinal elements  $\pi_s$  that were effectively found along the signal are counted to estimate  $p_i$ , and zero elsewhere. The empirical permutation entropy can be calculated from the histogram as,

$$H(\mathbf{p}) = \sum_{i=1}^{m!} p_i \log \frac{1}{p_i}. \quad (1.13)$$

The implemented code was derived from [?], and the model description from [9]. This procedure produces a scalar number for the given signal window of size  $W$ . To derive a

feature, a sliding window procedure must be implemented to cover an entire segment of length  $N$ . Thus, the length of the feature is  $N - (W + \tau(m - 1))$ .

$$f = \left\{ H(\mathbf{p})_u \right\}_{W+\tau m}^N. \quad (1.14)$$

with  $u$  varying on a sample by sample basis along the signal, starting from the specified index.

### Slope Horizontal Chain Code - SHCC

This algorithm [4] proceeds by generating a coding scheme from a sequence of sample points. This encoding is based on the angle between the horizontal line on a 2D-plane and any segment produced by two consecutive sample points, regarding them as coordinates on that plane.

A signal of length  $N$ , can be represented by a list of ordered-pairs  $e$ ,

$$e = [(x, y)_1, (x, y)_2, \dots, (x, y)_N] \quad (1.15)$$

and it can be divided into  $G$  different blocks. These blocks are obtained by resampling the original signal from the index

$$G = \lfloor n + (m\Delta) + 0.5 \rfloor \quad (1.16)$$

with  $n$  being the original sampling index on  $1 \leq n \leq N$  and  $\lfloor \cdot \rfloor$  being the floor operation, i.e. rounding of the number argument to the closest smaller integer number. On the other hand,  $\Delta$  can be obtained by

$$\Delta = \left\lceil \frac{N}{G+1} \right\rceil \quad (1.17)$$

with  $G < N$  and using instead  $\lceil \cdot \rceil$  as the ceil operation, the rounding to the closest bigger integer number. Lastly, the value  $m$  can be derived from

$$m = sign\left(\frac{N-1}{\Delta}\right) \left\lfloor \left| \frac{N-1}{\Delta} \right| \right\rfloor. \quad (1.18)$$

This resampling produces a new sequence of values,

$$e' = [(x', y')_1, \dots, (x', y')_s, \dots, (x', y')_G]. \quad (1.19)$$

The next step is the normalization of each ordered-pair as vectors  $\mathbf{x}' = (x'_1, \dots, x'_G)$  and  $\mathbf{y}' = (y'_1, \dots, y'_G)$  according to

$$\hat{\mathbf{x}} = \frac{\mathbf{x}' - \min(\mathbf{x}')\mathbf{1}}{\max(\mathbf{x}') - \min(\mathbf{x}')} \quad (1.20)$$

$$\hat{\mathbf{y}} = \frac{\mathbf{y}' - \min(\mathbf{y}')\mathbf{1}}{\max(\mathbf{y}') - \min(\mathbf{y}')} \quad (1.21)$$

with  $\mathbf{1}$  being the vector of length  $G$  with all their components equal to 1. Hence, the scalar components  $\hat{x}_s$  of  $\hat{\mathbf{x}}$ , and  $\hat{y}_s$  of  $\hat{\mathbf{y}}$ , with  $s$  varying between 1 and  $G$  are effectively normalized to  $\hat{x}_s, \hat{y}_s \in [0, 1]$ .

Finally, the feature is constructed by calculating the point-to-point slope against the horizontal plane,

$$f = \left\{ \frac{\hat{y}_s - \hat{y}_{s-1}}{\hat{x}_s - \hat{x}_{s-1}} \right\}_2^G \quad (1.22)$$

# Chapter 2

## From signals to images

A regular practice in image processing is to analyze images as bidimensional signals. In this Thesis the opposite is done and signals are studied by how they are represented on images. This chapter describes the procedure to plot an image from the digital EEG signal. This image is used to extract a feature which represents the waveform, the structure of the signal on a plot. By analyzing this feature, we hypothesize that the underlying cognitive process can be detected and it can be used to implement a brain-computer communication device.

### 2.1 Electroencephalographic Plotting

The plotting of the EEG is intrinsically mixed with the nuisances of the electroencephalography itself. Plotting proceed by using a chart recorded with a single pen [48]. Voltages are represented on a vertical axis while time is represented on the horizontal axis, in a Cartesian arrangement. The most salient characteristics of a plot are:

1. Sensitivity: also termed gain due the amplification procedure. Its units are  $\frac{mV}{mm}$ . In the digital form, it is  $\frac{\mu V}{pixel}$ .
2. Epoch/Paper speed: the time span that is represented in a single screen. For paper strips it is usually  $10s$ . In its digital counterpart is  $\frac{w}{pixel}$  with  $w$  being the length in milliseconds of the signal segment.

Additionally, on analog plotting montage is essential, though digital plotting allows flexible montage configuration from software. Montage can be monopolar or bipolar. On monopolar montages each electrode obtains the potential difference against a common reference. With bipolar montages, electrodes are paired, eventually in chained configurations, and the potential difference is obtained between each pair of electrodes [12].

## Neuroimaging

With the advent of digital computers and the digital revolution, plotting has become imaging. Neuroimaging [31] means mapping activity or structure to neuroanatomical regions.

There are currently three categories of neuroimaging: *structural* which includes CT (Computed Tomography), MRI (Magnetic Resonance Imaging) and DTI (Diffusion Tensor Imaging), *functional*, which encompass EEG, MEG (Magnetoencephalography), fMRI (functional MRI) PET (Positron Emission Tomography), SPECT (Single Positron Emission Computed Tomography), NIRS (Near-Infrared Spectroscopy) and *chemical* which involves special dyes which are sensible to neuron firing.

## 2.2 Signal to Image transformation

The EEG signal is represented by

$$x(n, c) \quad (2.1)$$

where  $n$  are sample points digitalized at sampling frequency  $F_s$ . This is a multichannel signal, for  $c$  varying between  $1 \leq c \leq C$ . Each one of this channels is assigned a name according to the 10-20 international system, and there are  $C$  available channels. The sample index  $n$  varies between 1 and  $N$ . The span of the signal  $\lambda$  is the length in milliseconds of the waveform under study.

The length of segment  $N$  in sample units, the sampling frequency  $F_s$  in Hz and the segment length  $w$  in ms are related by

$$N = \lfloor F_s w \rfloor. \quad (2.2)$$

To extract features from an image, it should be first constructed. The straightforward way to do it, replicating the analog or digital EEG plotting, is to draw a line on a contrast background. This line represents the voltage amplitude of a channel  $c$  in relation to a reference zero-level  $z(c)$ , with a positive deflection going upwards and downwards for negative deflection. Figure 2.1 shows an example of an EEG signal segment plot. This image is a black-and-white binary image. The color selection is arbitrary (white for the line, black for the background), but it has some implications in terms of the feature extraction procedure that will be described in Chapter 2.



Figure 2.1: Sample EEG signal plot. For this sample image, the length of the signal is 1s, which is 250 sample points. The height of the image is 73 pixels, which is the peak-to-peak amplitude of the signal segment. Channel Oz of baseline EEG activity is being shown.

This chapter mostly deal with the coordinates transformation that need to be enforced while converting the signal into a plot. Figure 2.2 shows the image coordinate system where the  $(z_1, z_2)$  represents the horizontal and vertical location, and the  $(0, 0)$  value is the upper-left position of the image.

In order to convert the EEG original signal  $x(n, c)$  into an image  $I(z_1, z_2)$ , the following six alternatives can be used.

1. Channel-by-channel binary image

The standard plotting, on a black-and-white image with lines representing voltage amplitude.

$$I^{(c)}(z_1, z_2) = \begin{cases} 255 & \text{if } z_1 = n; z_2 = x(n, c) + z(c) \\ 0 & \text{otherwise} \end{cases} \quad (2.3)$$

2. Channel-by-channel greyscale image

The voltage amplitudes are represented in greyscale, that could range between 0 and 255. The function  $\phi(\cdot)$  is a bounded linear mapping between  $[0, 255]$

$$I^{(c)}(z_1, z_2) = \begin{cases} \phi(x(n, c)) & \text{if } z_1 = n; z_2 = z(c) \\ 0 & \text{otherwise} \end{cases} \quad (2.4)$$

3. Multichannel full greyscale image

The image is greyscale. Voltage amplitudes are represented by the pixel content and each channel is represented on the vertical axis. The height of the signal is equal to

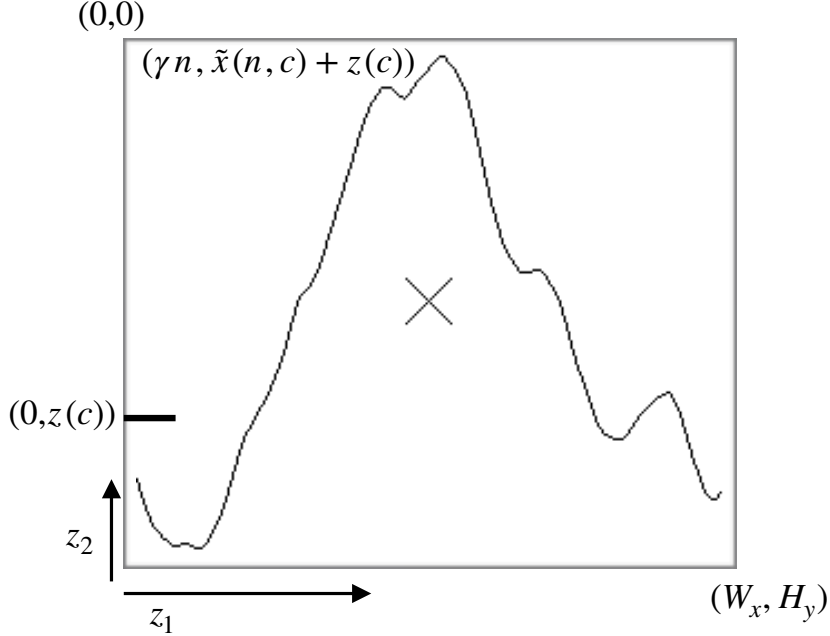


Figure 2.2: The image coordinate system and the mapping from the signal segment. The origin is the  $(0, 0)$  position at the upper-left corner of the image. Time is represented as sample points on the horizontal axis, and the amplitude in  $\mu V$  is shown on the vertical axis. Image height  $H_y$  and width  $W_x$  are obtained based on signal parameters. The signal's zero-level  $z(c)$  is the vertical location where the signal zero value is located. The plot of the signal is obtained by first setting the sample points on the predetermined image locations according to equation 2.9 and then applying a discrete interpolation algorithm to connect them with straight lines.

the number of channels. This is used in Neuroimaging plots of ERP events.

$$I(z_1, z_2) = \begin{cases} \phi(x(n, c)) & \text{if } z_1 = n; z_2 = c \\ 0 & \text{otherwise} \end{cases} \quad (2.5)$$

#### 4. Multichannel stationary binary image

The horizontal axis of the image is not time, but it is channels instead. In this representation different contributions from different channels can be explored at the same time, but time dynamics is lost.

$$I^{(n)}(z_1, z_2) = \begin{cases} 255 & \text{if } z_1 = c; z_2 = x(n, c) + z(n) \\ 0 & \text{otherwise} \end{cases} \quad (2.6)$$

### 5. Multichannel stationary greyscale image

This is a variant of the previous one, where the horizontal axis also represent the channel. In this form, the intensity of the contribution of each channel is represented by the greyscale pixel value. Combined with head models and forward projection solutions this is the methodology used to represent scalp heatmaps [34].

$$I^{(n)}(z_1, z_2) = \begin{cases} \phi(x(n, c)) & \text{if } z_1 = c; z_2 = z(n) \\ 0 & \text{otherwise} \end{cases} \quad (2.7)$$

### 6. Channel by channel full greyscale image

This is similar to a raster plot [22] but the greyscale image representing voltages in pixel intensities can be replicated or epoched  $H$  times, which at the same time is the height of the image. The selection of this value depends on the number of epochs or repetitions to show. In this case, the mapping is

$$I^{(c)}(z_1, z_2) = \begin{cases} \phi(x(n, c)) & \text{if } z_1 = n; z_2 = H \\ 0 & \text{otherwise} \end{cases} \quad (2.8)$$

## 2.3 EEG Signal Plot

A binary image  $\mathcal{I}^{(c)}$  can be constructed from a variant of the method specified in 2.3 according to

$$\mathcal{I}^{(c)}(z_1, z_2) = \begin{cases} 255 & \text{if } z_1 = \gamma_t n; z_2 = \lfloor \gamma \tilde{x}(n, c) \rceil + z(c) \\ 0 & \text{otherwise} \end{cases} \quad (2.9)$$

with 255 being white and representing the signal's voltage in relation to the zero-level  $z(c)$ , and 0 for black which is the background contrast. This scheme produces a black-and-white plot of the signal. Pixel arguments  $(z_1, z_2) \in \mathbb{N} \times \mathbb{N}$  iterate over the width  $W_x$  and height  $H_y$  of the image plot with  $1 \leq n \leq N$  and  $1 \leq c \leq C$ . There is one image per channel. The parameters  $\gamma$  and  $\gamma_t$  are the amplitude and time scaling factors. They are used to determine the image size and at the same time the image resolution.

To analyze effectively an EEG signal, many signal segments must be produced. Hence, the transformation from signal to image is continuously repeated, and many images need to be crafted for the EEG signal under analysis. How to determine the size of all the images so that they can be effectively compared between them ? The first option is to regularize the

signal and fit in an equal size for every image. An alternative choice is to autoscale every image according to the zero-level position. Figure 2.3 shows two sample artificial impulse signals and their alternative transformation into images.

### 2.3.1 Standardized plotting

The *z-score* is a widely used method to regularize a signal [110].

This standardization procedure is defined for  $1 \leq n \leq N$  and  $1 \leq c \leq C$  by doing

$$\tilde{x}(n, c) = \frac{x(n, c) - \bar{x}(c)}{\hat{\sigma}(c)} \quad (2.10)$$

where  $x(n, c)$  is the multichannel EEG signal segment for the sample point  $n$  and for channel  $c$ . The values

$$\bar{x}(c) = \frac{1}{N} \sum_{n=1}^N x(n, c)$$

and

$$\hat{\sigma}(c) = \left\{ \frac{1}{N-1} \sum_{n=1}^N [x(n, c) - \bar{x}(c)]^2 \right\}^{\frac{1}{2}}$$

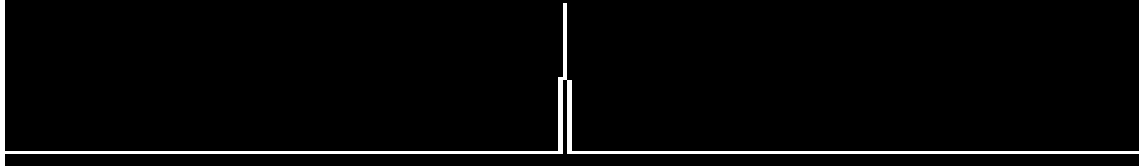
are the mean and estimated standard deviation of  $x(n, c), 1 \leq n \leq N$ , for each channel  $c$ . Figure 2.3(a) shows an impulse signal and their standardized representation.

### 2.3.2 Autoscaled plotting

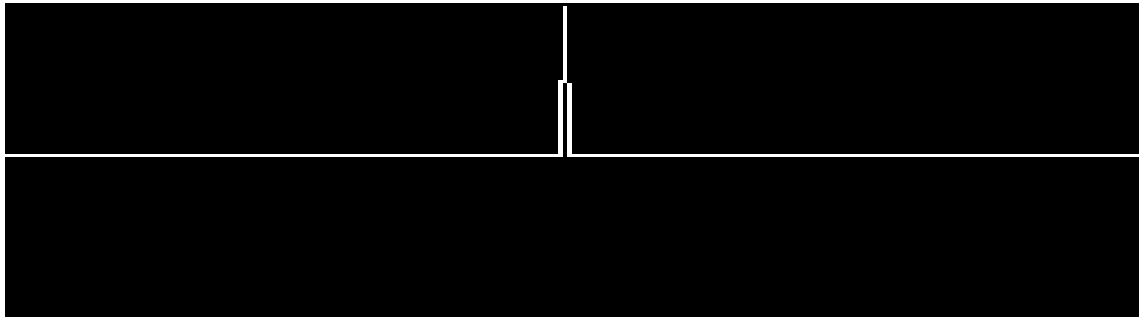
This plotting scheme allows each image to adapt to the underlying signal. The height is set at twice the value of the zero-level, and the signal mean is subtracted from the signal, producing a vertical displacement.

$$\tilde{x}(n, c) = x(n, c) - \bar{x}(c) \quad (2.11)$$

Figure 2.3(b) shows the results of the plotting for an impulse signal. Equation 2.11 has the advantage that any low frequency component, particularly the EEG DC drift is eliminated, due to the fact that plot of the signal is always centered on each image.



(a) An artificial signal pulse and their plotting representation. The signal is standardized and the height of the image is determined according to the peak-to-peak amplitude, which is the same for every image and equal to  $\gamma$ .



(b) The plotted image height is twice the zero-level. In this case, the height is also determined according to the peak-to-peak amplitude of each segment, proportional to  $\gamma$ , and not constant. Transformed images do not have the same height, but the zero-level is always located at half the height of the image.

Figure 2.3: Signal plotting schemes.

### 2.3.3 Zero-Level

The zero-level  $z(c)$  is the image vertical position where the signal's zero value has to be situated in order to fit the entire signal within the image for each channel  $c$ :

$$z(c) = \left\lfloor \frac{\max_n \tilde{x}(n, c) - \min_n \tilde{x}(n, c)}{2} \right\rfloor - \left\lfloor \frac{\max_n \tilde{x}(n, c) + \min_n \tilde{x}(n, c)}{2} \right\rfloor \quad (2.12)$$

where the minimization and maximization are carried out for  $n$  varying between  $1 \leq n \leq N$ , and  $\lfloor \cdot \rfloor$  denote the rounding to the smaller nearest integer of the number. This value represents the vertical location on the image where the signal goes to zero.

### 2.3.4 Image Size

#### Height

The height of the image is calculated according to the peak-to-peak amplitude of the signal,

$$H_y = \max [\gamma \tilde{x}(n, c)] - \min [\gamma \tilde{x}(n, c)] \quad (2.13)$$

while for the autoscalable version, it is just twice the value of the zero-level.

$$H_y = 2 z(c) \quad (2.14)$$

#### Width

The width on the other hand is obtained based on the length of the signal segment, scaled by the  $\gamma_t$  time factor,

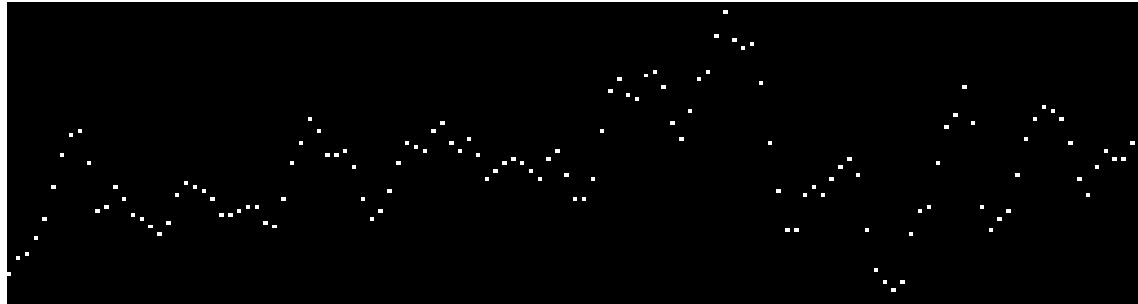
$$W_x = \gamma_t N \quad (2.15)$$

### 2.3.5 Interpolation

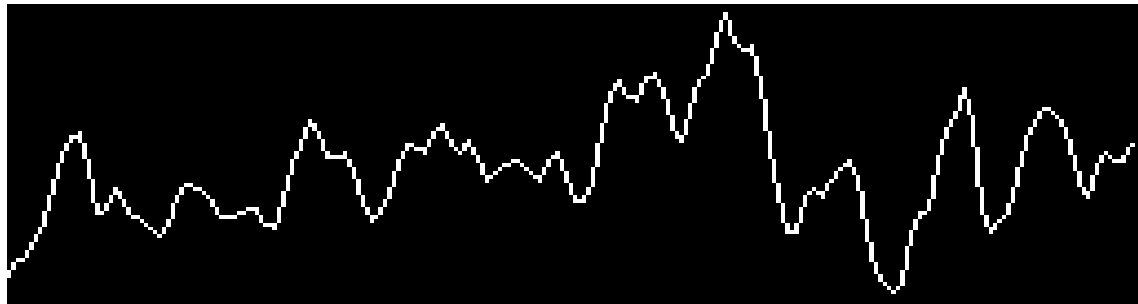
Equation 2.9 produces a set of isolated pixels over the image. To produce the plot  $I^{(c)}$ , the Bresenham [11, 76] algorithm is used to digitally interpolate straight lines between each pair of consecutive pixels. Figure 2.4(a) shows an image plot constructed by only using the sample points, while (b) shows the digital interpolation produced by the Bresenham algorithm.

On Figure 2.4(c) the same signal can be observed produced when the time scaling factor  $\gamma_t$  is increased to 4. It can be observed that there are very sharp edges around sample pixels. This can lead to a quantization of histogram gradients that will be discussed in the next Chapter. To reduce this sharpness of the signal on the plot, an alternative is to use a smoothing interpolation of the signal  $\tilde{x}(n, c)$  using splines. Instead of just situating time point values at a bigger step according to Equation 2.9, intermediate values are produced according to a linear quadratic or cubic interpolation, hence smoothing the curve around each point. This procedure is similar to what the Matlab's **resample** function does which also includes an antialiasing FIR lowpass filter.

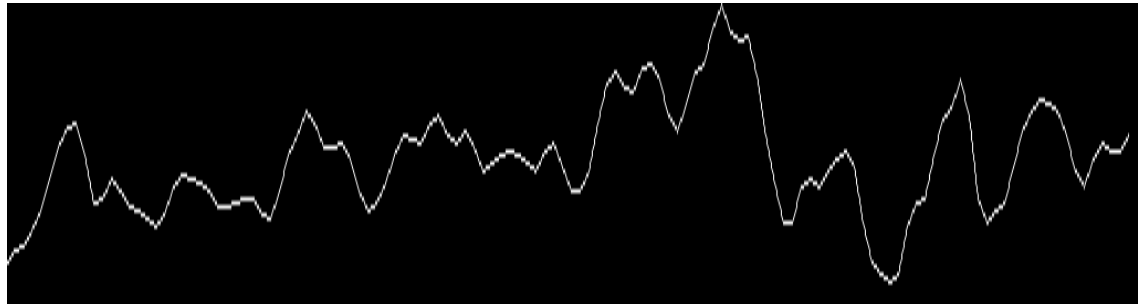
Special care must be taken by the presence of artifacts around the signal endpoints, at the edges of the image. Those regions are excluded from further analysis.



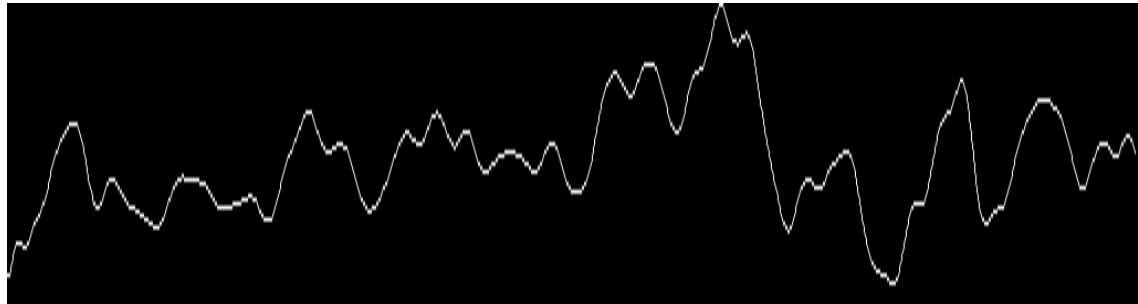
(a) Sample points are located on the image according to Equation 2.9.



(b) Sample points are linearly interpolated in a discrete procedure using the Bresenham algorithm.



(c) The digital signal is scaled 4 times ( $\gamma_t = 4$ ) and the generated sample points are interpolated using the Bresenham algorithm.



(d) The digital signal is upsampled 4 times and the generated sample points are interpolated using the Bresenham algorithm.

Figure 2.4: Generated images based on different interpolation schemes.

### 2.3.6 Resolution and Precision

The resolution [22] of the image transformation can be determined based on the characteristics of the digital signal and the parameter selection.

On the horizontal axis of the image, one pixel is equivalent  $\equiv$  to

$$1P_x \equiv \frac{1}{F_s \gamma_t} [\text{s}] \quad (2.16)$$

where  $F_s$  is the sampling frequency in Hertz, and  $\gamma_t$  is the time scale factor. This gives a value in seconds. For example, for Figure 2.1, the sampling frequency is  $200\text{Hz}$ , the length is  $0.65\text{s}$  and  $\gamma_t = 1$ , which gives a resolution of  $1P_x \equiv 0.0077\text{s}$ .

Consistently, on the vertical axis, one pixel is analogous to

$$1P_y \equiv \frac{1}{\gamma} [\mu\text{V}] \quad (2.17)$$

where  $\gamma$  is the amplitude scale factor. As EEG time-series are digitalized in  $\mu\text{V}$ , this is the unit of choice. In Figure 2.2, 1 vertical pixel represents exactly  $1\mu\text{V}$ .

Regarding the *Precision*, EEG time-series are floating-point numbers and the image is constructed based on discrete and integer pixels. Image's pixel values ( $z_1, z_2$ ) are obtained according to Equation 2.9. Thus, on the horizontal axis,  $z_1$ , no discretization is needed because time is already digitalized in sample units. Hence, there is no loss of precision in time from the one generated by the digital device.

$$z_1 = \gamma_t n. \quad (2.18)$$

On the other hand, on the vertical axis, pixels are discretized according to

$$z_2 = \lfloor \gamma \tilde{x}(n, c) \rfloor \quad (2.19)$$

where  $\gamma$  is the scale amplitude factor parameter, which also affects the height of the image in Equation 2.13. A rounding operation  $\lfloor \cdot \rfloor$  is applied to obtain an integer value. Hence, precision is lost on the voltage amplitude. Additionally, the dynamic range of the digital capturing device is reduced to what is actually needed for each segment. Table 2.1 shows some reference values.

Table 2.1: Reference Values for Precision and Resolution

$\gamma$	$1P_x$	Decimal Precision	$\parallel$	$\gamma_t$	$1P_y$
1	$1\mu V$	$NN$		1	$\frac{1}{F_s} s$
2	$\frac{1}{2}\mu V$	$NN \pm 0.5$		2	$\frac{1}{2} \frac{1}{F_s} s$
3	$\frac{1}{3}\mu V$	$NN \pm 0.3$		3	$\frac{1}{3} \frac{1}{F_s} s$
10	$\frac{1}{10}\mu V$	$NN.N$		10	$\frac{1}{10} \frac{1}{F_s} s$
100	$\frac{1}{100}\mu V$	$NN.NN$		100	$\frac{1}{100} \frac{1}{F_s} s$



# Chapter 3

## The Histogram of Gradient Orientations of Signal Plots

This Chapter presents and introduce the EEG feature extraction procedure based on the Histogram of Gradient Orientations. This method is grounded on an extension and modification of the SIFT [59] Descriptor which is used in Computer Vision to extract and map local regions of an image. At the same time, this Chapter fill in and end the previous Chapter, describing how to mine the information from the Plot and build a feature out of it.

### 3.1 Introduction

The work of Edelman, Intrator and Poggio [27] on how the visual cortex sense features was the inspiration to the development of an algorithm to identify and decode salient local information from image regions. SIFT is composed of two parts, the SIFT Detector and the SIFT Descriptor. The first one is the procedure to identify relevant areas of an image. The second one is the procedure to describe and characterize a region of an image using the Histogram of Gradient Orientations<sup>1</sup>. The SIFT algorithm is biomimetically inspired in how the visual cortex detects shapes by analyzing orientations [27]. The patch description is also based on the Theory of Receptive Fields and other related ideas [54].

---

<sup>1</sup>It should not to be confused with HOG [24], the Histogram Of Gradients which is another method from Computer Vision based on similar ideas. Actually, the descriptor part of the SIFT Method has no specific name, but as it is based on building a histogram of gradient orientations, that is the reason why it is described here in that way.

### 3.2 Feature Extraction: Histogram of Gradient Orientations

On the image generated by the procedure detailed in previous Chapter, a keypoint  $\mathbf{kp}$  is placed on a pixel  $(x_{kp}, y_{kp})$  over the image plot and a window around the keypoint is considered. A local image patch of size  $\mathbf{S}_x \times \mathbf{S}_y$  pixels is constructed by dividing the window in 16 blocks. It is arranged in a  $4 \times 4$  grid and the pixel  $\mathbf{kp}$  is the patch center.

A local representation of the signal shape within the patch can be described by obtaining the gradient orientations on each of the 16 blocks and creating a histogram of gradients. This technique is the basis of Lowe's SIFT Descriptor method. In order to calculate the histogram, the interval  $[0 - 360]$  of possible angles is divided in 8 bins, each one at 45 degrees.

Hence, for each spacial bin  $i, j = \{0, 1, 2, 3\}$ , corresponding to the indexes of each block  $B_{i,j}$ , the orientations are accumulated in a 3-dimensional histogram  $h$  through the following equation:

$$h(\theta, i, j) = \sum_{\mathbf{p}} w_{\text{ang}}(\angle J(\mathbf{p}) - \theta) w_{ij}(\mathbf{p} - \mathbf{kp}) |J(\mathbf{p})| \quad (3.1)$$

where  $\mathbf{p}$  is a pixel from within the patch,  $\theta$  is the angle bin with  $\theta \in \{0, 45, 90, 135, 180, 225, 270, 315\}$ ,  $|J(\mathbf{p})|$  is the norm of the gradient vector in the pixel  $\mathbf{p}$  and it is computed using finite differences and  $\angle J(\mathbf{p})$  is the angle of the gradient vector. The scalar  $w_{\text{ang}}(\cdot)$  and vector  $w_{ij}(\cdot)$  functions are linear interpolations used by [59] and [97] to provide a weighting contribution to eight adjacent bins. They are calculated as

$$w_{ij}(\mathbf{v}) = w\left(\frac{v_x - x_i}{3 \mathbf{S}_x}\right) w\left(\frac{v_y - y_i}{3 \mathbf{S}_y}\right) \quad (3.2)$$

$$w_{\text{ang}}(\alpha) = \sum_k w\left(\frac{8\alpha}{2\pi} + 8r\right) \quad (3.3)$$

where  $x_i$  and  $y_i$  are the spatial bin centers located in  $x_i, y_i = \{-\frac{3}{2}, -\frac{1}{2}, \frac{1}{2}, \frac{3}{2}\}$ . The function parameter  $\mathbf{v} = (v_x, v_y)$  is a vector variable and  $\alpha$  a scalar variable. On the other hand,  $r$  is an integer that can vary freely which allows the argument  $\alpha$  to be unconstrained in terms of its values in radians. The interpolating function  $w(\cdot)$  is defined as:

$$w(z) = \max(0, |z| - 1). \quad (3.4)$$

These binning functions conform a trilinear interpolation that has a combined effect of sharing the contribution of each oriented gradient between their eight adjacent bins in a tridimensional cube in the histogram space, and zero everywhere else.

Lastly, the fixed value of 3 is a magnification factor, a fixed parameter. As the patch has 16 blocks and 8 bin angles are considered, a feature called *descriptor* of 128 dimension is obtained.

Figure 3.1 shows an example of a patch and a scheme of the histogram computation. In (A) a plot of the signal and the patch centered around the keypoint is shown. In (B) the possible orientations on each patch are illustrated. Only the upper-left four blocks are visible. The first eight orientations of the first block, are labeled from 1 to 8 clockwise. The orientations of the second block  $B_{1,2}$  are labeled from 9 to 16. This labeling continues left-to-right, up-down until the eight orientations for all the sixteen blocks are assigned. They form the corresponding **kp**-descriptor of 128 coordinates. Finally, in (C) an enlarged image plot is shown where the oriented gradient vector for each pixel can be seen.

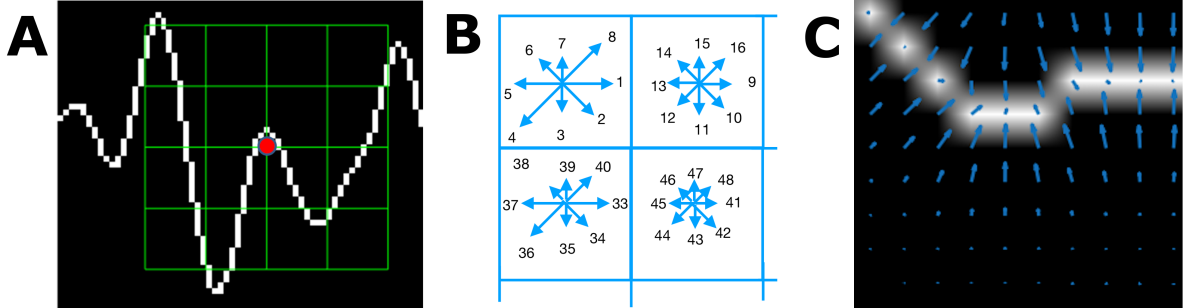


Figure 3.1: (A) Example of a plot of the signal, a keypoint and the corresponding patch. (B) A scheme of the orientation's histogram computation. Only the upper-left four blocks are visible. The first eight orientations of the first block, are labeled from 1 to 8 clockwise. The orientation of the second block  $B_{1,2}$  is labeled from 9 to 16. This labeling continues left-to-right, up-down until the eight orientations for all the sixteen blocks are assigned. They form the corresponding descriptor of 128 coordinates. The length of each arrow represent the value of the histogram on each direction for each block. (C) Vector field of oriented gradients. Each pixel is assigned an orientation and magnitude calculated using finite differences.

### 3.3 Keypoint Location

The keypoint **kp** location must be accurate specified in order to establish the region from the signal where the waveform is located.

For the horizontal position, the localization of the keypoint is based on a priori information, based on the characteristics of the event under study. For instance certain ERP have a specific timing that can be explored to elucidate in which position the expected signal pattern will be generated.

But the main answer to respond is how many descriptors, and this also leads to density of descriptors. How many per pixel or per sample point.

Additionally, there can be more than just one patch located over the signal plot. This is particular important for oscillatory processes and defines a descriptor density parameter  $s_d$ .

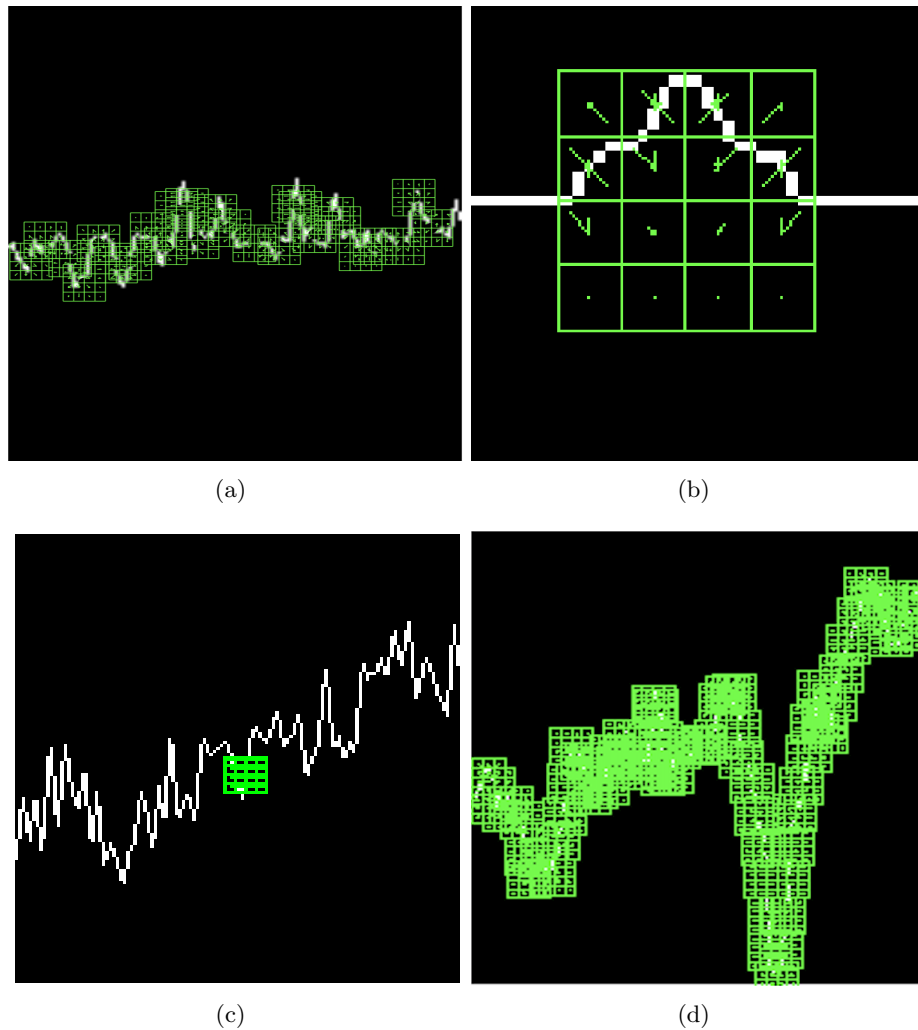


Figure 3.2:

Regarding the Vertical Location, there are two options. The first one is along the signal, exactly on the sample points calculated by the Equation 2.9. The second is on a fixed position over the zero-level as described by 2.12.

### 3.4 Patch Geometry

The Horizontal Patch Scale  $S_t$  determines the size of the patch on the image horizontal axis, and it is related to the span  $\lambda$  of the waveform to analyze according to

$$S_t = \frac{\lambda}{\Delta_s} F_s \gamma_t \quad (3.5)$$

where  $F_s$  is the sample frequency,  $\gamma_t$  is the time scale factor and  $\Delta_s$  is the pixel conversion factor.

On the other hand, on the vertical axis, the vertical patch scale depends on the peak-to-peak amplitude  $\Delta\mu V$ .

$$S_v = \frac{S_t \gamma}{\Delta_s} \quad (3.6)$$

The vertical scale can be dynamically adjusted according to the peak-to-peak amplitude of each segment, or it can be set fixed. This is more appropriate if the underlying signal is bounded which is the case if the standardized procedure described in 2.3.1 is applied.

Figure 3.3 shows the different parameters of the patch.

Once these parameters are set, the size in pixels of the patch can be obtained in both dimensions. The Horizontal Patch Size in pixels is

$$\mathbf{S}_x = \Delta_s S_t + 1. \quad (3.7)$$

The Vertical Patch Size in pixels can be calculated from

$$\mathbf{S}_y = \Delta_s S_v + 1 \quad (3.8)$$

where  $\Delta_s$  is a fixed parameter value which depends on the SIFT implementation. The parameters  $S_t$  and  $S_v$  are the scales of the local patch. This region is arranged in a  $4 \times 4$  grid and the pixel  $\mathbf{kp}$  is the patch center.

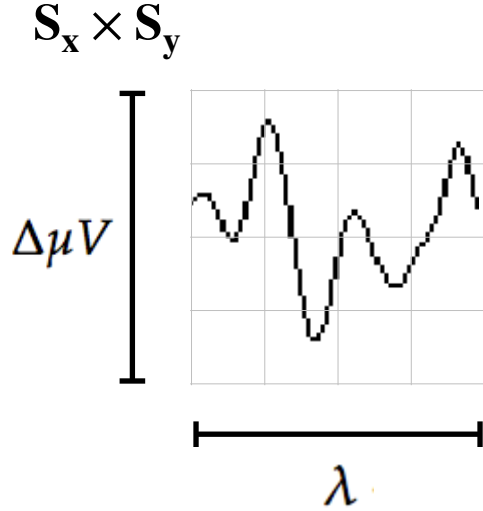


Figure 3.3: The scale of local patch is selected in order to capture the whole transient event. The size of the patch is  $S_y \times S_x$  pixels. The vertical size consists of 4 blocks of size  $S_y$  pixels which should be high enough as to contain the signal  $\Delta\mu V$ , the peak-to-peak amplitude of the signal component. The horizontal size includes 4 blocks up to  $S_x$  and should cover the entire duration in seconds of the signal waveform,  $\lambda$ .

The patch size cannot be bigger than the image. This is reflected by the following two inequalities that restrict the size of the patch according to

$$\frac{W_x - 1}{\Delta_s} \geq S_t \quad (3.9)$$

on the horizontal axis, and on the vertical axis,

$$\frac{H_y - 1}{\Delta_s} \geq S_v. \quad (3.10)$$

### 3.4.1 Oscillatory Processes

For these patterns, the central idea is to locate keypoints, and their patches and descriptors, all along the signal trace and filling the entire signal segments with all the possible descriptors. In this case, the descriptor density determines the step at which a keypoint is located along the trace of the signal, pixel after pixel. Close to the margins, there is a gap to avoid locating incomplete patches. This can be observed in Figure 3.2(a).

### 3.4.2 Transient Events

For transient events, descriptors are treated as representatives of the signals itself so there is just one descriptor that is located in a meaningful position along the time axis.

Additionally, particularly for autoscale plotting, the zero level can be used to localize keypoints.

## 3.5 Classification

A discriminative [102] semi-supervised classification method based on Naive Bayes Nearest Neighbor [10] was applied to classify EEG signals using the features provided by the calculated descriptors. One problem that frequently arises when using local features is how to go back from the classification of those local characteristics to the image where those descriptors came from. The NBNN technique overcomes this problem by comparing each image against a whole class which is characterized by the set of descriptors that are closest to each one of the descriptors of the query image. This algorithm is very easy to implement, and is based on (5).

$$\hat{class} = \arg \min_{class} \sum_{\mathbf{d}_i^{(c)}} \sum_{q \in N_T(\mathbf{d}_i^{(c)})} \|q - \mathbf{d}_i^{(c)}\|^2 \quad (3.11)$$

The estimated class C of a query image is calculated as the class C that minimize the summation of the L2 distance between each descriptor  $\mathbf{d}_i$  that belongs to the query image and its corresponding near neighbor  $NN_c(\mathbf{d}_i)$  descriptor for each class.

In brief, based on segmented signals from at least two labeled classes, a set of images is first generated. For each image, descriptors are extracted during the training or calibration step of a BCI procedure and they are grouped in KD-tree [59] structures for each one of the classes.

Hence, given a new unlabeled signal segment, an image plot is generated as well, and their descriptors extracted. They are fed into Equation 5 in order to determine the class which minimizes the summation and thus provide the information bit to the BCI controller.

## 3.6 BCI Algorithm

In brief, based on segmented signals from at least two labeled classes, a set of images is first generated. For each image, descriptors are extracted during the training or calibration

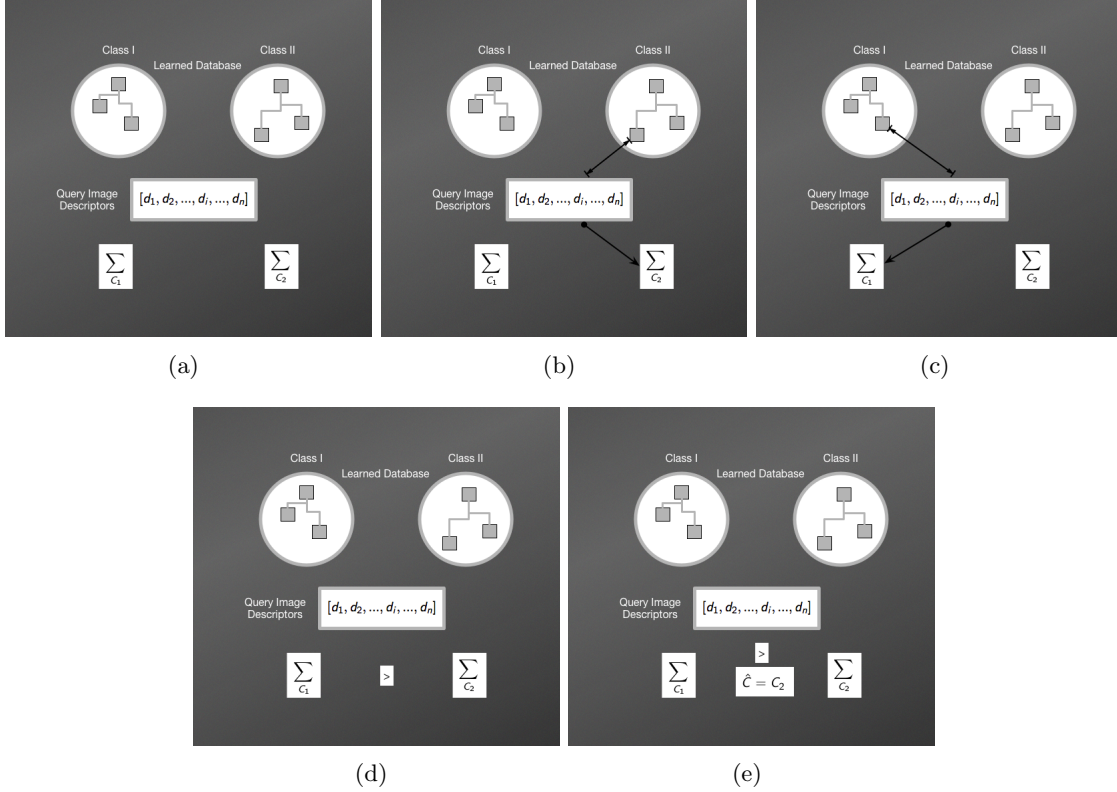


Figure 3.4: (a) Two Dictionaries contain templates descriptors for two different classes. A set of query descriptors are extracted from a new image that needs to be categorized.(b) Distances from every descriptor  $d_i$  is calculated against the closest one from the Dictionary of Class 2. Distances are accumulated.(c) Distances from every descriptor  $d_i$  is calculated against the closest one from the Dictionary of Class 1. Distances are accumulated. (d) The two different values are compared.(e) The summation that achieved the lesser value is the one that more closely resemble the set of templates, thus is the one predicted by the classification algorithm.

step of a BCI procedure and they are grouped in KD-tree [59] structures for each one of the classes.

Hence, given a new unlabeled signal segment, an image plot is generated as well, and their descriptors extracted. They are fed into Equation 5 in order to determine the class which minimizes the summation and thus provide the information bit to the BCI controller.

## 3.7 Implementation

### 3.7.1 Matlab, C++ and VLFeat

The implemented code is published in <https://bitbucket.org/itba/hist/> by using Matlab, python and the VLFeat library.

## 3.8 Mapping Cheat-Sheet

This section provides a mapping cheat sheet to convert and obtain the parameters of the algorithm for a given set of signal parameters.

The input signal parameters are  $N, F_s$  and  $\lambda$ . The peak-to-peak amplitude of the waveform to study is  $\Delta\mu V$ . The unit length of the patch is  $\Delta_s = \sqrt{2} 15$ .

Output parameters are:  $N, \lambda, F_s, \Delta_s, \Delta\mu V, \gamma, \gamma_t, H_y, W_x, S_t, S_v, \mathbf{S}_y, \mathbf{S}_x, w, \mathbf{k}, \mathbf{p}$

Amplitude scale factor

$$\gamma \equiv \frac{H_y}{\Delta\mu V} \quad (3.12)$$

Time scale factor

$$\gamma_t \equiv \frac{W_x}{F_s w} \quad (3.13)$$

Restriction on the waveform time scale

$$\frac{W_x - 1}{\sqrt{2} 15} \geq S_t \quad (3.14)$$

Restriction on the waveform amplitude scale

$$\frac{H_y - 1}{\sqrt{2} 15} \geq S_v \quad (3.15)$$

Horizontal Patch scale

$$S_t = \frac{\lambda F_s \gamma_t}{\Delta_s} \quad (3.16)$$

Vertical Patch scale

$$S_v = \frac{\Delta\mu V \gamma}{\Delta_s} \quad (3.17)$$

Time to sample point conversion

$$n = \lfloor F_s \Delta_t \rfloor \gamma_t \quad (3.18)$$

Horizontal Patch size in pixels

$$\mathbf{S}_x = \Delta_s S_t + 1 \quad (3.19)$$

Vertical Patch Size in pixels

$$\mathbf{S}_y = \Delta_s S_v + 1 \quad (3.20)$$

Span of a Patch

$$\Delta_t = \frac{S_t \Delta_s}{F_s \gamma_t} \quad (3.21)$$

# Chapter 4

## Alpha Wave: inhibition signal

The electroencephalogram represents a continuous curve with continuous oscillations in which... one can distinguish larger first order waves with an average duration of 90 milliseconds...

---

Berger

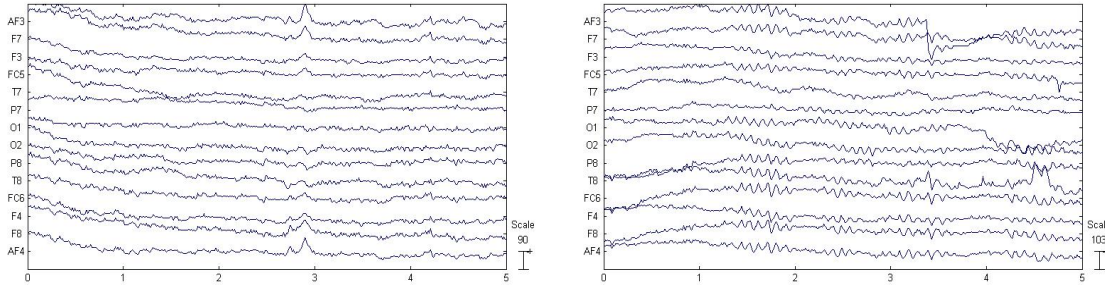
This Chapter describes the experiments performed over a well-established but still mysterious EEG cognitive signal: The Berger Rhythm or Visual Occipital Alpha Waves. An own dataset of resting subjects with and without alpha blocking is produced and the details of their generation are outlined. Additionally, an experiment on a public Dataset is also delineated. Conclusions and discussion are described in the last section.

### 4.1 Introduction

Alpha Waves were the first signals ever spotted from the Electroencephalography. They are regularly characterized as 10Hz, or more broadly between the frequency band of 8-12 Hz. They are physiologically consistent across subjects, though it has been reported inter- and intra- variations with functional cognitive implications [38]. Moreover, they are associated with synchronous inhibitory processes and attention shifting [83]. They tend to be more prominent while subject's eyes are closed and appear stronger in occipital regions, around  $O_1$  and  $O_2$  [103, 89]. These waves are also called Prominent Posterior Alpha or Posterior Dominant Rhythm due to their pervasiveness in EEG [85, 38].

Figure 4.1 shows two records of 8-channels signals. Figure 4.1(a) contains the registered

alpha waves of a subject with their eyes open while the (b) contains the same information with their eyes closed. The characteristic pattern of wiggles can be spotted in the latter, while their absence entails the blocking of alpha waves in the former [7].



(a) EEG signals of a relaxed healthy subject with (b) EEG signals of the same relaxed subject with their eyes closed. Alpha Waves wiggles can be spotted since the first second.

Figure 4.1: Five seconds of EEG signals obtained from the Emotiv EPOC device. Fourteen channels are shown.

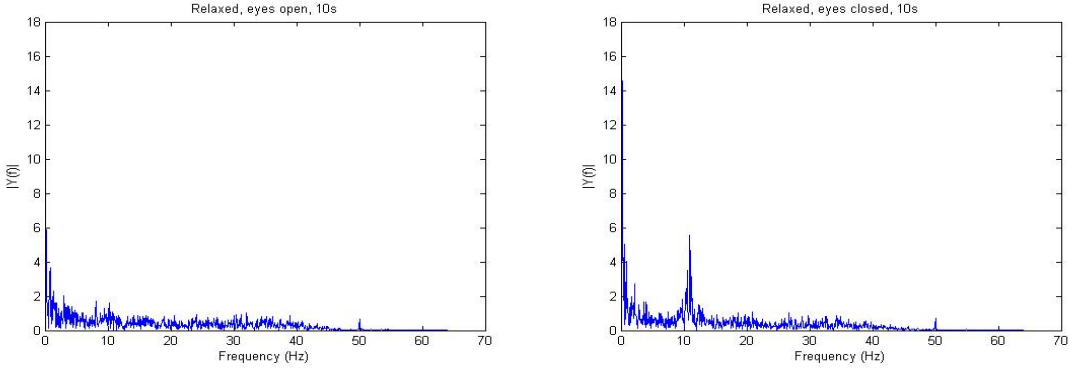
This important rhythm is an oscillatory process. As such, it is understood and studied in the frequency-domain. Figure 4.2 show the results of applying the Fast Fourier Transform to two different segments of 10s length. For each segment, the Power Spectral Density is calculated and their values are shown on the vertical axis. Frequency values are shown on the horizontal axis. On Figure (a) no particular frequency component can be spotted. However, on Figure (b) the prevalence of the 10-Hz alpha wave component can be observed.

## 4.2 Materials and Methods

These experiments consist in performing a binary classification of EEG signal segments between the two defined classes. Class 2 is assigned to segments containing significant alpha waves (i.e. eyes closed), whereas class 1 identifies those where these signals are blocked (i.e. eyes open).

### 4.2.1 Dataset I - Emotiv EPOC alpha waves own dataset

The first dataset is gathered using the EEG EPOC Emotiv Headset. Although this is a commercial-grade device, it provides an acceptable price-performance ratio and it has been used to investigate basic EEG processes [26, 25]. In order to obtain the multichannel raw



(a) Subject was sit, relaxed in front of the Computer Monitor with his eyes open. (b) Subject was sit, relaxed in front of the Computer Monitor with his eyes closed. A strong 10Hz component can be observed.

Figure 4.2: Spectrum components of a 10s signal segment of a subject with their eyes open. Horizontal axis shows different frequencies while the vertical axis represents the PSD. In both diagrams a 50Hz line component can be visualized.

EEG signal, a C++ SDK library provided by the manufacturer is used and an in-house software program is developed. This device has 14 channels, and a sampling rate of 128 Hz[89]. Available channels are AF3, F7, F3, FC5, T7, P7, O1, O2, P8, T8, FC6, F4, F8, AF4. Ten healthy subjects between ages 20-50 are recruited and they accept to wear the device and to participate in the experiments.

A 30 minutes procedure is required to adjust the headset to each user, in order to decrease the impedance on each electrode (below  $5\text{k}\Omega$ ). This is achieved by physically adjusting the headset position over the scalp, and by embedding each electrode electrode pad in saline solution. Once the set up is finished, each subject is instructed to sit in a relaxed position. Subsequently, she/he is commanded to watch the screen for 15 seconds, trying to avoid, as much as possible, to abruptly move its body or head. During that time, a single-trial of 10 seconds-length window of EEG signals data is transferred to a PC and logged into standard binary files. After a 5 minutes pause, the subject is asked to close the eyes avoiding any movement while keeping the same pose for another batch of 15 seconds. Again, 10 seconds of EEG information are transferred and logged into the PC. This finally produce a dataset of 10 subjects, 2 classes per subject, composed of 14 channels, 10-seconds length or 1280 samples per window. These windows are further divided into 10 segments per class and per subject.

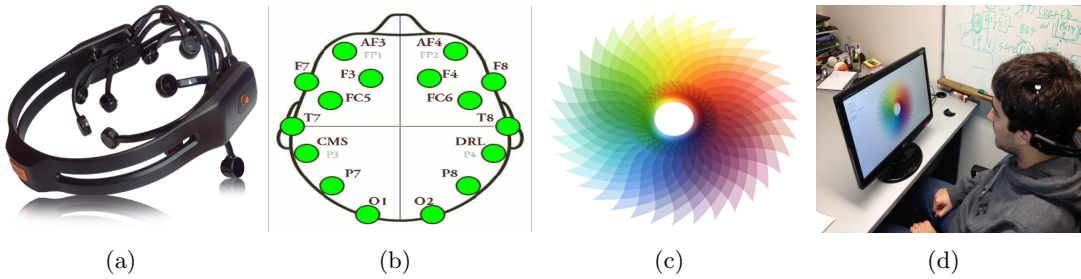


Figure 4.3: (a) EPOC Emotiv consumer-grade 14-channels Wireless EEG.(b) This device has a fixed set of positions according to the 10-20 International System.(c) While resting and sitting comfortable in a chair, subjects had to fixate their sight to the center of this image which was being displayed on a computer monitor, 1 meter away from the subject.(d) Subject performing the experiment described to produce the Dataset described in 4.2.1

#### 4.2.2 Dataset II - AlphaNet Dataset

Additionally, the performance of HIST was tested against the public dataset EEG Motor Movement/Imagery Dataset of the PhysioNet effort published and maintained by the NHS [84, 33].

Baseline records and motor/imagery tasks were performed by 109 healthy volunteers, using the BCI2000 system [84]. At the same time 64-channel EEG records were registered where each subject completed 14 tasks, called Runs. The first two are the baseline calibration tasks, of relevance for this Chapter. These Runs 1 and 2 are each one-minute records of resting subjects with eyes open and eyes closed. From these records, 60 segments of 1-second length are further extracted per subject. Class labeling is the same as Dataset I. The experiment was performed on 25 of the 109 subjects.

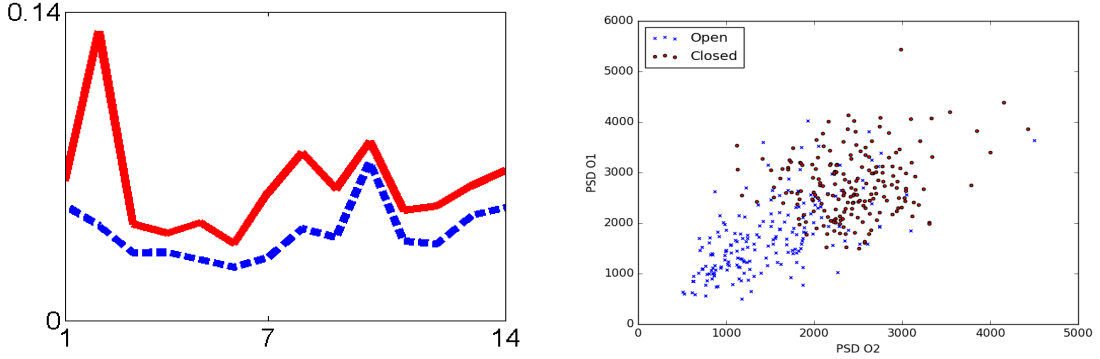
#### 4.2.3 Parameters

Descriptors are extracted from all the generated images, from both classes, and they are used to classify images from the same set. Keypoint localization is determined by following the trace of the signal, as detailed in section 3 of Chapter 3. The classification method is what is described in section 2 of Chapter 3. The parameters  $\gamma$  is set to 1, as well as  $\gamma_t$ .

### 4.3 Results

Dataset I was controlled and verified by processing it with a 8-12Hz band-pass filter, and calculating the average power spectral density across subjects for each channels. It can

be observed on Figure 4.4(a) that values corresponding to class 2 (eyes closed) are always higher than the values obtained for class 1 (eyes open). On the other hand, for the sake of illustration, a scatter plot of the obtained segment's PSD for O1 vs O2 for Subject 2 is shown, where a clear separation of classes can be devised. In brief, there is discriminative information in the frequency-domain.



(a) PSD averaged across 10 subjects for each channel. (b) Scatterplot of PSD for the channel O1 vs O2. Values for Class 2 (red) are always higher than values for Class 1 (blue). There is a separation of classes between the red (class 2) and blue(Class 1) dots.

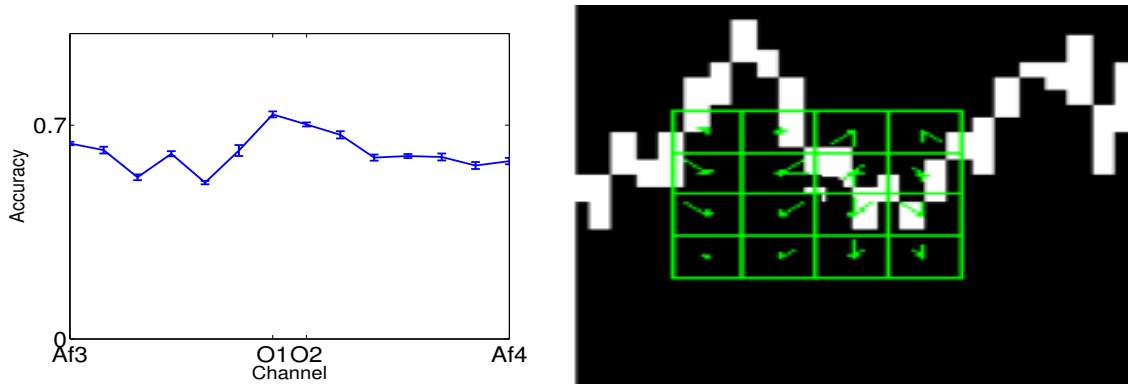
Figure 4.4: Verification and control of the obtained Dataset I.

Results of applying a 10-Fold Cross Validation procedure on the entire set of labeled descriptors is shown on Figure 4.5. Descriptors from different subjects were used as part of the different training set to classify unknown images, so the obtained accuracy level was subject-independent. Moreover, a classification level with average above 70% was obtained in Occipital channels.

For the Dataset II, an accuracy median higher than 70% for 25 subjects, also on occipital channels O1, Oz, O2 and Iz (numbered 61 to 64) is obtained while discriminating Runs 1 and 2 (Baseline eyes open vs Baseline eyes closed). This information can be devised on Figure 4.6 (a) where boxplots of the averaged classification accuracies for all the subjects are represented. On the other hand, Figure 4.6(b) shows the 10-Fold Validated Accuracy for one random subject. A higher accuracy in the classification of the signals can also be seen over occipital channels.

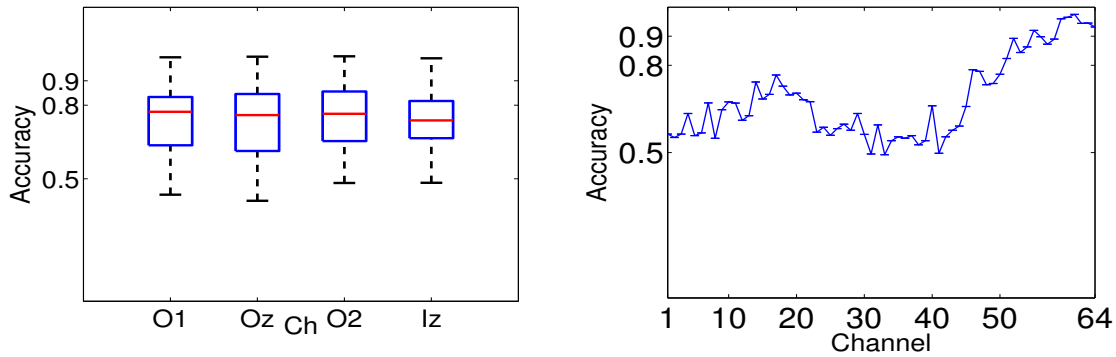
#### 4.4 Conclusion

It is known and it was verified here that the discriminative information in EEG alpha waves is mostly contained in the frequency-domain. In spite of this, there is enough discriminative



(a) 10-Fold Cross-validated accuracy values for 10 subjects. Descriptors were mixed for all the subjects. (b) Sample Descriptor patch located on one of the images generated for one 1-second long segment of this Dataset.

Figure 4.5: The classification accuracy is maximum on occipital channels O1 and O2. The descriptor size is 12x12 pixels which corresponds to a variation of  $\Delta\mu V = 12$  microvolts in the signal amplitude during  $\lambda = 0.09$  seconds.



(a) 10-Fold Cross-validated accuracies for O1, Oz, O2 and Iz channels for 25 subjects of the Alphanet subject number 12, using Runs 1 and 2 of the Dataset. Medians are above 75%. (b) 10-Fold Cross-validated accuracies values for Alphanet Dataset.

Figure 4.6: Classification Accuracy for discriminating windows of 1s ( $N = 160$ ) of EEG for Alpha Waves differences between subjects with eyes opened and closed.

information to classify alpha waves signals solely on the information contained on the wiggles of the plot that is captured by the HIST method presented in this Thesis. Offline Alpha Waves presence was detected from plots of single segments of EEG signals with an accuracy level 10-fold cross validated of 70%.

It was also showed and proved here that there is information within the plot of a signal related to 8-12 Hz oscillatory alpha waves is higher around the occipital region and that an automated procedure which analyze visually the image structure can detect them. This

important oscillatory rhythm has many connections with shifting of attention and with volitional changes and is of quite relevance in BCI research. Particularly, the BCI paradigm of Covert Spatial Visual Attention is a further area of research for this method due to the fact that it is entirely based on analyzing alpha waves. Moreover, the posterior rythm has many implications outside the field of BCI and is very important to assess healthy EEG patterns.



# Chapter 5

## Motor Imagery: the hunt for a greek letter

...utilizing the brain signals in man-computer dialogue.

---

Vidal

### 5.1 Introduction

Motor Imagery is an EEG or ECoG based BCI paradigm originated on changes of SMR, sensorimotor rhythms, that are altered when a person engages in motor behavior, but it can also be elicited when a person imagines to perform any movement. Particularly, the Rolandic wicket rhythm, the  $\mu$  rhythm, is of the same frequency (e.g. 8-12 Hz) of visual occipital alpha waves, but from a spatially different location (posterior frontal and anterior parietal areas)[102]. Although SMR patterns presents a high inter- and intra-subjects variability regarding the signal features required to identify them, an Event Related Desynchronization/Synchronization of  $\mu$  rhythm is in general consistent across subjects, regardless of the specificity of the imagined movement (i.e. what is being imagined to move).

### 5.2 Materials and Methods

In order to verify if this ERD/ERS could be detected by the method presented in this work, i.e. by automatically extracting the information from the signal plots, a BCI Simulation was performed against the public Motor Imagery Dataset 002-2014, published by BNCI-Horizon

2020 website and initiative [88]. This dataset is composed of 8 runs for 14 participants. The first 5 runs were used for training without feedback, and the remaining 3 runs were used to test the results. The original online experiment was performed with 20 trials on each run, 10 corresponding to imagining moving the right hand and the other 10 to feet movement. Figure 5.1 schematize the protocol and the structure of the published dataset. This BCI simulation experiment was divided in two. In the first simulation, baseline signals, corresponding to the 1st second of each trial were compared against right hand motor imagery, 4.5 seconds ahead of the beginning of each trial. Signal segments of 1s length were processed for 10 trials for each of 5 runs and their descriptors extracted for both classes. The second BCI simulation was similar but only extracting trials corresponding to feet movement imagery.

#### **BCI Simulation or Cross Validation?**

The decoding part of BCI Research inherits practices from Machine Learning and a cross-validation procedure is a common practice. However, in terms of the data extracted from the brain of a person who is learning and changing how to perform a certain operation does not make too much sense to use information from a future brain to derive outputs in the past.

The idea of implementing a BCI Simulation is not very well defined in BCI research, but their practice without naming it has been the regular approach for BCI Competitions. The idea is to use an offline dataset simulating what would have happened if the system has been tested in real-time following the same sequence of operations that what was used to generate the dataset.

Regardless, of any definition, the Online Validation with feedback of any BCI system is the Gold Standard due to Man-Machine Dilemma.

### **5.3 Results**

Binary classification accuracies are calculated based on the output of the BCI simulation on the remaining 3 runs for each participant, in a single-trial approach: for each sampled segment of 1-second length, classification based on the classification algorithm described in 3.5 is applied and a match or mismatch is obtained. Results are shown in Figure 5.2 where for right-hand detection *RH*, average accuracies of around 70% are obtained for the channel C3, the best-performing channel, coincidentally with the contralateral structure of the imagined movement. On the other hand, the binary classification accuracy for feet

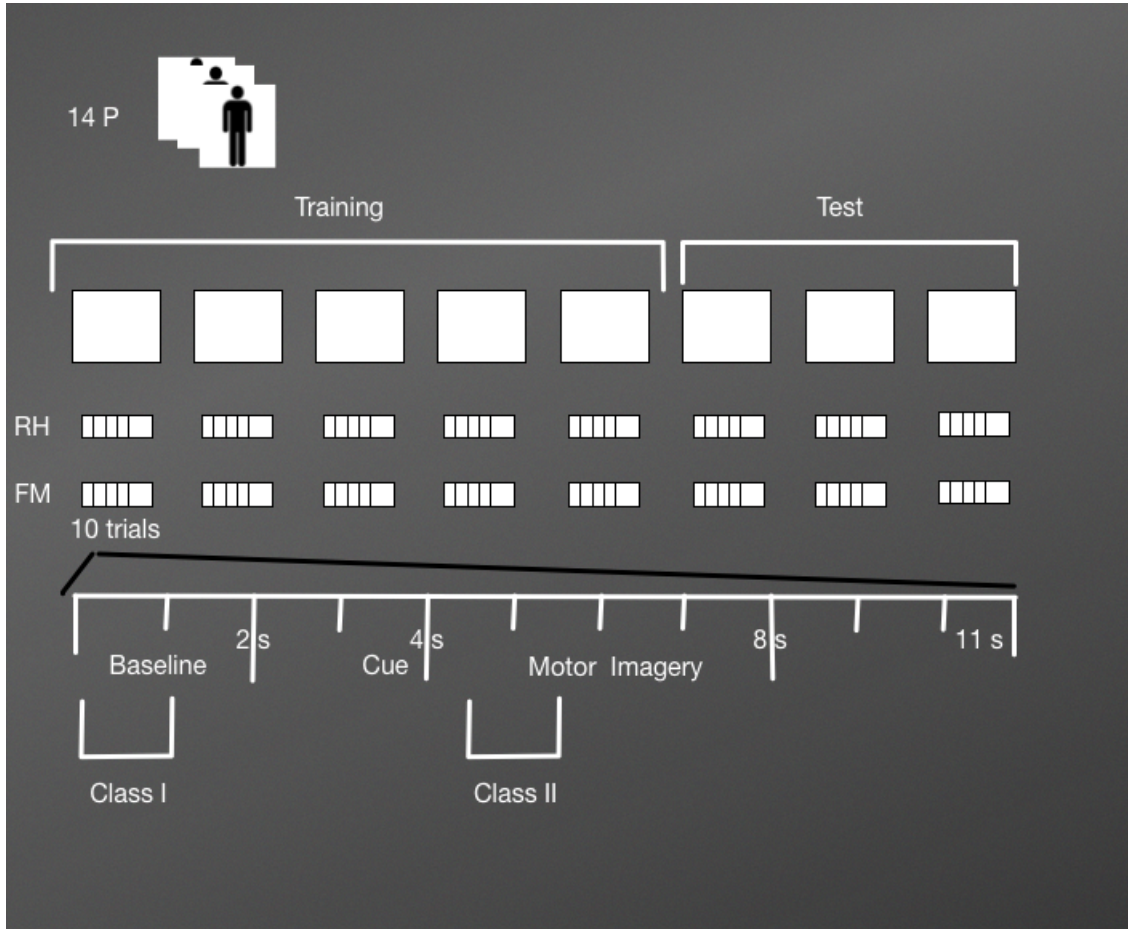


Figure 5.1: Fourteen voluntary Participants performed 5 sessions of training and 3 sessions of testing. On each session each subject had 10 trials to perform Right Hand Motor Imagery and 10 trials for Feet Movement. At the same time, each trial has a 2-seconds baseline and a 4-seconds section to perform the imagery task. For each BCI Simulation, Class 1 is defined from EEG information obtained from the baseline section, while Class 2 is based on extracting segments from the imagery section of the EEG signal.

imagery detection  $FM$ , achieves in all the channels accuracies of just above chance level.

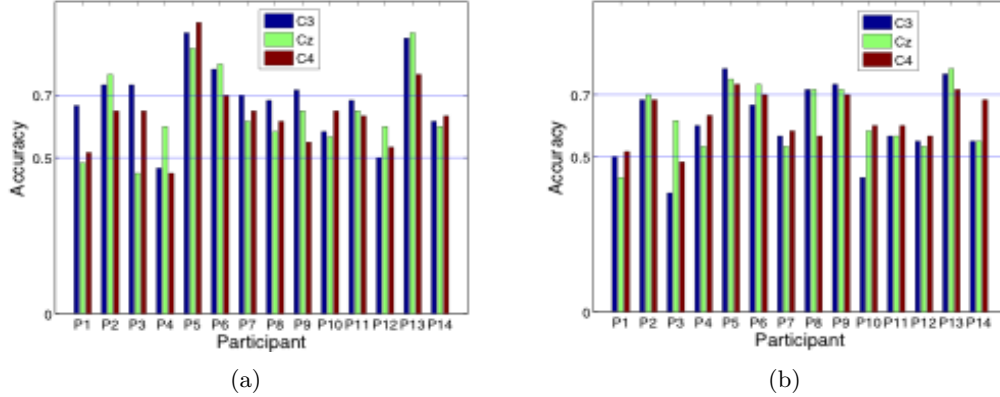


Figure 5.2: Classification Accuracy for discriminating segments of 1s ( $N = 512$ ) of EEG for Motor Imagery detection BCI simulation. (a) Accuracy values for channels C3, Cz and C4 for the 14 participants of the described MI dataset discriminating between baseline and right-hand imagery. (b) The same procedure for feet imagery. Accuracy levels averaged to 70% are obtained only for right-hand movement on the contralateral channel C3. The SIFT descriptor size for this dataset was adjusted to 72x72 pixels

## 5.4 Conclusion

Offline BCI Simulation of single trial asynchronous triggering for right hand MI based on signal plots was implemented with a level of success of 70% for 7 out of 14 Participants. Single trial asynchronous triggering of BCI can be implemented with this paradigm, particularly for right-hand motor imagery. The name  $\mu$  rhythm was precisely coined because the shape of the waves have some resemblance to the greek letter [23]. Additionally, in line with previous chapter results, the frequency of these components is exactly the same as alpha waves, 10 Hz.

# Chapter 6

## Event Related Potential: The P300 Wave

Talking off the top of your head....

---

Farwell and Donchin

### 6.1 Introduction

The P300 [28, 51] is a positive deflection of the EEG signal which occurs around 300 ms after the onset of a rare and deviant stimulus that the subject is expected to attend. It is produced under the oddball paradigm [102] and it is consistent across different subjects. It has a lower amplitude ( $\pm 5\mu V$ ) compared to basal EEG activity, reaching a Signal to Noise Ratio (SNR) of around  $-15$  db estimated based on the amplitude of the P300 response signal divided by the standard deviation of the background EEG activity [41]. This signal can be used to implement a speller application by means of a Speller Matrix [28]. Fig. 6.1 shows an example of the Speller Matrix used in the OpenVibe open source software [79], where the flashes of rows and columns provide the deviant stimulus required to elicit this physiological response. Each time a row or a column that contains the desired letter flashes, the corresponding synchronized EEG signal should also contain the P300 signature and by detecting it, the selected letter can be identified.



Figure 6.1: Example of the  $6 \times 6$  Speller Matrix used in the study obtained from the OpenVibe software. Rows and columns flash in random permutations.

## 6.2 Materias and Methods

### 6.2.1 Feature Extraction from Signal Plots

In this section, the signal preprocessing, the method for generating images from signal plots, the feature extraction procedure and the Speller Matrix identification are described. Figure 6.2 shows a scheme of the entire process.

#### Preprocessing Pipeline

The data obtained by the capturing device is digitalized and a multichannel EEG signal is constructed.

The 6 rows and 6 columns of the Speller Matrix are intensified providing the visual stimulus. The number of a row or column is a location. A sequence of twelve randomly permuted locations  $l$  conform an intensification sequence. The whole set of twelve intensifications is repeated  $k_a$  times.

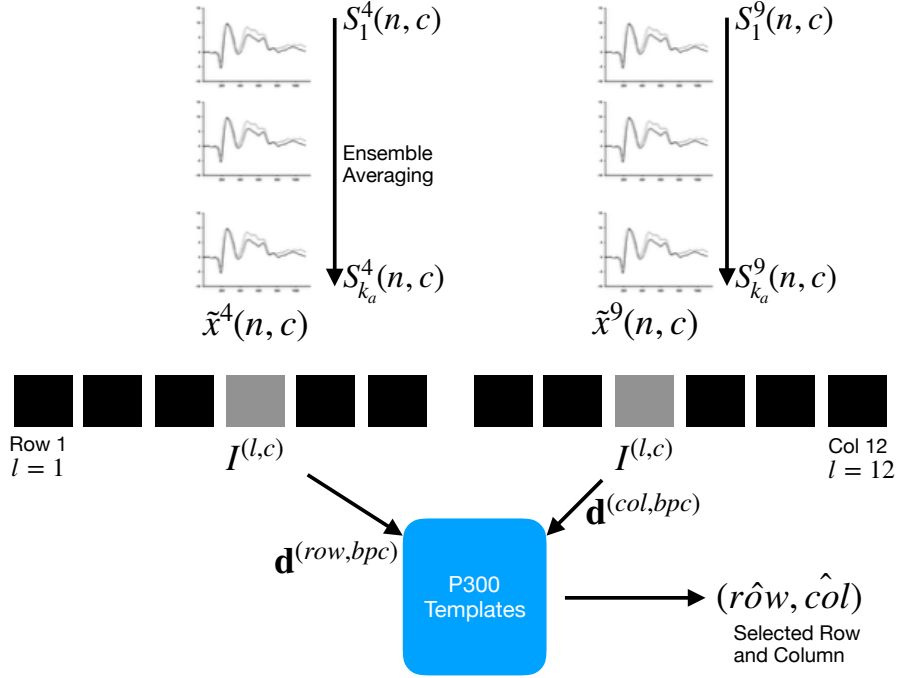


Figure 6.2: For each column and row, an averaged, standardized and scaled signal  $\tilde{x}^l(n, c)$  is obtained from the segments  $S_i^l$  corresponding to the  $k_a$  intensification sequences with  $1 \leq i \leq k_a$  and location  $l$  varying between 1 and 12. From the averaged signal, the image  $I^{(l,c)}$  of the signal plot is generated and each descriptor is computed. By comparing each descriptor against the set of templates, the P300 ERP can be detected, and finally the desired letter from the matrix can be inferred.

- **Signal Enhancement:** This stage consists of the enhancement of the SNR of the P300 pattern above the level of basal EEG. The pipeline starts by applying a notch filter to the raw digital signal, a 4th degree 10 Hz lowpass Butterworth filter and finally a decimation with a Finite Impulse Response (FIR) filter of order 30 from the original sampling frequency down to 16 Hz [52].
- **Artifact Removal:** For every complete sequence of 12 intensifications of 6 rows and 6 columns, a basic artifact elimination procedure is implemented by removing the entire sequence when any signal deviates above/below  $\pm 70\mu V$ .
- **Segmentation:** For each of the 12 intensifications of one intensification sequence, a segment  $S_i^l$  of a window of  $t_{max}$  seconds of the multichannel signal is extracted, starting from the stimulus onset, corresponding to each row/column intensification  $l$  and to the intensification sequence  $i$ . As intensifications are permuted in a random order, the

segments are rearranged corresponding to row flickering, labeled 1-6, whereas those corresponding to column flickering are labeled 7-12. Two of these segments should contain the P300 ERP signature time-locked to the flashing stimulus, one for the row, and one for the column.

- **Signal Averaging:** The P300 ERP is deeply buried under basal EEG so the standard approach to identify it is by point-to-point averaging the time-locked stacked signal segments. Hence the values which are not related to, and not time-locked to the onset of the stimulus are canceled out [53].

This last step determines the operation of any P300 Speller. In order to obtain an improved signal in terms of its SNR, repetitions of the sequence of row/column intensification are necessary. And, at the same time, as long as more repetitions are needed, the ability to transfer information faster is diminished, so there is a trade-off that must be acutely determined.

The procedure to obtain the point-to-point averaged signal goes as follows:

1. Highlight randomly the rows and columns from the matrix. There is one row and one column that should match the letter selected by the subject.
2. Repeat step 1  $k_a$  times, obtaining the  $1 \leq l \leq 12$  segments  $S_1^l(n, c), \dots, S_{k_a}^l(n, c)$ , of the EEG signal where the variables  $1 \leq n \leq n_{max}$  and  $1 \leq c \leq C$  correspond to sample points and channel, respectively. The parameter  $C$  is the number of available EEG channels whereas  $n_{max} = F_s t_{max}$  is the segment length and  $F_s$  is the sampling frequency. The parameter  $k_a$  is the number of repetitions of intensifications and it is an input parameter of the algorithm.
3. Compute the Ensemble Average by

$$x^l(n, c) = \frac{1}{k_a} \sum_{i=1}^{k_a} S_i^l(n, c) \quad (6.1)$$

for  $1 \leq n \leq n_{max}$  and for the channels  $1 \leq c \leq C$ . This provide an averaged signal  $x^l(n, c)$  for the twelve locations  $1 \leq l \leq 12$ .

### Speller Matrix letter Identification

**P300 ERP Extraction** Segments corresponding to row flickering are labeled 1-6, whereas those corresponding to column flickering are labeled 7-12. The extraction process has the following steps:

- **Step A:** First highlight rows and columns from the matrix in a random permutation order and obtain the Ensemble Average as detailed in steps 1, 2 and 3 in Section 6.2.1.
- **Step B:** Plot the signals  $\tilde{x}^l(n, c)$ ,  $1 \leq n \leq n_{max}$ ,  $1 \leq c \leq C$ , according Section ?? in order to generate the images  $I^{(l,c)}$  for rows and columns  $1 \leq l \leq 12$ .
- **Step C:** Obtain the descriptors  $\mathbf{d}^{(l,c)}$  for rows and columns from  $I^{(l,c)}$  in accordance to the method described in Section 3.2.

**Calibration** A trial, as defined by the BCI2000 platform [84], is every attempt to select just one letter from the speller. A set of trials is used for calibration and once the calibration is complete it can be used to identify new letters from new trials.

During the calibration phase, two descriptors  $\mathbf{d}^{(l,c)}$  are extracted for each available channel, corresponding to the locations  $l$  of a selection of one previously instructed letter from the set of calibration trials. These descriptors are the P300 templates, grouped together in a template set called  $T^c$ . The set is constructed using the steps described in Section 6.2.1 and the steps A, B and C of the P300 ERP extraction process.

Additionally, the best performing channel,  $bpc$  is identified based on the the channel where the best Character Recognition Rate is obtained.

**Letter identification** In order to identify the selected letter, the template set  $T^{bpc}$  is used as a database. Thus, new descriptors are computed and they are compared against the descriptors belonging to the calibration template set  $T^{bpc}$ .

- **Step D:** Match to the calibration template  $T^{bpc}$  by computing

$$\hat{row} = \arg \min_{l \in \{1, \dots, 6\}} \sum_{q \in N_T(\mathbf{d}^{(l,bpc)})} \left\| q - \mathbf{d}^{(l,bpc)} \right\|^2 \quad (6.2)$$

and

$$\hat{col} = \arg \min_{l \in \{7, \dots, 12\}} \sum_{q \in N_T(\mathbf{d}^{(l,bpc)})} \left\| q - \mathbf{d}^{(l,bpc)} \right\|^2 \quad (6.3)$$

where  $N_T(\mathbf{d}^{(l,bpc)})$  is defined as  $N_T(\mathbf{d}^{(l,bpc)}) = \{\mathbf{d} \in T^{bpc} / \mathbf{d} \text{ is the k-nearest neighbor of } \mathbf{d}^{(l,bpc)}\}$  for the best performing channel. This set is obtained by sorting all the elements in  $T^{bpc}$  based on distances between them and  $\mathbf{d}^{(l,bpc)}$ , choosing the  $k$  with

smaller values, with  $k$  a parameter of the algorithm. This procedure is based on the k-NBNN algorithm [10].

By computing the aforementioned equations, the letter of the matrix can be determined from the intersection of the row  $\hat{row}$  and column  $\hat{col}$ . Figure 6.2 shows a scheme of this process.

### 6.2.2 Experimental Protocol

To verify the validity of the proposed framework and method, the public dataset 008-2014 [80] published on the BNCI-Horizon website [13] by IRCCS Fondazione Santa Lucia, is used. Additionally, an own dataset with the same experimental conditions is generated. Both of them are utilized to perform an offline BCI Simulation to decode the spelled words from the provided signals.

The algorithm is implemented using VLFeat [97] Computer Vision libraries on MATLAB V2014a (Mathworks Inc., Natick, MA, USA). Furthermore, in order to enhance the impact of our paper and for a sake of reproducibility, the code of the algorithm has been made available at: <https://bitbucket.org/itba/hist>.

In the following sections the characteristics of the datasets and parameters of the identification algorithm are described.

#### P300 ALS Public Dataset

The experimental protocol used to generate this dataset is explained in [80] but can be summarized as follows: 8 subjects with confirmed diagnoses but on different stages of ALS disease, were recruited and accepted to perform the experiments. The Visual P300 detection task designed for this experiment consisted of spelling 7 words of 5 letters each, using the traditional P300 Speller Matrix [28]. The flashing of rows and columns provide the deviant stimulus required to elicit this physiological response. The first 3 words are used for calibration and the remaining 4 words, for testing with visual feedback. A trial is every attempt to select a letter from the speller. It is composed of signal segments corresponding to  $k_a = 10$  repetitions of flashes of 6 rows and  $k_a = 10$  repetitions of flashes of 6 columns of the matrix, yielding 120 repetitions. Flashing of a row or a column is performed for 0.125 s, following by a resting period (i.e. inter-stimulus interval) of the same length. After 120 repetitions an inter-trial pause is included before resuming with the following letter.

The recorded dataset was sampled at 256 Hz and it consisted of a scalp multichannel EEG signal for electrode channels Fz, Cz, Pz, Oz, P3, P4, PO7 and PO8, identified according to the 10-20 International System, for each one of the 8 subjects. The recording device was a research-oriented digital EEG device (g.Mobilab, g.Tec, Austria) and the data acquisition and stimuli delivery were handled by the BCI2000 open source software [84].

In order to assess and verify the identification of the P300 response, subjects are instructed to perform a copy-spelling task. They have to fix their attention to successive letters for copying a previously determined set of words, in contrast to a free-running operation of the speller where each user decides on its own what letter to choose.

### P300 for healthy subjects

We replicate the same experiment on healthy subjects using a wireless digital EEG device (g.Nautilus, g.Tec, Austria). The experimental conditions are the same as those used for the previous dataset, as detailed in section 6.2.2. The produced dataset is available in a public online repository [77].

Participants are recruited voluntarily and the experiment is conducted anonymously in accordance with the Declaration of Helsinki published by the World Health Organization. No monetary compensation is handed out and all participants agree and sign a written informed consent. This study is approved by the *Departamento de Investigación y Doctorado, Instituto Tecnológico de Buenos Aires (ITBA)*. All healthy subjects have normal or corrected-to-normal vision and no history of neurological disorders. The experiment is performed with 8 subjects, 6 males, 2 females, 6 right-handed, 2 left-handed, average age 29.00 years, standard deviation 11.56 years, range 20-56 years.

EEG data is collected in a single recording session. Participants are seated in a comfortable chair, with their vision aligned to a computer screen located one meter in front of them. The handling and processing of the data and stimuli is conducted by the OpenVibe platform [79].

Gel-based active electrodes (g.LADYbird, g.Tec, Austria) are used on the same positions Fz, Cz, Pz, Oz, P3,P4, PO7 and PO8. Reference is set to the right ear lobe and ground is preset as the AFz position. Sampling frequency is slightly different, and is set to 250 Hz, which is the closest possible to the one used with the other dataset.

### P300 Pseudo-Real Dataset Generation

The template ERP is acquired from the Subject Number 8 of the public dataset 008-2014 [80] published on the BNCI-Horizon website [13] by IRCCS Fondazione Santa Lucia. Segments from the EEG signal containing the ERP are extracted for the trial number 2, and they are point-to-point coherently averaged. This P300 ERP can be seen in Figure 6.3.

An EEG stream with null-P300 signal is obtained by the following procedure: A subject participant is recruited voluntarily and the experiment is conducted anonymously in accordance with the Declaration of Helsinki published by the World Health Organization. No monetary compensation is handed out and she/he agrees and signs a written informed consent. This study is approved by the *Departamento de Investigación y Doctorado, Instituto Tecnológico de Buenos Aires (ITBA)*. The participant is healthy and have normal or corrected-to-normal vision and no history of neurological disorders. This voluntary subject is aged between 20-30 years old. EEG data is collected in a single recording session. She/He is seated in a comfortable chair, with her/his vision aligned to a computer screen located one meter in front of her/him. The handling and processing of the data and stimuli is conducted by the OpenVibe platform [79]. Gel-based active electrodes (g.LADYbird, g.Tec, Austria) are used on locations Fz, Cz, Pz, Oz, P3,P4, PO7 and PO8 according to the 10-20 international system. Reference is set to the right ear lobe and ground is preset as the AFz position. Sampling frequency is set to 250 Hz.

The participant is instructed to passively watch the flashing screen while not focusing on any particular letter. A questionnaire is handed out at the end of the experiment with questions about how the participant felt during it, without giving more details.

Figure 6.5 shows a 5s sample of the EEG trace obtained with the MNE library [34]. Channel  $S$  represents the twelve different stimulus markers (columns or rows) while channel  $L$  represent the label (*True* vs *False*). Labels are represented by square signals. *False* segments are marked with single amplitude square signals while *True* segments are identified by double-amplitude square signals. Subfigure (a) shows the signals before the ERP template is superimposed while subfigure (b) shows the same signals with the superimposed ERP template. At first-sight, differences are really hard to spot visually. Subfigures (c) and (d) show only one second of channels Cz and L from the same segment. The superimposed ERP can be devised enclosed by the vertical bars, around 31.5s, where in (d) the peak is slightly bigger. Figure 6.6 shows the obtained ensemble average ERPs as result of superimposing the template signal into the EEG stream, time-locked to the stimulus onset. These 12

point-to-point averaged segments correspond to the first trial of the EEG stream.

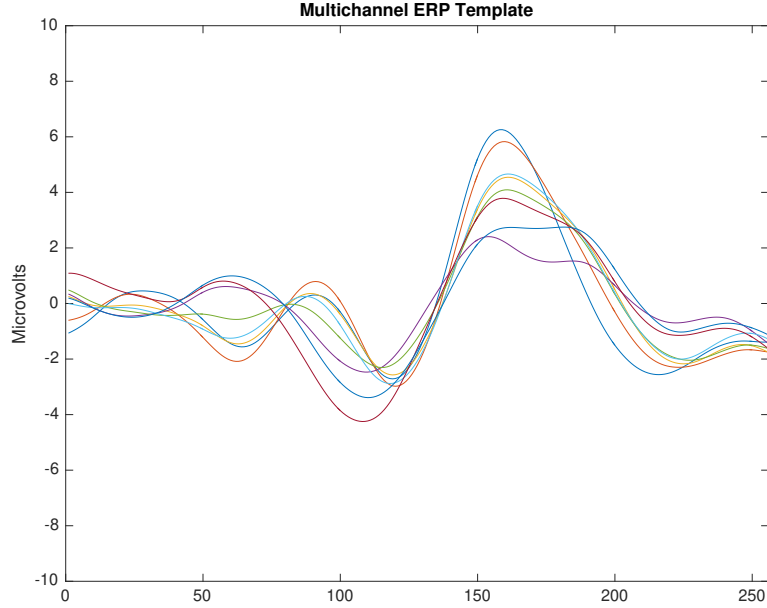


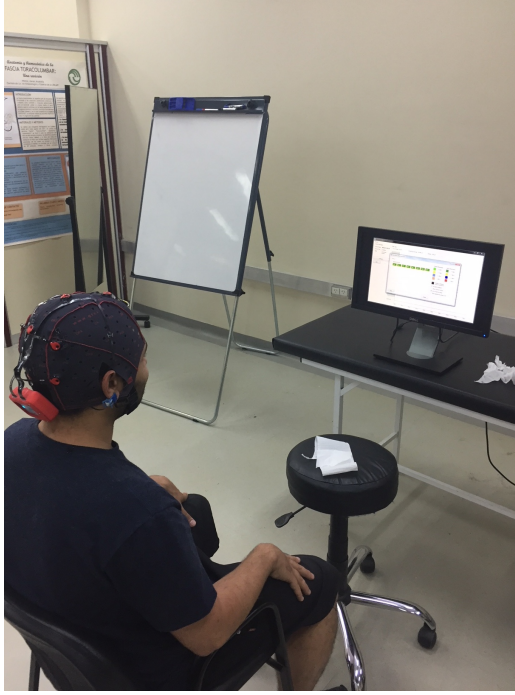
Figure 6.3: ERP Template obtained from the coherent point-to-point ensemble average from the signals of Subject Number Eight of the BNCI Horizon public dataset 008-2014. The template is 1s long which is 256 sample points, and the eight channels are superimposed with different colors. The P3b component can be seen around the sample index 150 and 200.

### P300 Dataset IIb BCI Competition II (2003)

Finally the performance at letter identifications for these same methods is evaluated by performing an offline BCI Simulation on the Dataset IIb of the BCI Competition II (2003) [?]. The protocol of this dataset is very similar to what was used to obtain the pseudo-real dataset. The sampling frequency of this dataset is 240, the number of letters are 73 where the first 42 are used to create the template dictionary for all the methods and the remaining 31 are used to test the character recognition rate performance. Additionally, in this dataset the number of available intensification number sequences is 15.

### Parameters

The patch size is  $X_P = 12s \times 12s$  pixels, where  $s$  is the scale of the local patch and it is an input parameter of the algorithm. The P300 event can have a span of 400 ms and its



(a) EEG trace of the original signal.

Figure 6.4: g.Tec device and subject

amplitude can reach  $10\mu V$  [78]. Hence it is necessary to utilize a signal segment of size  $t_{max} = 1$  second and a size patch  $X_P$  that could capture an entire transient event. With this purpose in consideration, the  $s$  value election is essential.

We propose the Equations 6.4 and 6.5 to compute the scale value in horizontal and vertical directions, respectively.

$$s_x = \frac{\gamma \lambda F_s}{12} \quad (6.4)$$

$$s_y = \frac{\gamma \Delta\mu V}{12} \quad (6.5)$$

where  $\lambda$  is the length in seconds covered by the patch,  $F_s$  is the sampling frequency of the EEG signal (downsampled to 16 Hz) and  $\Delta\mu V$  corresponds to the amplitude in microvolts that can be covered by the height of the patch. The geometric structure of the patch forces a squared configuration, then we discerned that by using  $s = s_x = s_y = 3$  and  $\gamma = 4$ , the local patch and the descriptor can identify events of  $9 \mu V$  of amplitude, with a span of  $\lambda = 0.56$  seconds. This also determines that 1 pixel represents  $\frac{1}{\gamma} = \frac{1}{4}\mu V$  on the vertical direction and  $\frac{1}{F_s \gamma} = \frac{1}{64}$  seconds on the horizontal direction. The keypoints  $\mathbf{p}_k$  are located at  $(x_{p_k}, y_{p_k}) = (0.55F_s \gamma, z^l(c)) = (35, z^l(c))$  for the corresponding channel  $c$  and location  $l$

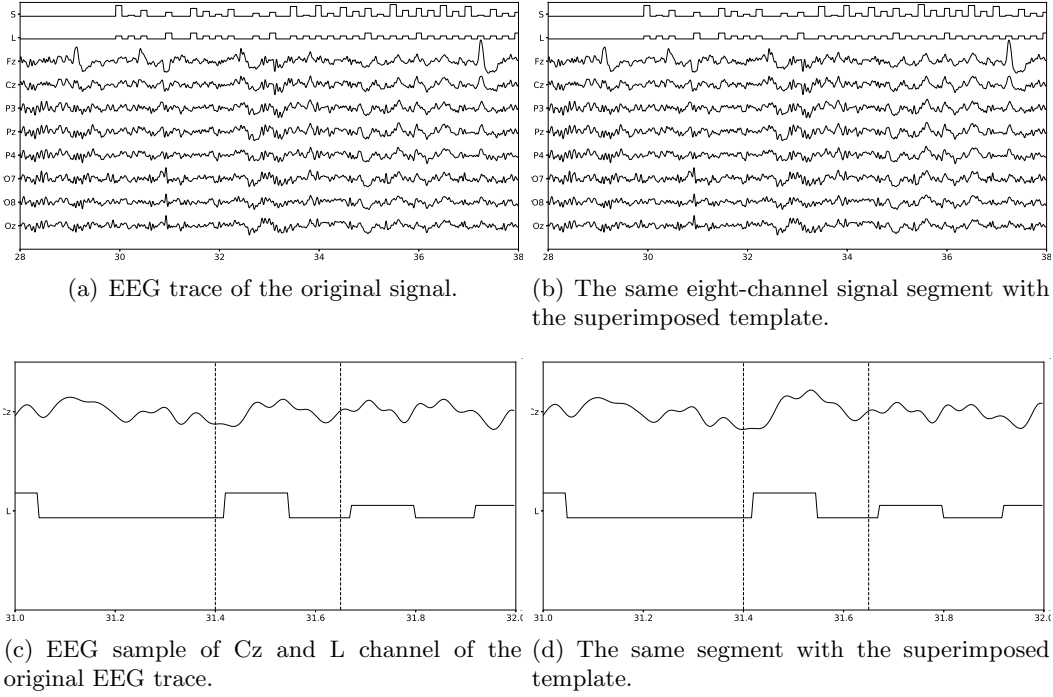


Figure 6.5: Eight-channel EEG signal without and with the superimposed ERP Template. The channel L, the mark which identifies where to superimpose the P300 ERP, is shown as well as the channel S which identifies the stimulus that was presented. On (c) and (d) the small variation that was introduced by the superimposition of the ERP can be seen enclosed by the vertical bars, where the slope of the bump on subfigure (d) is slightly bigger

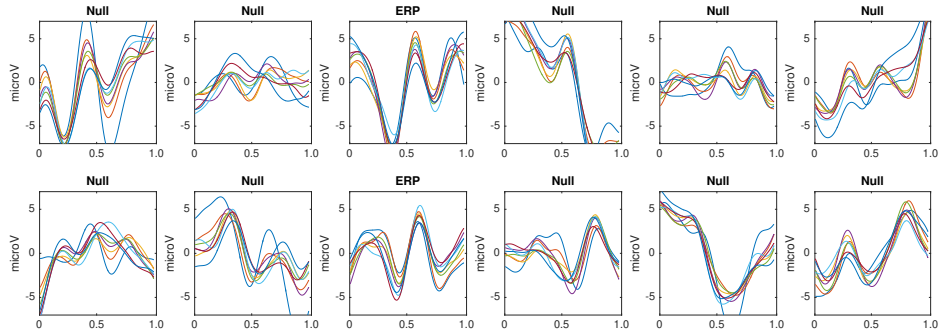


Figure 6.6: Point-to-point averaged signals for the first letter identification trial. The ERP is superimposed on classes 3 and 9. Class 3 is obtained while averaging the segments where the row of the speller matrix is intensified whereas class 9 is calculated from the intensification of the corresponding column.

(see Equation 2.12). In this way the whole transient event is captured. Figure 3.3 shows a patch of a signal plot covering the complete amplitude (vertical direction) and the complete

span of the signal event (horizontal direction).

Lastly, the number of channels  $C$  is equal to 8 for both datasets, and the number of intensification sequences  $k_a$  is fixed to 10. The parameter  $k$  used to construct the set  $N_T(\mathbf{d}^{(l,c)})$  is assigned to  $k = 7$ , which was found empirically to achieve better results. In addition, the norm used on Equations 6.2 and 6.3 is the cosine norm, and descriptors are normalized to  $[-1, 1]$ .

### 6.3 Results

Table 6.1 shows the results of applying the Histogram of Gradient Orientations (HIST) algorithm to the subjects of the public dataset of ALS patients. The percentage of correctly spelled letters is calculated while performing an offline BCI Simulation. From the seven words for each subject, the first three are used for calibration, and the remaining four are used for testing. The best performing channel  $bpc$  is informed as well. The target ratio is  $1 : 36$ ; hence theoretical chance level is 2.8%. It can be observed that the best performance of the letter identification method is reached in a dissimilar channel depending on the subject being studied. Table 6.1 and 6.2 show for comparison the obtained performance rates using single-channel signals with the Support Vector Machine (SVM) [?] classifier. This method is configured to use a linear kernel. The best performing channel, where the best letter identification rate was achieved, is also depicted.

Table 6.1: Character recognition rates for the public dataset of ALS patients using the Histogram of Gradient (HIST) calculated from single-channel plots. Performance rates using single-channel signals with the SVM classifier are shown for comparison. The best performing channel  $bpc$  for each method is visualized

Participant	$bpc$	HIST	$bpc$	Single Channel SVM
1	Cz	35%	Cz	15%
2	Fz	85%	PO8	25%
3	Cz	25%	Fz	5%
4	PO8	55%	Oz	5%
5	PO7	40%	P3	25%
6	PO7	60%	PO8	20%
7	PO8	80%	Fz	30%
8	PO7	95%	PO7	85%

The Information Transfer Rate (ITR), or Bit Transfer Rate (BTR), in the case of reactive BCIs [102] depends on the amount of signal averaging required to transmit a valid and robust

Table 6.2: Character recognition rates for the own dataset of healthy subjects using the Histogram of Gradient (HIST) calculated from single-channel plots. Performance rates using single-channel signals with the SVM classifier are shown for comparison. The best performing channel *bc* for each method is visualized.

Participant	<i>bc</i>	HIST	<i>bc</i>	Single Channel SVM
1	Oz	40%	Cz	10%
2	PO7	30%	Cz	5%
3	P4	40%	P3	10%
4	P4	45%	P4	35%
5	P4	60%	P3	10%
6	Pz	50%	P4	25%
7	PO7	70%	P3	30%
8	P4	50%	PO7	10%

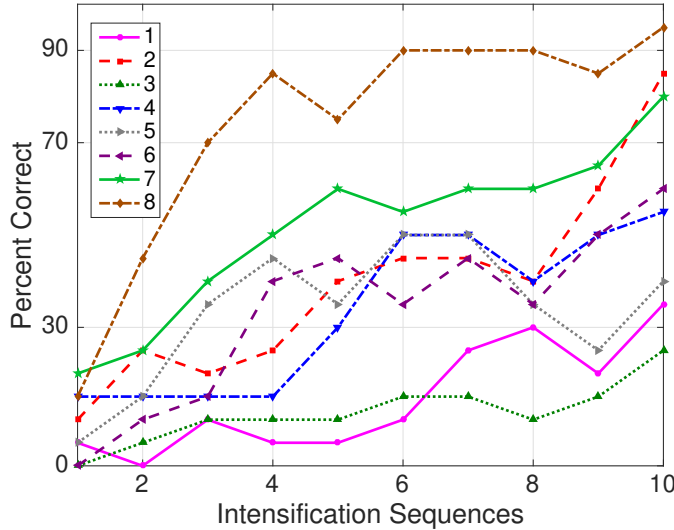


Figure 6.7: Performance curves for the eight subjects included in the dataset of ALS patients. Three out of eight subjects achieved the necessary performance to implement a valid P300 speller.

selection. Figure 6.7 shows the performance curves for varying intensification sequences for the subjects included in the dataset of ALS patients. It can be noticed that the percentage of correctly identified letters depends on the number of intensification sequences that are used to obtain the averaged signal. Moreover, when the number of intensification sequences tend to 1, which corresponds to single-intensification character recognition, the performance is reduced. As mentioned before, the SNR of the P300 obtained from only one segment of the intensification sequence is very low and the shape of its P300 component is not very

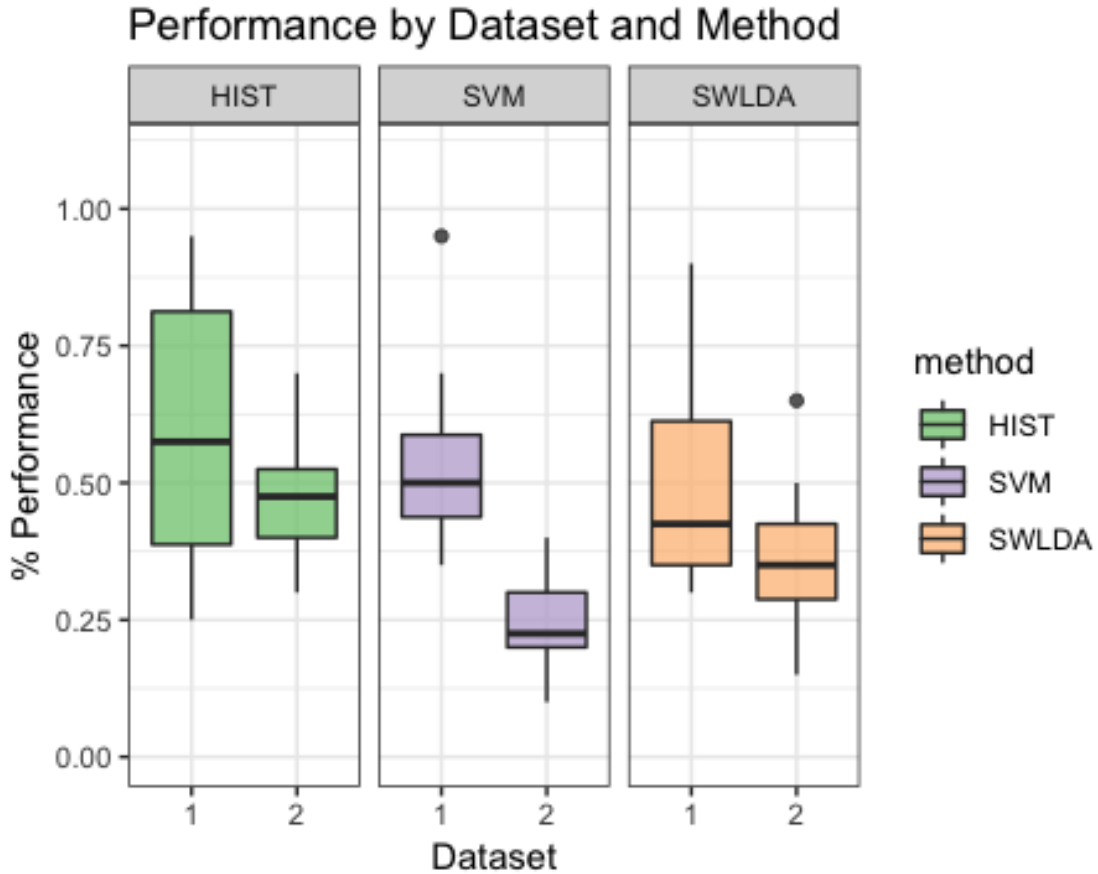


Figure 6.8: Obtained boxplots for the given algorithms.

well defined.

In Table 6.2 the results obtained for 8 healthy subjects are shown. It can be observed that the performance is above chance level. It was verified that HIST method has an improved performance at letter identification than SVM that process the signals on a channel by channel strategy (Wilcoxon signed-rank test,  $p = 0.004$  for both datasets).

Tables 6.3 and 6.4 are presented in order to compare the performance of the HIST method versus a multichannel version of the Stepwise Linear Discriminant Analysis (SWLDA) and SVM classification algorithms for both datasets. The feature was formed by concatenating all the channels [52]. SWLDA is the methodology proposed by the ALS dataset's publisher. Since authors [80] did not report the Character Recognition Rate obtained for this dataset, we replicate their procedure and include the performance obtained with the SWLDA algorithm at letter identification. It was verified for the dataset of ALS patients that it has similar performance against other methods like SWLDA or SVM, which use a multichannel feature

Table 6.3: Character recognition rates and the best performing channel  $bpc$  for the public dataset of ALS patients using the Histogram of Gradient (HIST) (repeated here for comparison purposes). Performance rates obtained by SWLDA and SVM classification algorithms with a multichannel concatenated feature.

Participant	$bpc$ for HIST	HIST	Multichannel SWLDA	Multichannel SVM
1	Cz	35%	45%	40%
2	Fz	85%	30%	50%
3	Cz	25%	65%	55%
4	PO8	55%	40%	50%
5	PO7	40%	35%	45%
6	PO7	60%	35%	70%
7	PO8	80%	60%	35%
8	PO7	95%	90%	95%

(Quade test with  $p = 0.55$ ) whereas for the dataset of healthy subjects significant differences were found (Quade test with  $p = 0.02$ ) where only the HIST method achieved a different performance than SVM (with multiple comparisons, significant difference of level 0.05).

Table 6.4: Character recognition rates and the best performing channel  $bpc$  for the own dataset of healthy subjects using the Histogram of Gradient (HIST) (repeated here for comparison purposes). Performance rates obtained by SWLDA and SVM classification algorithms with a multichannel concatenated feature.

Participant	$bpc$ for HIST	HIST	Multichannel SWLDA	Multichannel SVM
1	Oz	40%	65%	40%
2	PO7	30%	15%	10%
3	P4	40%	50%	25%
4	P4	45%	40%	20%
5	P4	60%	30%	20%
6	Pz	50%	35%	30%
7	PO7	70%	25%	30%
8	P4	50%	35%	20%

The P300 ERP consists of two overlapping components: the P3a and P3b, the former with frontocentral distribution while the later stronger on centroparietal region [74]. Hence, the standard practice is to find the stronger response on the central channel Cz [80]. However, [52] show that the response may also arise in occipital regions. We found that by analyzing only the waveforms, occipital channels PO8 and PO7 show higher performances for some subjects.

As subjects have varying *latencies* and *amplitudes* of their P300 components, they also have a varying stability of the *shape* of the generated ERP [64]. Figure 6.9 shows 10 sample P300 templates patches for patients 8 and 3 from the dataset of ALS patients. It can be discerned that in coincidence with the performance results, the P300 signature is more clear and consistent for subject 8 (A) while for subject 3 (B) the characteristic pattern is more difficult to perceive.

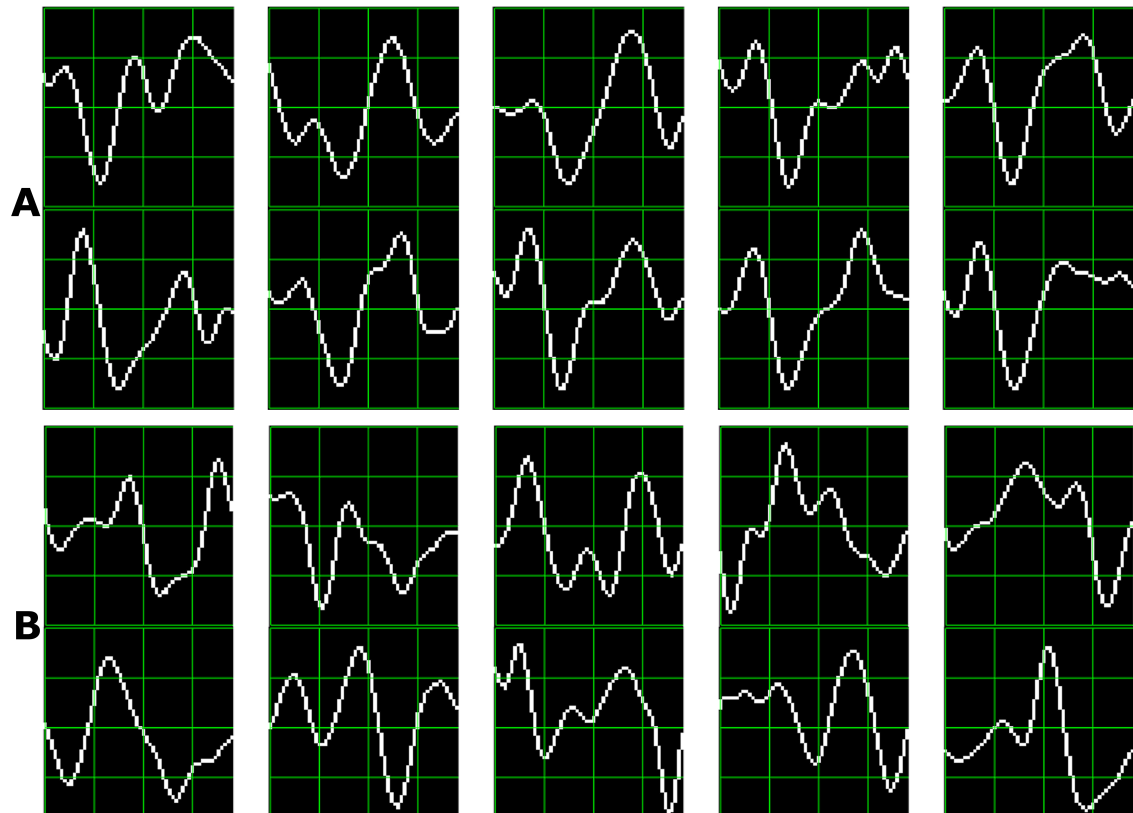


Figure 6.9: Ten sample P300 template patches for subjects 8 (A) and 3 (B) of the ALS Dataset. Downward deflection is positive polarity.

Additionally, the stability of the P300 component waveform has been extensively studied in patients with ALS [86, 60, 67, 61, 63] where it was found that these patients have a stable P300 component, which were also sustained across different sessions. In line with these results we do not find evidence of a difference in terms of the performance obtained by analyzing the waveforms (HIST) for the group of patients with ALS and the healthy group of volunteers (Mann-Whitney U Test,  $p = 0.46$ ). Particularly, the best performance is obtained for a subject from the ALS dataset for which, based on visual observation, the shape of they P300 component is consistently identified.

It is important to remark that when applied to binary images obtained from signal plots, the feature extraction method described in Section 3.2 generates sparse descriptors. Under this subspace we found that using the cosine metric yielded a significant performance improvement. On the other hand, the unary classification scheme based on the NBNN algorithm proved very beneficial for the P300 Speller Matrix. This is due to the fact that this approach solves the unbalance dataset problem which is inherent to the oddball paradigm [92].

## 6.4 Conclusion

Among other applications of Brain Computer Interfaces, the goal of the discipline is to provide communication assistance to people affected by neuro-degenerative diseases, who are the most likely population to benefit from BCI systems and EEG processing and analysis.

In this work, a method to extract an objective metric from the waveform of the plots of EEG signals is presented. Its usage to implement a valid P300-Based BCI Speller application is expounded. Additionally, its validity is evaluated using a public dataset of ALS patients and an own dataset of healthy subjects.

It was verified that this method has an improved performance at letter identification than other methods that process the signals on a channel by channel strategy, and it even has a comparable performance against other methods like SWLDA or SVM, which uses a multichannel feature. Furthermore, this method has the advantage that shapes of waveforms can be analyzed in an objective way. We observed that the shape of the P300 component is more stable in occipital channels, where the performance for identifying letters is higher. We additionally verified that ALS P300 signatures are stable in comparison to those of healthy subjects.

We believe that the use of descriptors based on histogram of gradient orientation, presented in this work, can also be utilized for deriving a shape metric in the space of the P300 signals which can complement other metrics based on time-domain as those defined by [61]. It is important to notice that the analysis of waveform shapes is usually performed in a qualitative approach based on visual inspection [86], and a complementary methodology which offer a quantitative metric will be beneficial to these routinely analysis of the waveform of ERPs.

The goal of this work is to answer the question if a P300 component could be solely determined by inspecting automatically their waveforms. We conclude affirmatively, though

two very important issues still remain:

First, the stability of the P300 in terms of its shape is crucial: the averaging procedure, montages, the signal to noise ratio and spatial filters all of them are non-physiological factors that affect the stability of the shape of the P300 ERP. We tested a preliminary approach to assess if the morphological shape of the P300 of the averaged signal can be stabilized by applying different alignments of the stacked segments (see Figure 6.2) and we verified that there is a better performance when a correct segment alignment is applied. We applied Dynamic Time Warping (DTW) [16] to automate the alignment procedure but we were unable to find a substantial improvement. Further work to study the stability of the shape of the P300 signature component needs to be addressed.

The second problem is the amplitude variation of the P300. We propose a solution by standardizing the signal, shown in Equation 2.10. It has the effect of normalizing the peak-to-peak amplitude, moderating its variation. It has also the advantage of reducing noise that was not reduced by the averaging procedure. It is important to remark that the averaged signal variance depends on the number of segments used to compute it [96]. The standardizing process converts the signal to unit signal variance which makes it independent of the number  $k_a$  of signals averaged. Although this is initially an advantageous approach, the standardizing process reduces the amplitude of any significant P300 complex diminishing its automatic interpretation capability.

In our opinion, the best benefit of the presented method is that a closer collaboration of the field of BCI with physicians can be fostered [18], since this procedure intent to imitate human visual observation. Automatic classification of patterns in EEG that are specifically identified by their shapes like K-Complex, Vertex Waves, Positive Occipital Sharp Transient [39] are a prospect future work to be considered. We are currently working in unpublished material analyzing K-Complex components that could eventually provide assistance to physicians to locate these EEG patterns, specially in long recording periods, frequent in sleep research [?]. Additionally, it can be used for artifact removal which is performed on many occasions by visually inspecting signals. This is due to the fact that the descriptors are a direct representation of the shape of signal waveforms. In line with these applications, it can be used to build a database [18] of quantitative representations of waveforms and improve atlases [39], which are currently based on qualitative descriptions of signal shapes.

Results are shown in Table 6.5 and in Figure 6.10, 6.11 and 6.12. Table 6.5 shows the

performance while identifying each letter of the standard P300 Speller Matrix, and the channel where the best performance is attained. Figure 6.10 shows the performance curves for six algorithms. Each one represents the percentage of letters that is actually predicted by the algorithms using a cross-validation procedure. As previously described the data is continuously divided in two sets, where the first 15 letters are used to derive the dictionary of templates while the remaining 20 letters are used to measure the letter identification performance. This is repeated one hundred times, and performances averaged. Figure 6.11 shows the same results for the Experiment 2, where a noisy latency lag was included. Finally, Figure 6.12 represents the performance values obtained for the Experiment 3, when the amplitude of the P3b component of the template is randomly attenuated. Furthermore, results obtained for the dataset BCI Competition 2003 IIb are shown in Figures 6.13 and in Table 6.6. For this experiment the number of available intensification sequences is 15.

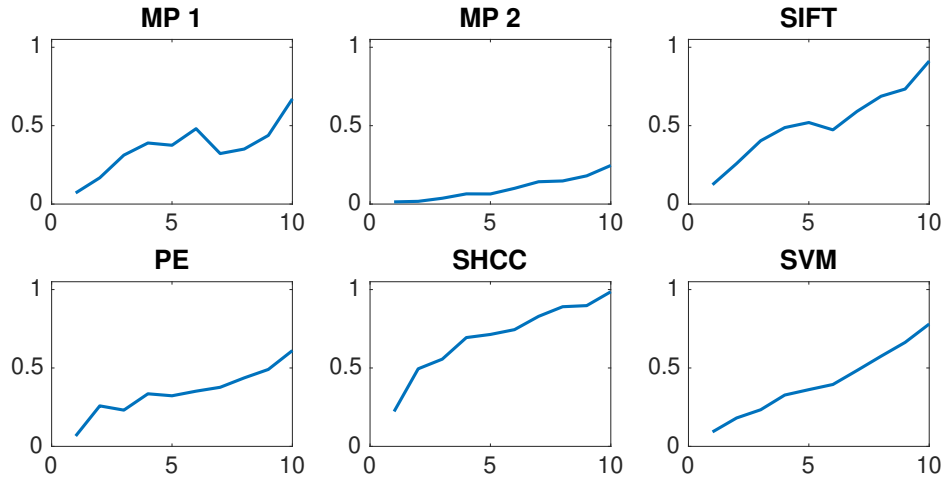


Figure 6.10: Speller performance obtained for each method for the Experiment 1. Y-axis shows performance accuracy while X-axis shows the number of intensification sequences used to calculate the point-to-point signal average.

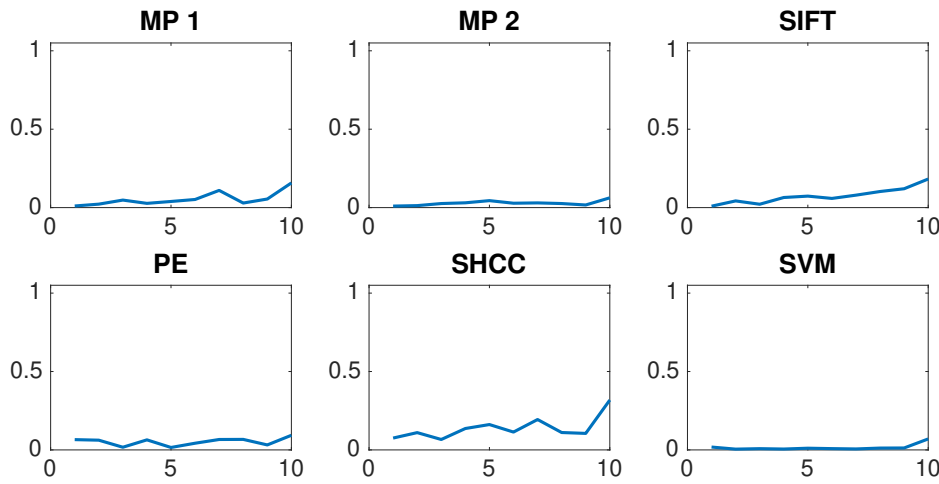


Figure 6.11: Speller performance obtained for each method while latencies are artificially added to each single-intensification segment corresponding to the Experiment 2. The achieved performance is significantly reduced for all methods. Y-axis shows letter identification performance while X-axis shows the number of intensification sequences used to calculate the ensemble average.

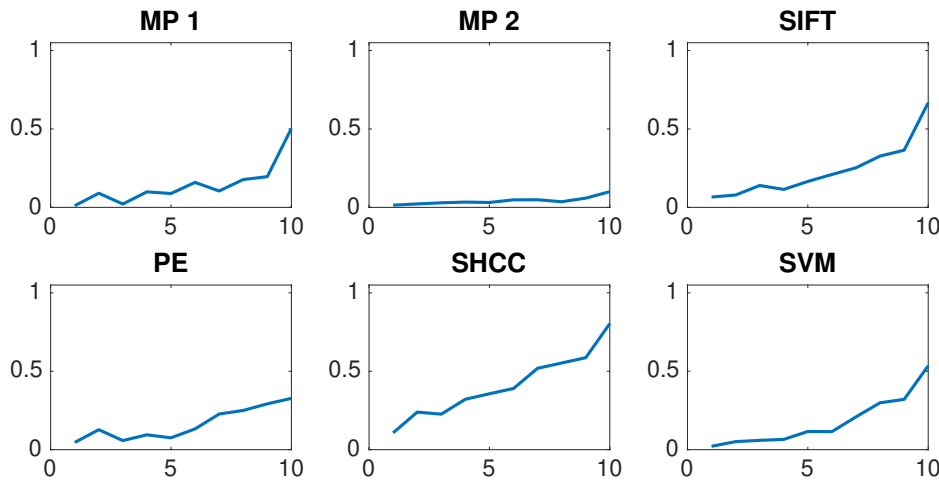


Figure 6.12: Speller performance obtained for the Experiment 3 while the amplitudes of the P3b component of the superimposed ERP is randomly reduced. Y-axis shows performance accuracy while X-axis shows the number of intensification sequences.

Table 6.5: Speller classification performance obtained for all the waveform-based algorithms: MP Matching Pursuit, SIFT Scale Invariant Feature Transform, PE Permutation Entropy and SHCC Slope Horizontal Code Chain. Additionally, the control algorithm SVM Support Vector Machines is included for comparison. All the methods process the signal on a channel-by-channel basis, hence the best performing channel is also shown. In this case with absence of null-signals, it can be interpreted as the channel that adds less noise to the ERP template. All the methods used 10 intensification sequences to coherently average the trials to obtain the averaged signal.

<b>Method</b>	<b>Channel</b>	<b>Performance</b>		
		<b>Experiment 1</b>	<b>Experiment 2</b>	<b>Experiment 3</b>
MP 1	PO8	67%	15%	50%
MP 2	PO7	24%	6%	10%
SIFT	PO8	91%	18%	66%
PE	Cz	61%	9%	32%
SHCC	P4	98%	31%	80%
SVM	PO8	78%	7%	53%

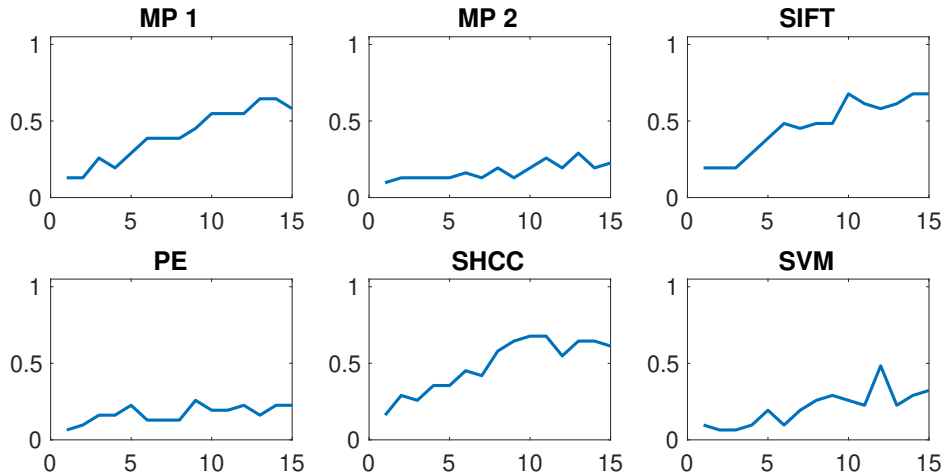


Figure 6.13: Speller performance obtained for the Dataset IIb of the BCI Competition II (2003) for each one of the algorithms. An offline BCI Simulation is performed using the first 42 trials as training and the remaining 31 as testing. The horizontal axis show the number of intensification sequences, from 0 to 15 for this dataset, while the vertical axis show the performance rate.

Table 6.6: Speller classification performance obtained for the dataset IIb of the BCI Competition II (2003) for each one of the algorithms using 15 repetitions of intensification sequences. The first 42 trials are used for training to build the template dictionary and the remaining 31 for testing. The channel where the best performance is attained, is also shown.

<b>Method</b>	<b>Channel</b>	<b>Performance</b>
MP 1	FC2	50%
MP 2	CPz	22%
SIFT	Cz	67%
PE	PO8	22%
SHCC	Cz	61%
SVM	C1	32%

# Chapter 7

## Conclusions and Future Work

A method to analyze EEG signals which is based on the waveform characterization is presented. The benefits of the proposed approach are twofold, (1) it has a universal applicability because the same basic methodology can be applied to detect different patterns in EEG signals with applications to BCI and (2) it has the potential to foster close collaboration with physicians and electroencephalograph technicians because the approach follows the established procedure of the clinical EEG community of analyzing waveforms by their shapes

1. intelligible property
2. The search for meaningfull or cognitive waveforms
3. Long Term recording
4. Foster clinical interaction.

Parte de las conclusiones pueden girar alrededor del debate de qEEG vs EEG. También las conclusiones en relación a otros métodos que hacen algo parecido y la necesidad de que el método explique el cómo llega a una decisión.

1. Keypoint Localization : scale space analysis on EEG
2. Usage to determine trial to trial variability (using general orientation)
3. Multichannel
4. Imaging

Provide tools to clinicians !!!!!



## Appendix A

# BCI en Argentina

El propósito de este apéndice es ofrecer información del estado de esta disciplina en Argentina. La inevitable omisión de trabajos o grupos específicos de ninguna manera ha sido adrede, y se solicita las pertinentes disculpas. Este relevamiento fue realizado durante el transcurso del desarrollo de esta tesis, y probablemente tenga una visión desde el mundo de las Ingenierías, sesgada en esta tremadamente interdisciplinaria disciplina.

Los pioneros en Argentina son los trabajos en la Universidad de La Plata, y los trabajos de la UNER. Estos últimos desarrollaron en el 2006 las primeras Jornadas Argentinas sobre Interfaces Cerebro-Computadora y las replicaron en el JAICC 2009.

- UNER, Facultad de Ingeniería, LIRINS,(Oro Verde) Bioingeniería Dr. Gerardo Gentilleti <http://cortex.loria.fr/Projects/STIC-AmSud-BCI>, [http://www.bioingenieria.edu.ar/postgrado/index.php?option=com\\_content&view=category&id=72&Itemid=61](http://www.bioingenieria.edu.ar/postgrado/index.php?option=com_content&view=category&id=72&Itemid=61) Interactive Dynamics ,Pyme Spin-off. Otros investigadores: Guerenstein, Pablo; Carolina B. Tabernig (BCI-FES system for neuro-rehabilitation of stroke patients)
- FRN: Fundación Rosarina de Neuro-Rehabilitación, Medicina y Rehabilitación, Dr. Carlos Ballario
  - BCI-FES
  - Stroke Neurorehabilitation
  - Trabajan con Interactive Dynamics.
- UBA, Facultad de Ingeniería, Laboratorio de Sergio Lew (<http://www.fi.uba.ar/es/node/1442>) , ”Instituto de Ingeniería Biomédicas” / Dr. Sergio Lew BCI Invasivo principalmente.

- UBA, Ingeniería Laboratorio de Sistemas Inteligentes Dr. Jorge Ierache <http://laboratorios.fi.uba.ar/lsi/>: control de robots por bioseñales, detección de emociones.
- UBA, Exactas <https://liaa.dc.uba.ar/> Applied Artificial Intelligence Lab Dr. Agustín Gravano / Dr. Diego Fernandez Slezak Tesis de grado Arneodo. Otros investigadores: Alejandro Sabatini
- INAUT, Instituto Nacional de Automática, San Juan, / Dr. Carlos Soria, Dr. Eugenio Orosco BCI Robótica (BCI híbridos, robótica asistiva) Trabajan con Teodiano Freire Bastos en Brasil [www.ncbi.nlm.nih.gov](http://www.ncbi.nlm.nih.gov) Otros investigadores: Mst. Ing. Fernando Auat Cheeín E-mail: fauat@inaut.unsj.edu.ar
- Instituto Argentino de Matemáticas Alberto Calderon / Bioing. Sergio Liberczuk, Dr. Bruno Cernuschi Frías Matemáticas y modelado del problema inverso.
- ITBA, / CiC del Dr Juan Santos, <http://www.itba.edu.ar/es/id/centros/cic-centro-de-inteligencia-computacional> Proyecto Doctorado Robótica Asistiva BCI Neurorehabilitación, Rodrigo Ramele [http://www.unsam.edu.ar/tss/controlar-maquinas-con-el-pensamiento/978-3-319-13117-7\\_142](http://www.unsam.edu.ar/tss/controlar-maquinas-con-el-pensamiento/978-3-319-13117-7_142)
- UNC, Universidad Nacional de Córdoba Trabajo Final de Ingeniería: <http://www.electronicosonline.com/2013/07/08/crean-jovenes-argentinos-interface-cerebral-para-discap> Carrera de Ingeniería Biomédica: Ing. Diego Beltramone
- UNLP, LEICI / Dr. Enrique Spinelli ([http://www.ing.unlp.edu.ar/leici/esp\\_pspinelli.html](http://www.ing.unlp.edu.ar/leici/esp_pspinelli.html)) Electrónica. Tesis de Grado de García Pablo: <http://sedici.unlp.edu.ar/handle/10915/3800631605> Tesis de Maestría de Andrea Noelia Bermudez Cicchino 31605 Cesar Caiafa (trabajó con Cichocki) <http://ccaiaca.wixsite.com/cesar>
- Universidad Nacional de Tucumán, Instituto Superior de Investigaciones Biológicas (INSIBIO) [www.lamein.org](http://www.lamein.org) Investigación sobre alternativas de codificación neural de los sistemas sensoriales. Investigadores responsables: Dr. Carmelo Felice, Mst. Ing. Fernando Farfán E-mail: cfelice@herrera.unt.edu.ar, ffarfan@herrera.unt.edu.ar
- Laboratorio de Investigación y Desarrollo en Nuevas Tecnologías (LIDeNTec) - ANSES Desarrollo de BCI Investigadores responsables: Dr. Mario Mastriani E-mail: mmastri@gmail.com

- INECO: Cercanía con BCI pero no parece ser el foco de lo que hacen. Eugenia Hesse Agustín Ibañez
- IBCN Silvia Kochen [http://www.ibcn.fmed.uba.ar/200\\_grupos-lab-epilepsia-kochen.html](http://www.ibcn.fmed.uba.ar/200_grupos-lab-epilepsia-kochen.html)
- Instituto Ferrero de Neurología y Sueño. Fundación Argentina de Estudio del Cerebro. Publicaron un excelente libro en castellano de *Análisis Computado de EEG*.



# Bibliography

- [1] *Towards Practical Brain-Computer Interfaces*, 2013.
- [2] *Gartner hype 2016*, 2016.
- [3] A. Bolu Ajiboye, Francis R. Willett, Daniel R. Young, William D. Memberg, Brian A. Murphy, Jonathan P. Miller, Benjamin L. Walter, Jennifer A. Sweet, Harry A. Hoyen, Michael W. Keith, P. Hunter Peckham, John D. Simeral, John P. Donoghue, Leigh R. Hochberg, and Robert F. Kirsch, *Restoration of reaching and grasping movements through brain-controlled muscle stimulation in a person with tetraplegia: a proof-of-concept demonstration*, *The Lancet* **389** (2017), no. 10081, 1821–1830.
- [4] Montserrat Alvarado-González, Edgar Garduño, Ernesto Bibiesca, Oscar Yáñez-Suárez, and Verónica Medina-Bañuelos, *P300 Detection Based on EEG Shape Features*, Computational and Mathematical Methods in Medicine (2016), 1–14.
- [5] Kai Keng Ang, Cuntai Guan, Karen Sui Geok Chua, Beng Ti Ang, Christopher Wee Keong Kuah, Chuanchu Wang, Kok Soon Phua, Zheng Yang Chin, and Haihong Zhang, *A large clinical study on the ability of stroke patients to use an EEG-based motor imagery brain-computer interface*, *Clinical EEG and Neuroscience* **42** (2011), no. 4, 253–258.
- [6] Jitka Annen, Séverine Blandiaux, Nicolas Lejeune, Mohamed A. Bahri, Aurore Thibaut, Woosang Cho, Christoph Guger, Camille Chatelle, and Steven Laureys, *BCI performance and brain metabolism profile in severely brain-injured patients without response to command at bedside*, *Frontiers in Neuroscience* **12** (2018), no. JUN, 370.
- [7] Erol Başar, *A review of alpha activity in integrative brain function: Fundamental physiology, sensory coding, cognition and pathology*, *International Journal of Psychophysiology* **86** (2012), no. 1, 1–24.
- [8] Christoph Bandt and Bernd Pompe, *Permutation Entropy: A Natural Complexity Measure for Time Series*, *Physical Review Letters* **88** (2002), no. 17, 174102.
- [9] Sebastian Berger, Gerhard Schneider, Eberhard Kochs, and Denis Jordan, *Permutation Entropy: Too Complex a Measure for EEG Time Series?*, *Entropy* 2017, Vol. 19, Page 692 **19** (2017), no. 12, 692.
- [10] O. Boiman, E. Shechtman, and M. Irani, *In defense of nearest-neighbor based image classification*, 26th IEEE Conference on Computer Vision and Pattern Recognition, CVPR (2008).
- [11] J. E. Bresenham, *Algorithm for computer control of a digital plotter*, *IBM Systems Journal* **4** (1965), no. 1, 25–30.

- [12] Jeffrey W. Britton, Lauren C. Frey, Jennifer L. Hopp, Pearce Korb, Mohamad Z. Koubeissi, William E. Lievens, Elia M. Pestana-Knight, and Erik K. St. Louis, *Electroencephalography (eeg): An introductory text and atlas of normal and abnormal findings in adults, children, and infants*, 2016.
- [13] Clemens Brunner, Benjamin Blankertz, Febo Cincotti, Andrea Kübler, Donatella Mattia, Felip Miralles, Anton Nijholt, and Begonya Otal, *BNCI Horizon 2020 – Towards a Roadmap for Brain / Neural Computer Interaction*, Lecture Notes in Computer Science **8513** (2014), no. 1, 475–486.
- [14] György Buzsáki, Costas A. Anastassiou, and Christof Koch, *The origin of extracellular fields and currents-EEG, ECoG, LFP and spikes*, Nature Reviews Neuroscience **13** (2012), no. 6, 407–420.
- [15] T. Carlson and J. del R. Millan, *Brain-controlled wheelchairs: A robotic architecture*, IEEE Robotics & Automation Magazine **20** (2013), no. 1, 65–73.
- [16] S. Casarotto, A.M. Bianchi, S. Cerutti, and G.A. Chiarenza, *Dynamic time warping in the analysis of event-related potentials*, IEEE Engineering in Medicine and Biology Magazine **24** (2005), no. 1, 68–77.
- [17] S. Chandran KS, A. Mishra, V. Shirhatti, and S. Ray, *Comparison of Matching Pursuit Algorithm with Other Signal Processing Techniques for Computation of the Time-Frequency Power Spectrum of Brain Signals*, Journal of Neuroscience **36** (2016), no. 12, 3399–3408.
- [18] Ricardo Chavarriaga, Melanie Fried-Oken, Sonja Kleih, Fabien Lotte, and Reinhold Scherer, *Heading for new shores! Overcoming pitfalls in BCI design*, Brain-Computer Interfaces **4** (2017), no. 1-2, 60–73.
- [19] Andy Clark, *Supersizing the mind: Embodiment, action, and cognitive extension*, OUP USA, 2008.
- [20] M. Clerc, L. Bougrain, and F. Lotte, *Brain-computer interfaces, technology and applications 2(cognitive science)*, ISTE Ltd. and Wiley, 2016.
- [21] Maureen Clerc, Laurent Bougrain, and Fabien Lotte, *Brain-Computer Interfaces 2: Technology and Applications*, 2016.
- [22] Mike X Cohen, *Analyzing Neural Time Series Data: Theory and Practice*, 2014.
- [23] Scott R. Cole and Bradley Voytek, *Brain Oscillations and the Importance of Waveform Shape*, Trends in Cognitive Sciences **21** (2017), no. 2, 137–149.
- [24] Navneet Dalal and Bill Triggs, *Histograms of oriented gradients for human detection*, Proceedings - 2005 IEEE Computer Society Conference on Computer Vision and Pattern Recognition, CVPR 2005, vol. I, IEEE, 2005, pp. 886–893.
- [25] M. De Vos and S. Debener, *Mobile EEG: Towards brain activity monitoring during natural action and cognition*, International Journal of Psychophysiology **91** (2014), no. 1, 1–2.

- [26] Stefan Debener, Falk Minow, Reiner Emkes, Katharina Gandras, and Maarten de Vos, *How about taking a low-cost, small, and wireless EEG for a walk?*, *Psychophysiology* **49** (2012), no. 11, 1617–21.
- [27] Shimon Edelman, Nathan Intrator, and Tomaso Poggio, *Complex cells and object recognition*, 1997.
- [28] L A Farwell and E Donchin, *Talking off the top of your head: toward a mental prosthesis utilizing event-related brain potentials.*, *Electroencephalography and clinical neurophysiology* **70** (1988), no. 6, 510–23.
- [29] Faranak Farzan, Sravya Atluri, Matthew Frehlich, Prabhjot Dhami, Killian Kleffner, Rae Price, Raymond W. Lam, Benicio N. Frey, Roumen Milev, Arun Ravindran, Mary Pat McAndrews, Willy Wong, Daniel Blumberger, Zafiris J. Daskalakis, Fidel Vila-Rodriguez, Esther Alonso, Colleen A. Brenner, Mario Liotti, Moyez Dharsee, Stephen R. Arnott, Kenneth R. Evans, Susan Rotzinger, and Sidney H. Kennedy, *Standardization of electroencephalography for multi-site, multi-platform and multi-investigator studies: Insights from the canadian biomarker integration network in depression*, *Scientific Reports* **7** (2017), no. 1, 7473.
- [30] Klein F.F., *A waveform analyzer applied to the human EEG*, *IEEE Transactions on Biomedical Engineering* **23** (1976), no. 3, 246–252.
- [31] Walter J. Freeman and Rodrigo Quian Quiroga, *Imaging brain function with EEG: Advanced temporal and spatial analysis of electroencephalographic signals*, vol. 9781461449843, Springer New York, New York, NY, 2013.
- [32] B. Giagante, S. Oddo, W. Silva, D. Consalvo, E. Centurion, L. D'Alessio, P. Solis, P. Salgado, E. Seoane, P. Saidon, and S. Kochen, *Clinical-electroencephalogram patterns at seizure onset in patients with hippocampal sclerosis*, *Clinical Neurophysiology* **114** (2003), no. 12, 2286–2293.
- [33] A. L. Goldberger, L. A. N. Amaral, L. Glass, J. M. Hausdorff, P. Ch. Ivanov, R. G. Mark, J. E. Mietus, G. B. Moody, C.-K. Peng, and H. E. Stanley, *PhysioBank, PhysioToolkit, and PhysioNet : Components of a New Research Resource for Complex Physiologic Signals*, *Circulation* **101** (2000), no. 23, e215–e220.
- [34] Alexandre Gramfort, Martin Luessi, Eric Larson, Denis A. Engemann, Daniel Strohmeier, Christian Brodbeck, Roman Goj, Mainak Jas, Teon Brooks, Lauri Parkkonen, and Matti Hämäläinen, *MEG and EEG data analysis with MNE-Python*, *Frontiers in Neuroscience* **7** (2013), no. 7 DEC, 267.
- [35] Christoph Guger, Brendan Z. Allison, and Mikhail A. Lebedev, *Introduction*, *Brain Computer Interface Research: A State of the Art Summary* 6, Springer, Cham, 2017, pp. 1–8.
- [36] Christoph Guger, Shahab Daban, Eric Sellers, Clemens Holzner, Gunther Krausz, Roberta Carabalona, Furio Gramatica, and Guenter Edlinger, *How many people are able to control a P300-based brain-computer interface (BCI)?*, *Neuroscience Letters* **462** (2009), no. 1, 94–98.

- [37] Marcelo Alejandro Haberman and Enrique Mario Spinelli, *A multichannel EEG acquisition scheme based on single ended amplifiers and digital DRL*, IEEE Transactions on Biomedical Circuits and Systems **6** (2012), no. 6, 614–618.
- [38] Saskia Haegens, Helena Cousijn, George Wallis, Paul J. Harrison, and Anna C. Nobre, *Inter- and intra-individual variability in alpha peak frequency*, NeuroImage **92** (2014), 46–55.
- [39] a. L. Hartman, *Atlas of EEG patterns*, vol. 65, Lippincott Williams & Wilkins, 2005.
- [40] Hochberg, Serruya, Friehs, Mukand, Saleh, Capla, Branner, Chen, Penn, and Donoghue, *Neuronal ensemble control of prosthetic devices by a human with tetraplegia*, Nature **442** (2006), no. 7099, 164–171.
- [41] L. Hu, A. Mouraux, Y. Hu, and G. D. Iannetti, *A novel approach for enhancing the signal-to-noise ratio and detecting automatically event-related potentials (ERPs) in single trials*, NeuroImage **50** (2010), no. 1, 99–111.
- [42] Jane E. Huggins, Ramses E. Alcaide-Aguirre, and Katya Hill, *Effects of text generation on P300 brain-computer interface performance*, Brain-Computer Interfaces **3** (2016), no. 2, 112–120.
- [43] Jane E. Huggins, Aisha A. Moinuddin, Anthony E. Chiodo, and Patricia A. Wren, *What would brain-computer interface users want: Opinions and priorities of potential users with spinal cord injury*, Archives of Physical Medicine and Rehabilitation **96** (2015), no. 3, S38–S45.
- [44] Alice F. Jackson and Donald J. Bolger, *The neurophysiological bases of eeg and eeg measurement: A review for the rest of us*, Psychophysiology **51** (2014), no. 11, 1061–1071.
- [45] Abeg Kumar Jaiswal and Haider Banka, *Local pattern transformation based feature extraction techniques for classification of epileptic EEG signals*, Biomedical Signal Processing and Control **34** (2017), 81–92.
- [46] Ben H. Jansen, *Quantitative analysis of electroencephalograms: is there chaos in the future?*, International Journal of Bio-Medical Computing **27** (1991), no. 2, 95–123.
- [47] Piotr Jaśkowski and Rolf Verleger, *An evaluation of methods for single-trial estimation of P3 latency*, Psychophysiology **37** (2000), no. 2, 153–162.
- [48] J. Jestico, P. Fitch, R. W. Gilliatt, and R. G. Willison, *Automatic and rapid visual analysis of sleep stages and epileptic activity. A preliminary report*, Electroencephalography and Clinical Neurophysiology **43** (1977), no. 3, 438–441.
- [49] Camille Jeunet, Alison Cellard, Sriram Subramanian, Martin Hachet, N Kaoua, Fabien Lotte, Camille Jeunet, Alison Cellard, Sriram Subramanian, Martin Hachet, Bernard N Kaoua, Camille Jeunet, Alison Cellard, Sriram Subramanian, and Martin Hachet, *How Well Can We Learn With Standard BCI Training Approaches ? A Pilot Study . To cite this version : How Well Can We Learn With Standard BCI Training Approaches ? A Pilot Study .*, (2014), no. SEPTEMBER, 1–5.

- [50] F. Jure, L. Carrere, G. Gentiletti, and C. Tabernig, *BCI-FES system for neuro-rehabilitation of stroke patients*, Journal of Physics: Conference Series **705** (2016), no. 1, 1–8.
- [51] Kevin H. Knuth, Ankoor S. Shah, Wilson A. Truccolo, Mingzhou Ding, Steven L. Bressler, and Charles E. Schroeder, *Differentially variable component analysis: Identifying multiple evoked components using trial-to-trial variability*, Journal of Neurophysiology **95** (2006), no. 5, 3257–3276.
- [52] Dean J Krusienski, Eric W Sellers, François Cabestaing, Sabri Bayoudh, Dennis J McFarland, Theresa M Vaughan, and Jonathan R Wolpaw, *A comparison of classification techniques for the P300 Speller*, Journal of Neural Engineering **3** (2006), no. 4, 299–305.
- [53] Nanying Liang and Laurent Bougrain, *Averaging techniques for single-trial analysis of oddball event-related potentials*, 4th International Brain-Computer (2008), 1–6.
- [54] Tony Lindeberg, *A computational theory of visual receptive fields*, Biological Cybernetics **107** (2013), no. 6, 589–635.
- [55] Peter Lloyd-Sherlock, *Population ageing in developed and developing regions: Implications for health policy*, Social Science and Medicine **51** (2000), no. 6, 887–895.
- [56] F. Lotte, L. Bougrain, A. Cichocki, M. Clerc, M. Congedo, A. Rakotomamonjy, and F. Yger, *A review of classification algorithms for EEG-based brain-computer interfaces: A 10 year update*, Journal of Neural Engineering **15** (2018), no. 3, 031005.
- [57] F. Lotte, M. Congedo, A. Lécuyer, F. Lamarche, and B. Arnaldi, *A review of classification algorithms for EEG-based brain-computer interfaces*, 2007.
- [58] Fabien Lotte, Josef Faller, Christoph Guger, Yann Renard, Gert Pfurtscheller, Anatole Lécuyer, and Robert Leeb, *Combining bci with virtual reality: Towards new applications and improved bci*, pp. 197–220, Springer Berlin Heidelberg, Berlin, Heidelberg, 2013.
- [59] G Lowe, *SIFT - The Scale Invariant Feature Transform*, International Journal **2** (2004), 91–110.
- [60] Tomohiro Madarame, Hisaya Tanaka, Takenobu Inoue, Minoru Kamata, and Motoki Shino, *The development of a brain computer interface device for amyotrophic lateral sclerosis patients*, Conference Proceedings - IEEE International Conference on Systems, Man and Cybernetics, IEEE, oct 2008, pp. 2401–2406.
- [61] Joseph N. Mak, Dennis J. McFarland, Theresa M. Vaughan, Lynn M. McCane, Phillipa Z. Tsui, Debra J. Zeitlin, Eric W. Sellers, and Jonathan R. Wolpaw, *EEG correlates of P300-based brain-computer interface (BCI) performance in people with amyotrophic lateral sclerosis*, Journal of Neural Engineering **9** (2012), no. 2.
- [62] Stephane G. Mallat and Zhifeng Zhang, *Matching Pursuits With Time-Frequency Dictionaries*, IEEE Transactions on Signal Processing **41** (1993), no. 12, 3397–3415.

- [63] Lynn M McCane, Susan M Heckman, Dennis J McFarland, George Townsend, Joseph N Mak, Eric W Sellers, Debra Zeitlin, Laura M Tenteromano, Jonathan R Wolpaw, and Theresa M Vaughan, *P300-based brain-computer interface (BCI) event-related potentials (ERPs): People with amyotrophic lateral sclerosis (ALS) vs. age-matched controls*, Clinical Neurophysiology **126** (2015), no. 11, 2124–2131.
- [64] Chang S. Nam, Yueqing Li, and Steve Johnson, *Evaluation of P300-based brain-computer interface in real-world contexts*, International Journal of Human-Computer Interaction **26** (2010), no. 6, 621–637.
- [65] F. (Ed.). Nam, C. (Ed.), Nijholt, A. (Ed.), Lotte, *Brain-Computer Interfaces Handbook*, CRC Press, Boca Raton, jan 2018.
- [66] Nicoletta Nicolaou and Julius Georgiou, *Permutation entropy: A new feature for brain-computer interfaces*, 2010 IEEE Biomedical Circuits and Systems Conference, BioCAS 2010, IEEE, nov 2010, pp. 49–52.
- [67] Femke Nijboer and Ursula Broermann, *Brain Computer Interfaces for Communication and Control in Locked-in Patients*, Graumann B., Pfurtscheller G., Allison B. (eds) Brain-Computer Interfaces. The Frontiers Collection., Springer Berlin Heidelberg, 2009, pp. 185–201.
- [68] Amin Nourmohammadi and Mohammad Jafari, *A Survey on Unmanned Aerial Vehicle Remote Control Using Brain– Computer Interface*, IEEE Transactions on Human-Machine Systems (2018), no. May, 1–12.
- [69] Domen Novak, Roland Sigrist, Nicolas J. Gerig, Dario Wyss, Rene Bauer, Ulrich Gotz, and Robert Riener, *Benchmarking brain-computer interfaces outside the laboratory: The cybathlon 2016*, Frontiers in Neuroscience **11** (2018), 756.
- [70] Guang Ouyang, Andrea Hildebrandt, Werner Sommer, and Changsong Zhou, *Exploiting the intra-subject latency variability from single-trial event-related potentials in the P3 time range: A review and comparative evaluation of methods*, Neuroscience and Biobehavioral Reviews **75** (2017), 1–21.
- [71] Chethan Pandarinath, Paul Nuyujukian, Christine H. Blabe, Brittany L. Sorice, Jad Saab, Francis R. Willett, Leigh R. Hochberg, Krishna V. Shenoy, and Jaimie M. Henderson, *High performance communication by people with paralysis using an intracortical brain-computer interface*, eLife **6** (2017), e18554.
- [72] Lucas Parra, Christoforos Christoforou, Adam Gerson, Mads Dyrholm, An Luo, Mark Wagner, Marios Philiastides, and Paul Sajda, *Spatiotemporal Linear Decoding of Brain State*, IEEE Signal Processing Magazine **25** (2008), no. 1, 107–115.
- [73] S. Perdikis, R. Leeb, J. Williamson, A. Ramsay, M. Tavella, L. Desideri, E. J. Hoogerwerf, A. Al-Khadairy, R. Murray-Smith, and J. D R Millán, *Clinical evaluation of BrainTree, a motor imagery hybrid BCI speller*, Journal of Neural Engineering **11** (2014), no. 3, 036003.

- [74] John Polich, *Updating P300: An integrative theory of P3a and P3b*, Clinical Neurophysiology **118** (2007), no. 10, 2128–2148.
- [75] Alain Rakotomamonjy and Vincent Guigue, *BCI Competition III: Dataset II-Ensemble of SVMs for BCI P300 Speller*, IEEE Transactions on Biomedical Engineering **55** (2008), no. 3, 1147–1154.
- [76] R. Ramele, A. J. Villar, and J. M. Santos, *BCI classification based on signal plots and SIFT descriptors*, 4th International Winter Conference on Brain-Computer Interface, BCI 2016 (Yongpyong), IEEE, feb 2016, pp. 1–4.
- [77] ———, *P300-dataset rrid scr\_015977*, <https://www.kaggle.com/rramele/p300samplingdataset>, 2017.
- [78] Rajesh P. N. Rao, *Brain-computer interfacing: An introduction*, Cambridge University Press, New York, NY, USA, 2013.
- [79] Yann Renard, Fabien Lotte, Guillaume Gibert, Marco Congedo, Emmanuel Maby, Vincent Delannoy, Olivier Bertrand, and Anatole Lécuyer, *OpenViBE: An Open-Source Software Platform to Design, Test, and Use Brain Computer Interfaces in Real and Virtual Environments*, Presence: Teleoperators and Virtual Environments **19** (2010), no. 1, 35–53.
- [80] Angela Riccio, Luca Simione, Francesca Schettini, Alessia Pizzimenti, Maurizio Inghilleri, Marta Olivetti Belardinelli, Donatella Mattia, and Febo Cincotti, *Attention and P300-based BCI performance in people with amyotrophic lateral sclerosis*, Frontiers in Human Neuroscience **7** (2013), no. November, 732.
- [81] Robert Riener and Linda J. Seward, *Cybathlon 2016*, 2014 IEEE International Conference on Systems, Man, and Cybernetics (SMC) (2014), 2792–2794.
- [82] Andrea Rodenbeck, Ralf Binder, Peter Geisler, Heidi Danker-Hopfe, Reimer Lund, Friedhart Raschke, Hans Günther Weiß, and Hartmut Schulz, *A review of sleep EEG patterns. Part I: A compilation of amended rules for their visual recognition according to Rechtschaffen and Kales*, Somnologie **10** (2006), no. 4, 159–175.
- [83] Sanei and Chambers, *Eeg signal processing*, John Wiley & Sons, 2008.
- [84] Gerwin Schalk, Dennis J McFarland, Thilo Hinterberger, Niels Birbaumer, and Jonathan R Wolpaw, *BCI2000: a general-purpose brain-computer interface (BCI) system*, IEEE transactions on bio-medical engineering **51** (2004), no. 6, 1034–43 (English).
- [85] Donald L Schomer and Fernando Lopes Da Silva, *Niedermeyer's electroencephalography: Basic principles, clinical applications, and related fields*, Walters Klutter -Lippincott Williams & Wilkins, 2010.
- [86] Eric W. Sellers, Andrea Kübler, and Emanuel Donchin, *Brain-computer interface research at the University of South Florida cognitive psychophysiology laboratory: The P300 speller*, IEEE Transactions on Neural Systems and Rehabilitation Engineering **14** (2006), no. 2, 221–224.

- [87] Nidhi Agrawal Shah and Courtney Jane Wusthoff, *How to use: Amplitude-integrated EEG (aEEG)*, Archives of Disease in Childhood: Education and Practice Edition **100** (2015), no. 2, 75–81.
- [88] David Steyrl, Reinhold Scherer, Josef Faller, and Gernot R Müller-Putz, *Random forests in non-invasive sensorimotor rhythm brain-computer interfaces: a practical and convenient non-linear classifier.*, Biomedizinische Technik. Biomedical engineering (2015).
- [89] Stopczynski, Stahlhut, Larsen, Petersen, and Hansen, *The smartphone brain scanner: A portable real-time neuroimaging system*, PloS one **9** (2014), no. 2, e86733.
- [90] Nitish V. Thakor and Shanbao Tong, *Advances in Quantitative Electroencephalogram Analysis Methods*, Annual Review of Biomedical Engineering **6** (2004), no. 1, 453–495.
- [91] Nv Thakor, *Quantitative EEG analysis methods and clinical applications*, 2009.
- [92] Roni Tibon and Daniel A Levy, *Striking a balance: analyzing unbalanced event-related potential data.*, Frontiers in psychology **6** (2015), 555.
- [93] Sunao Uchida, Irwin Feinberg, Jonathan D. March, Yoshikata Atsumi, and Tom Maloney, *A comparison of period amplitude analysis and FFT power spectral analysis of all-night human sleep EEG*, Physiology and Behavior **67** (1999), no. 1, 121–131.
- [94] Sunao Uchida, Masato Matsuura, Shigeki Ogata, Takuji Yamamoto, and Naoyuki Aikawa, *Computerization of Fujimori's method of waveform recognition a review and methodological considerations for its application to all-night sleep EEG*, Journal of Neuroscience Methods **64** (1996), no. 1, 1–12.
- [95] Lukáš Vařeka, *Matching pursuit for p300-based brain-computer interfaces*, 2012 35th International Conference on Telecommunications and Signal Processing, TSP 2012 - Proceedings (2012), no. 2, 513–516.
- [96] Wim Van Drongelen, *Signal processing for neuroscientists: an introduction to the analysis of physiological signals*, Academic press, 2006.
- [97] A. Vedaldi and B. Fulkerson, *VLFfeat - An open and portable library of computer vision algorithms*, Design **3** (2010), no. 1, 1–4.
- [98] E. Vincent and Y. Deville, *Handbook of Blind Source Separation - Independent Component Analysis and Applications*, Elsevier, 2010.
- [99] Sophie Wang, C. Janice Hsu, Lauren Trent, Tiffany Ryan, Nathan T. Kearns, Eugene F. Civillico, and Kimberly L. Kontson, *Evaluation of Performance-Based Outcome Measures for the Upper Limb: A Systematic Review*, Pm&R (2018).
- [100] Wouter D. Weeda, Raoul P P P Grasman, Lourens J. Waldorp, Maria C. van de Laar, Maurits W. van der Molen, and Hilde M. Huizenga, *A fast and reliable method for simultaneous waveform, amplitude and latency estimation of single-trial EEG/MEG data*, PLoS ONE **7** (2012), no. 6.

- [101] Wessberg, Stambaugh, Kralik, Beck, Laubach, Chapin, Kim, Biggs, Srinivasan, and Nicolelis, *Real-time prediction of hand trajectory by ensembles of cortical neurons in primates*, *Nature* **408** (2000), no. 6810, 361–365.
- [102] J. Wolpaw and Wolpaw E., *Brain-computer interfaces: Principles and practice*, Oxford University Press, 2012.
- [103] J. Wolpaw and E. W. Wolpaw, *Brain-computer interfaces: principles and practice*, Oxford University Press, 2011.
- [104] T. Yamaguchi, M. Fujio, K.o Inoue, and G. Pfurtscheller, *Design method of morphological structural function for pattern recognition of EEG signals during motor imagery and cognition*, Fourth International Conference on Innovative Computing, Information and Control (ICICIC), 2009, pp. 1558–1561.
- [105] Robert Maxwell Young, *Mind, brain, and adaptation in the nineteenth century: Cerebral localization and its biological context from gall to ferrier*, no. 3, Oxford University Press, USA, 1970.
- [106] Rafael Yuste, Sara Goering, Blaise Agüeray Arcas, Guoqiang Bi, Jose M. Carmena, Adrian Carter, Joseph J. Fins, Phoebe Friesen, Jack Gallant, Jane E. Huggins, Judy Illes, Philipp Kellmeyer, Eran Klein, Adam Marblestone, Christine Mitchell, Erik Parens, Michelle Pham, Alan Rubel, Norihiro Sadato, Laura Specker Sullivan, Mina Teicher, David Wasserman, Anna Wexler, Meredith Whittaker, and Jonathan Wolpaw, *Four ethical priorities for neurotechnologies and AI*, *Nature* **551** (2017), no. 7679, 159–163.
- [107] Thorsten O. Zander, Christian Kothe, Sabine Jatzke, and Matti Gaertner, *Enhancing Human-Computer Interaction with Input from Active and Passive Brain-Computer Interfaces*, Springer, London, 2010, pp. 181–199.
- [108] Thorsten O. Zander, Laurens R. Krol, Niels P. Birbaumer, and Klaus Gramann, *Neuroadaptive technology enables implicit cursor control based on medial prefrontal cortex activity*, *Proceedings of the National Academy of Sciences* **113** (2016), no. 52, 14898–14903.
- [109] Dandan Zhang and Yuejia Luo, *The P1 latency of single-trial ERPs estimated by two peak-picking strategies*, *Proceedings - 2011 4th International Conference on Biomedical Engineering and Informatics, BMEI 2011* **2** (2011), 882–886.
- [110] Jian Zhang, Junzhong Zou, Min Wang, Lanlan Chen, Chunmei Wang, and Guisong Wang, *Automatic detection of interictal epileptiform discharges based on time-series sequence merging method*, *Neurocomputing* **110** (2013), 35–43.